Master Thesis in Geosciences

Paleogene sedimentation in Central Basin of Svalbard – Depositional conditions, geochemical and mineralogical variations across PETM

Ahmad Salman

UNIVERSITY OF OSLO

FACULTY OF MATHEMATICS AND NATURAL SCIENCES

Paleogene sedimentation in Central Basin of Svalbard – Depositional conditions, geochemical and mineralogical variations across PETM

Ahmad Salman

Master Thesis in Geosciences

Discipline: Petroleum Geology and Geophysics

Department of Geosciences

Faculty of Mathematics and Natural Sciences

UNIVERSITY OF OSLO

June 8th, 2011

Abstract

This study deals with the recunstruction of depositional environments and development of transgressive-regressive sequences within the upper Grumantbyen Formation and lower Frysjaodden Formation in the Central Basin. Data from sedimentary field logging, XRD and geochemical analysis has been integrated to elucidate the depositional environments.Emphasis has been laid on use of clay mineralogy as proxy for peleoclimate conditions, especially PETM: The most pronounced climatic anomaly of the Cenozoic era.

In the studied sections, deepnig upwards developments have been identified from the Grumantbyen Formation to lower Frysjaodden Formation. Two maximum flooding intervals have been identified the basal parts of Marstranderbreen Member and Gilsonryggen Member. Shallowing upward developents have also been noticed in the middle part of two cores containing Hollendardallen Member. The upper part of all cores display a transgressive development into homogenous laminated shales of Gilsonryggen Member.

PETM intervals have been identified in all three core just below and within the Maximum flooding intervals of basal Gilsonryggen Member. Kaolinite/(kaolinite+chlorite) and kaolinite/(kaolinite+chlorite) ratios forms the basis of PETM recognition and its stratigraphic position coincides earlier studies from Svalbard.

Keywords: Sedimentology, PETM, clay mineralogy, kaolinite, Svalbard, XRD

Contents

1 Introduction

This master thesis has been written as part of an international collaboration of 7 universities under the paleo Arctic Climate and Environment (pACE) project, which was initiated in 2005 by World Universities Network (WUN). The primary objective of this cooperation is to provide a vivid understanding and reconstruction of paleoenvironmental and paleoclimatic conditions during the deposition of paleogene sedimentary strata in Svalbard and the Arctic region. The study aims to explore the causes and effects of subsequent transition from Paleocene-Eocene greenhouse to the Eocene-to-modern icehouse conditions and relate them to the current climatic change. The Paleocene Eocene Thermal maximum (PETM), a dramatic and abrupt climatic change during the Paleocene-Eocene (56.3 Ma) transition will be of special interest.

The task of Oslo subgroup in this project is to provide the sedimentological, petrographic, micro paleontological and geochemical analyses of the Frysjaodden Formation and Hollendardalen member. These formations have been studies in detail by Burca (2008), Ruther (2007), Jargvoll (2009) and Riber (2009) and papers are subsequently published by Dypvik et al., (2011) and Harding et al., (2011). Present master thesis is based on three cores BH 7/08, BH 9/06 and 10/06 (Figure 1) covering the lower part of Frysjaodden Formation including the Horllenderdalen and Marstranderbreen Member.

In this thesis, the three cores are sedimentologically logged and sampled in detail. The sample material is treated in various geochemical analyses (organic carbon, carbonate, rockeval pyrolysis,main and trace elements), mineralogical analyses and petrographic analyses (thin sections and XRD). The main purpose of this thesis is to elucidate the paleoenvironment of the lower frysjaodden formation, particularly at the PETM. Source properties of the formation will be observed. Clay mineralogy will be the key climate indicator. Sedimentary data will be integrated with biostratigraphic observations. Sedimentary data from this study will be set in a regional context to approach paleo-climate interpretation.

2 Geological evolution

The Svalbard archipelago covers a land area of 63,300 km^2 and forms the sub aerially exposed northwestern margins of the Barents shelf (Worsley, 2006). It comprises all the islands between 71-81^{o}N, 10-35^{o}E, Spitsbergen being the largest among them (Nøttvedt et al., 1993). In this master thesis, the Tertiary geological evolution will be discussed since the studied drill cores are located in the Paleogene Central Basin of Spitsbergen (Figure 1).

2.1 Paleogeography

Based on study of paleomegnetic data, Dalland (1976) deduced that Svalbard was located between 71^o and 72 ^{o}N latitude in Eocene. A narrow seaway existed between Greenland and Svalbard since widening of the Norwegian Sea had not occurred at this time. Therefore, continental climatic conditions prevailed with snowfalls during winters and warm summers. On the contrary, an annual mean temperature of 15-18 degree is proposed during this time based on the study of conifers from the early Paleocene and Eocene horizons (Schweitzer, 1980). Green house climate is also proposed for the arctic by Moran et al.(2006) and Sluijs et al.(2006).

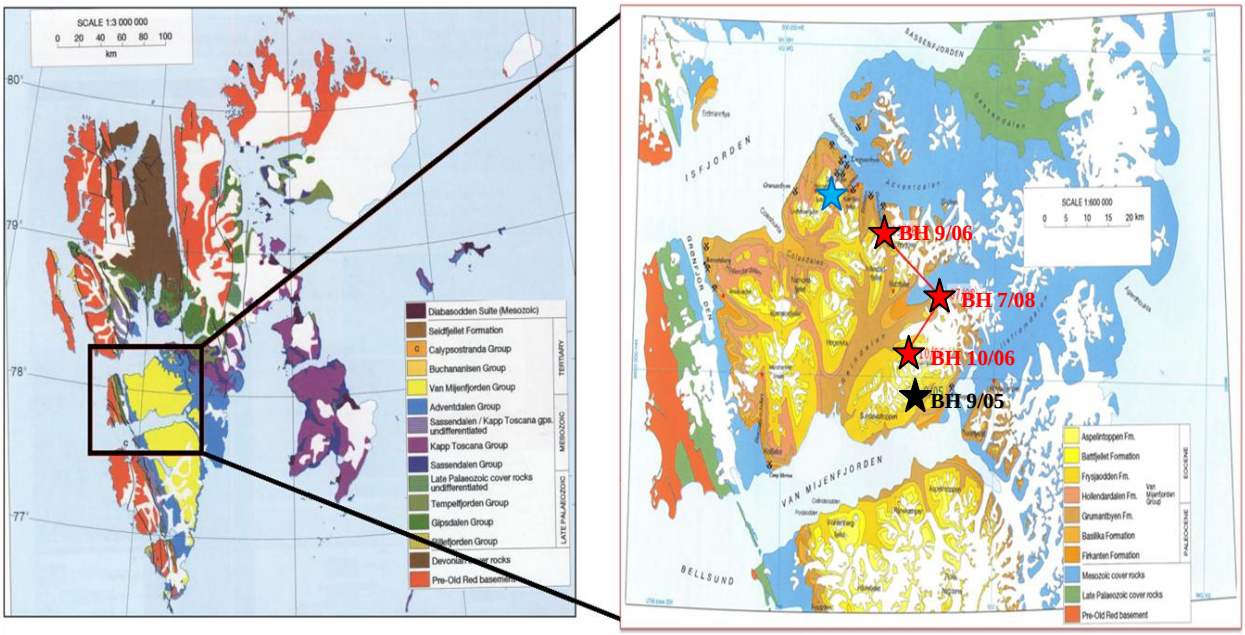

Figure 1: Geloigical map showing location of Svalbard (from Dallmann, 1999). Position of BH 7/08, BH 9/06 BH 10/06 (Red color) and studies of Ribers, 2009 (Black star) and Ruther and Burca (Blue star) have been marked.

2.2 Tertiary regional tectonics and stratigraphy

Cenozoic sedimentary strata in Svalbard are restricted to the five depositional basins in Spitsbergen (Dallmann, 1999). The Tertiary Central basin is for the largest basin of these having dimensions of 200 km length and 60 km width, with approximately 2.3 km of clastic deposits.

Deposition of Tertiary sedimentary succession in the Central Tertiary Basin initiated in the early Paleocene and continued during the onset of Norwegian–Greenland Sea opening due to large-scale transcurrent movement between Greenland and Eurasia (Harland, 1965 and 1969; Steel et al., 1981). Harland (1969) proposed the name "West Spitsbergen Orogeny" for the orogeny created by the transcurrent movement of svalbard relative to Greenland. Further movement of Greenland away from Eurasia creating a large strike-slip zone, De Geer shear zone or the De Geer Hornsund Line (Crane et al., 1982).

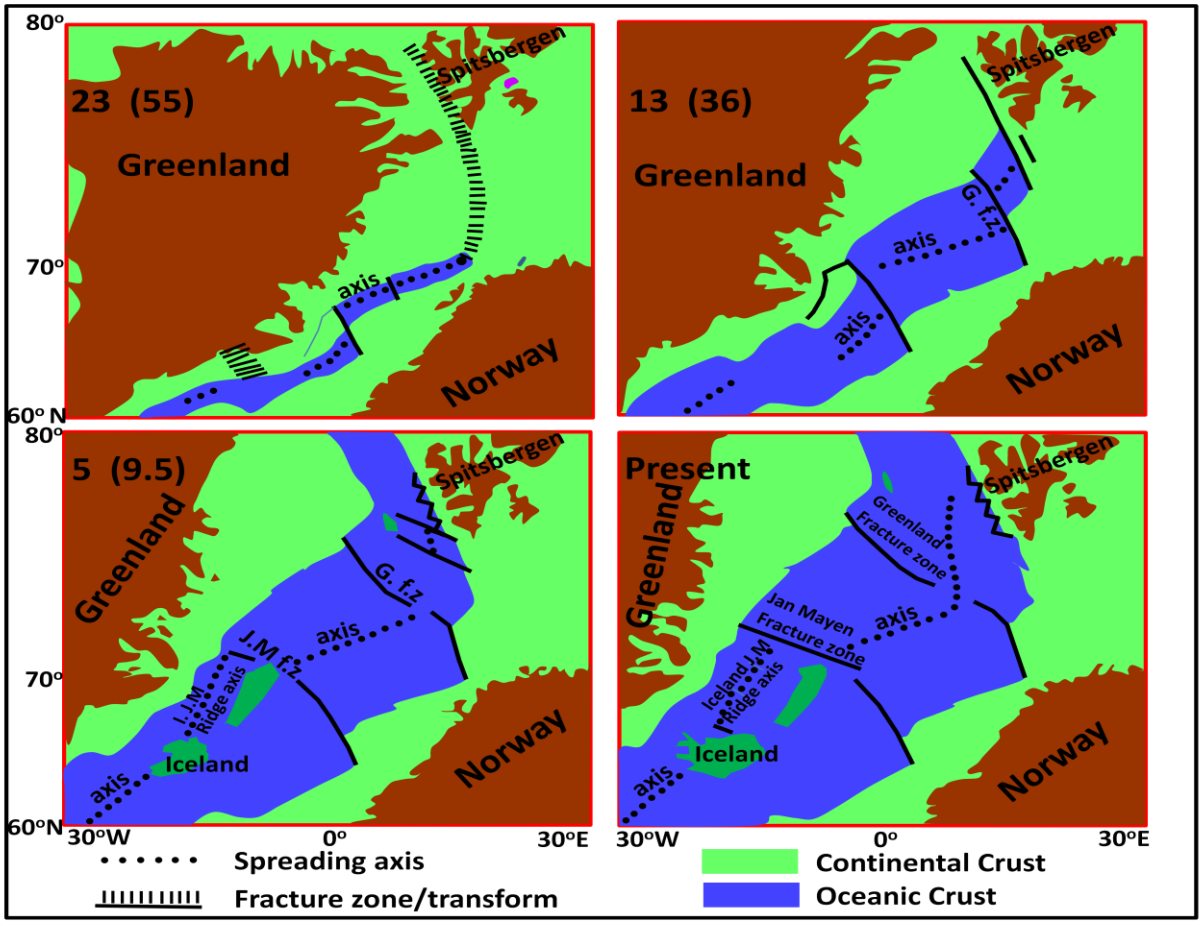

Figure 2: Evolution of Norwegian-Greenland sea (Modified from Eldhom, 1985)

This orogeny is interpreted as a product of this strike-slip movement, directly linked to the paleogene transcurrent motion in the De Geer Zone. The rifting event has been dated (57-58 Ma) on the basis of sea-floor magnetic anomalies (Sundvor, 1977; Talwani and Eldhom, 1977; Myhre et al., 1982). The tectonic development that caused the separation of Greenland from Svalbard took place later (36-37 Ma) due to change in pole rotation and plate movement (Talwani and Eldhom, 1977; Steel, 1985).

This plate boundary has been reffered as Hornsund Fault (Sundvor and Eldhom, 1979), Hornsund Escarpment (Vogt et al., 1981) and Hornsund fault zone (Myhre et al., 1982). Eldhom (1985) simplified this model of principal tectonic events (Figure 1). The mid oceanic ridge is segmented into smaller ridges namely: Jan Mayens ridge, Mohns Ridge and the Knipovich Ridge (Talwani and Eldhom, 1977) (Figure 2).

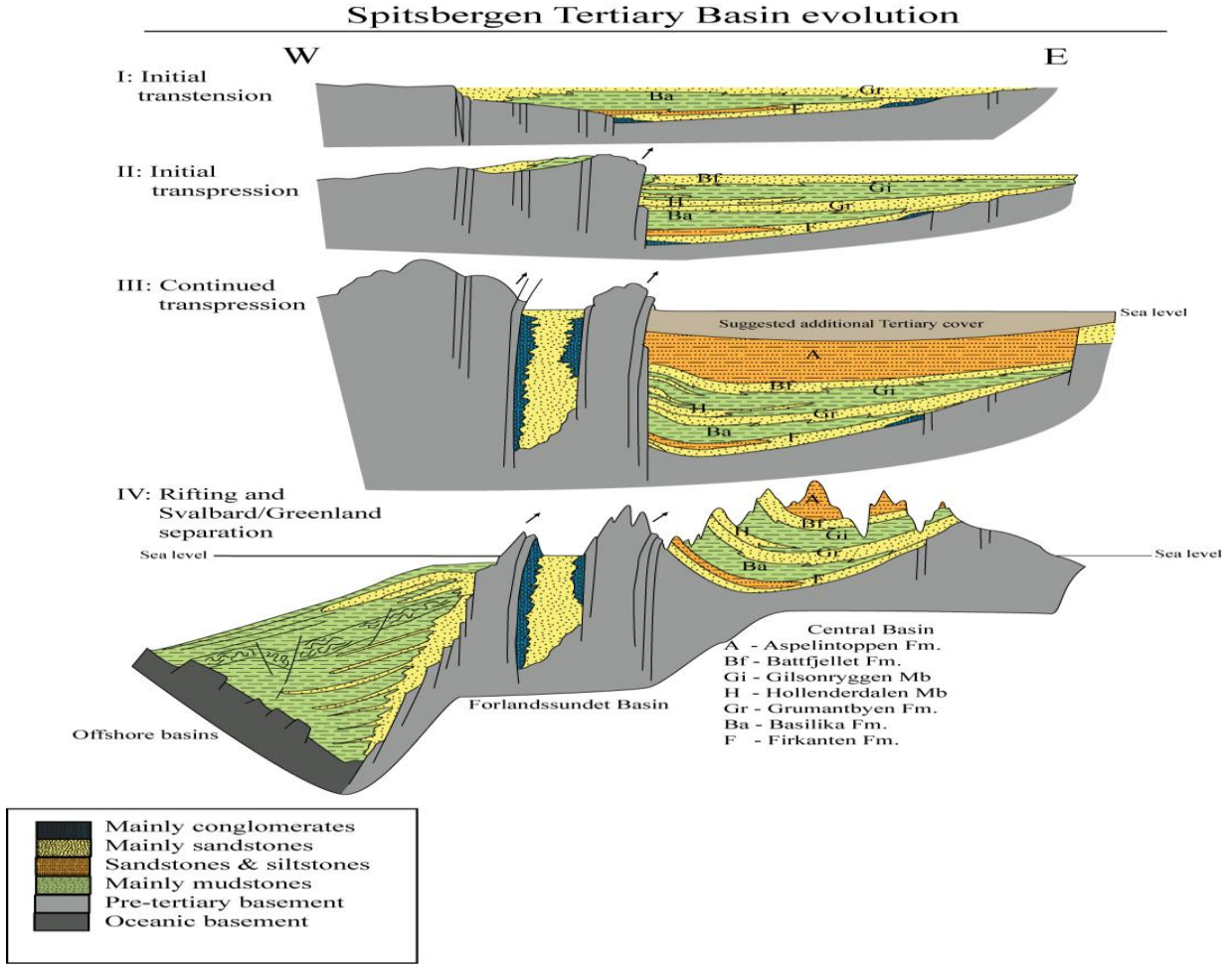

Figure 3: Paleogene depositional model for Central Basin (Modified from Steel et al., 1985; by Ribers, 2009).

Several refined and modified tectonic models were published in the coming years (e.g. Schluter and Hinz, 1978; Myhre et al., 1982; Spencer et al., 1984). The most widely accepted tectonic model for evolution of Tertiary Central Basin was proposed by Steel et al., (1981 and 1985). This interpretation was based on the study of available onshore and offshore record of sea-floor spreading, structural elements (faults) and sedimentology. The main feature of this model is that there were two discrete phases in the tectonic development. The first: an extensional tectonic setting for the early to mid-Paleocene Central Basin. To support this three evidences have been postulated: (1) considerable thickness of sedimentary strata in the basin and its thickening towards the De Geer Line; (2) presence of volcanic ash layers in Firkanten formation indicative of igneous activity during rifting (Major and Nagy, 1972); (3) Unavailability of evidence for uplift in the western part during that time . There are evidences present to suggest that a component of strike-slip was associated with this extension (Steel et al., 1985). During the second phase (Late Paleocene-Early Eocene), the tectonic regime changed to transpression (Myhre et al., 1982; Steel et al., 1985). A drainage reversal occurred and sandstones of Frysjaodden and Battfjellet formations, with a source derived from the western side of the basin were deposited. From this point onwards, the basin became a foreland basin, depressed by the loading of thrust sheets (Steel et al., 1985).

Bruhn and Steel (2003) challenged this complex transtensional-transpressional mode and presented an alternative model for Tertiary Central Basin evolution based on recent time constraints on Late Cretaceous and Paleogene seafloor spreading in Norwegian-Greenland Sea and Arctic Ocean, coupled with sedimentary data from Spitsbergen (Figure 4). The new interpretation suggests that the entire Paleocene-Eocene sedimentation in The Central Basin can be incorporated into a foreland basin setting. The Tertiary fold belt which was earlier thought to be result of strike-slip movement (Steel et al., 1985) shows minimal impact of such deformation. It is now established that it predominantly reflects compressional deformation (Helland-Hansen, 1990; Bruhn and Steel, 2003). The deposition of Paleocene sediments with an overall landward stepping trend was sourced by an eastward migrating peripheral bulge created east of the basin (Bruhn and Steel, 2003).

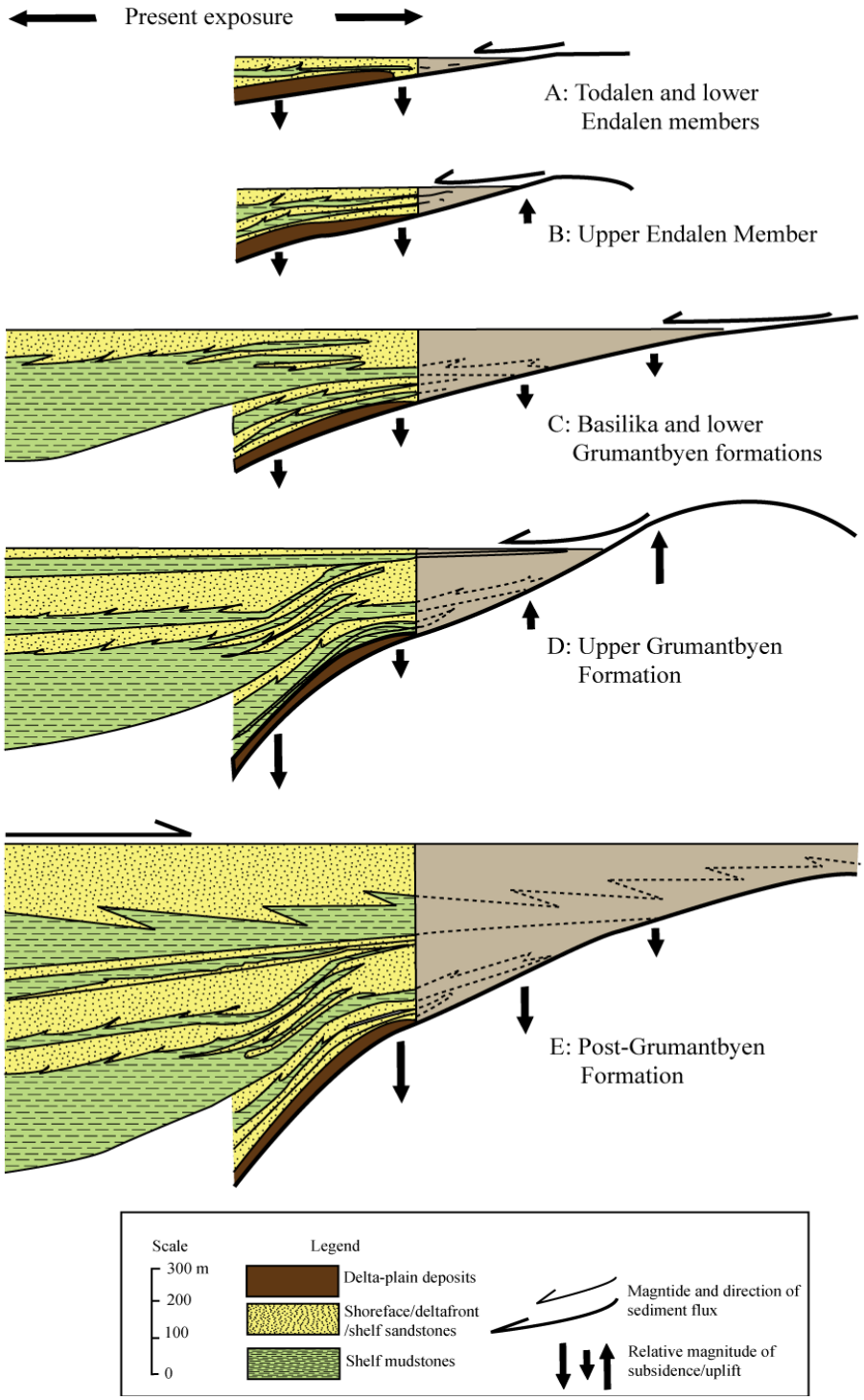

Figure 4: Development of depositional architecture (Modified from Bruhn and Steel, 2003, by Ribers, 2009).

2.3 Stratigraphic position

In Spitsbergen, Tertiary sediments are confined to mainly five depositional basins (Dallmann et al., 1999). The Central Basin, a NW-SE trending synclinorium is the largest and hosts the most complete Paleogene succession (Nagy, 2005). Cenozoic deposits have also been reported in Forlandsundet, Bellsund, Kongsfjorden and Northern Spitsbergen (Dallmann et al., 1999). The Paleogene sedimentary package has been assembled into the van Mijenfjorden Group. This group has a depositional thickness of 2100m (Bruhn and Steel, 2003) and is subdivided into seven formations: The Paleocene Firkanten, Basilika and Grumantbyen Formations and the Eocene Frysjaodden, Hollenderdalen, Battfjellet and Aspelintoppen Formations (Steel et al., 1981; Dallmann et al., 1999; Bruhn and Steel, 2003). In this study Hollenderdalen Formation is reduced to member rank. Age relationships within the group are only roughly defined due to scarcity of stratigraphically significant fossils (Nagy, 2005). The different figures are mentioned in both Figure 4 and 5.

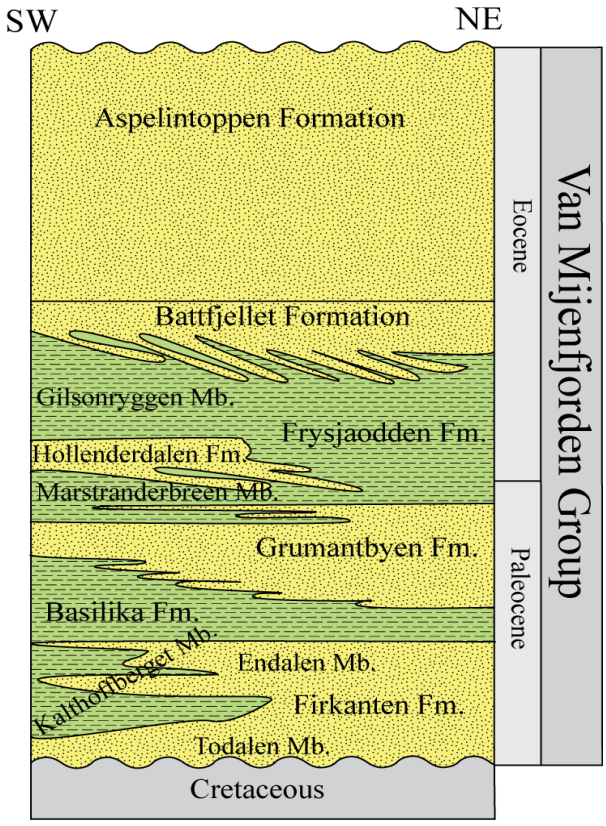

Figure 5: Paleocene-Eocene stratigraphy of Central basin (Modified from Helland-Hansen, 1992, by Ribers 2009).

2.3.1 Paleocene Stratigraphy

The Paleocene succession in the Central Basin had a clastic source area located in the east to northeast and is up to 700m thick. These sediments represent the deepest water conditions in the basin (Bruhn and Steel, 2003). It constitutes the following formations:

1. **Firkanten Formation (Figure 5):** The early Paleocene Firkanten Formation (Vonderbank, 1970; Harland, 1997) is the lower most Tertiary unit and is deposited unconformably on a low angle ravinement surface formed in the late Cretaceous (Müller and Spielhagen, 1990; Nagy, 2005). The dominant lithology is coal bearing delta plain and paralic facies (Steel et al., 1981). These terrigenous clastic sediments are interpreted as a major depositional sequence, formed in deltaic coastal plain to delta front to prodelta environment (Nagy, 2005). The deposition of Firkanten Formation was terminated by a broad regression (Kellogg, 1975). The formation is subdivided into three members:

    i. **Todalen Member (Figure 5):** This basal unit of the Firkanten Formation begins with fluvial conglomerates at the base (Müller and Spielhagen, 1990; Dallmann et al., 1999) which is interpreted as a regional unconformity (Nagy, 2005). These conglomerates are overlain by shale-sandstone-coal succession of the Todalen Member representing coastal marine to delta plain origin (Nøttvedt et al., 1985; Nagy, 2005).

    ii. **Endalen Member (Figure 5):** The Endalen Member consists of upward coarsening sandstone units which were deposited in a prograding delta front environment (Nagy, 2005). This member dominates the northern part of the basin. Bruhn and Steel (2003) have placed the maximum flooding surface in the middle of this member. Fluvial conglomerates overlie the Endalen Member (Steel et al., 1981).

    iii. **Kolthoffberget Member (Figure 5):** The Endalen Member interfingers with the Kolthoffberget Member in the western and southern part of the basin (Steel et al., 1981; Müller and Spielhagen, 1990) and consists of alternating

marine shale, siltstone and sandstone beds (Steel et al., 1985; Nagy et al., 2000). These sediments were deposited in prodelta environment (Nagy, 2005).

2. **Basilika Formation (Figure 5):** The Basilika Formation has been roughly assigned an age between early and late Paleocene on the basis of dynocyst observations (Nagy, 2005). The dominant lithology is black colored shale with an increase in silt and sand upwards (Steel et al., 1981). The lower part of this formation consists of fining upward mudstone and siltstone (Bruhn and Steel, 2003). A series of upward-coarsening units dominate the upper part of the formation (Steel et al., 1981). Anoxic environments have been proposed during the deposition of Basilika Formation on the basis of scarcity of fossils and abundance of pyrite (Müller and Spielhagen, 1990). These shales were deposited as outer shelf mud complex (Steel et al., 1981).
3. **Grumantbyen Formation (Figure 5):** This formation forms the uppermost unit of Paleocene stratigraphy in the Central Basin and consists mainly of upward coarsening sandstones (Nagy, 2005). These sandstones are matrix rich with massive character and high level of bioturbation (Müller and Spielhagen, 1990) which makes its origin problematic (Steel et al., 1981). However, these evidences point to a lower shoreface environment (Müller and Spielhagen, 1990) in which these sandstones were deposited as inner to mid shelf sand barrier complex (Nagy, 2005). Five such sandstone sheets have been observed in the norther western part of the central basin (Steel et al., 1985). The top of Grumantbyen formation is marked by the presence of conglomerates (Kellogg, 1975).

2.3.2 Eocene Stratigraphy

During the deposition of Eocene succession, the West Spitsbergen Orogeny in the west of the Central Basin provided the sediment source and these deposits form a large scale regressive unit (Bruhn and Steel, 2003). Manum and Throndsen (1986) placed the maximum flooding surface in the lowermost part of Frysjaodden Formation. The thickness of overlying Eocene strata is 1400m (Bruhn and Steel, 2003) and the formations are:

1. **Frysjaodden Formation (Figure 5):** A sharp conglomeratic horizon separates the Grumantbyen Formation sandstones and the overlying Frysjaodden Formation. This formation was deposited in a prodelta/shelf system (Steel et al., 1985). Its lithology comprises primarily shales and siltstones (Kellogg, 1975). Some irregularly shaped

conglomerates lenses exist close to the basal part (Dallmann, 1999) and exclusive turbidite deposits have been reported in the western side of the basin (Steel, 1985). The sandstones wedge of the Hollendardalen Member results in subdivision of the Frysjaodden Formation into three members (Steel et al., 1985):

i. **Mastranderbreen Member (Figure 5):** This member, an offshore marine deposit is distinguished at the localities where Hollendardalen Member exists (Dallman, 1999). This is the lowermost member of the Frysjaodden formation. These shales have accumulated in a restricted basin (Burca, 2008).

ii. **Gilsonryggen Member (Figure 5)**: The Gilsonryggen Member consists of deep marine silty shale (Steel et al., 1981; Dallmann, 1999), mudstones, and subordinate sandstones (Helland-Hansen, 1990). The sandstone interbeds in the Gilsonryggen Member are a result of turbiditic events (Steel et al., 1985*)*. An abrupt change is observed form underlying sandstones (Grumantbyen Formation and Hollendardalen Member) to the shales.

iii. **Hollendardalen Member (Figure 5):** The deposition of Hollendardalen Member is restricted to the northwestern part of the Central basin in the Nordenskiøld Land (Steel et al., 1981; Müller and Spielhagen, 1990) where it has a thickness of up to 150m. Dalland (1977) studied the formation in detail and reported this formation to consist of tidal-dominated, deltaic sandstone wedges thinning eastwards. Abundance of rock fragments and mineral cloritoid has been observed which indicates a nearby source, probably in the West Spitsbergen Orogeny (Müller and Spielhagen, 1990). In recent studies, Rüther (2007) and Burca (2008) have not been able to find any evidence of a fluvial terrestrial feeder system. They have interpreted the depositional environment of Hollenderdalen Member to be offshore transition to shoreface and foreshore, dominantly characterized by marine processes.

2. **Battfjellet Formation (Figure 5):** The formation is developed over the entire Central Basin (Steel et al., 1981) and exhibits a variation of facies type throughout the basin (Müller and Spielhagen, 1990). It consists of shales, siltstones and sandstones (Nagy, 2005) with prominent shoreline-deltafront, sheet sandstone body (Steel et al., 1981). Wave dominated sedimentary structures (e.g. hummocky cross-stratification) dominate

the lower part of the formation while predominantly current generated structures (e.g. trough and planar cross bedding) are observed in the upper part of the formation (Helland-Hansen, 1990). The Battfjellet formation was deposited in a prograding deltafront locally with coastal barrier bars (Nagy, 2005).

3. **Aspelintoppen Formation (Figure 5):** The Aspelintoppen Formation forms the top of Tertiary sucession in the Central Basin (Nagy, 2005). It consists of alternating fluvial and estuarine deposits (Steel et al, 1981; Plink and Björklund, 2006). These deposits represent the continental equivalent of the marine sediments of Gilsonryggen and Battfjellet Formation (Helland, 1990), representing the final regression in the Central Basin (Müller and Spielhagen, 1990) and were deposited in a coastal plain to delta plain system dominated by sandstones and mudstones (Nagy, 2005).

3 Paleogene Environmental conditions

The study of sedimentary archives reveals that the Earth's climate system has experienced a significant and complex evolution during much of the last 65 million years (Zachos et al., 2001). There occured swift transition in global environmental condition in early Paleogene from the extremes of a warm ice free green house, to a colder icehouse with massive continental ice sheets and polar ice caps in Neogene (Zachos et al., 2001; Moran et al., 2006). Although this conversion was previously thought to have developed gradually through the Paleogene (Savin et al., 1975), the detailed paleoclimatic information of Paleogene available through the DSDP (Deep Sea Drilling Project) and the ODP (Ocean Drilling Project) contradicted these findings. These projects were initiated during the 1970's and 1980's and this data revealed that instead of gradual developments, this transition occurred through several periods of rapid climatic changes (Kennett and Scott, 1991; Zachos et al., 1993). Tectonic processes such as the North Atlantic rifting and the isolation of Antarctic continent are proposed as the responsible forces for this large scale cooling of global climate (Zachos et al., 2001). Orbital variations in Earth's motion control the amount to solar energy absorbed, and recent evidences have proved that these cycles (The Milankovitch cycles) also contribute to the global climatic patterns (Berger, 1988) .

The initiation of The Integrated Ocean Drilling Program Arctic Coring Expedition (IODP ACEX) in August 2004 opened new horizons in understanding the paleoceanographic records and impact of Arctic ice on the Earth's climate (Moran et al., 2006). A 400m sediment core was acquired through ACEX, representing Cenozoic sediments from the Lomonosov ridge (Figure 5) in the Arctic Ocean. Based on ACEX results, Moran et al (2006) argued that tectonic changes may modify parts of planet's circulation system, but it cannot induce climatic changes to effect global cooling patterns. They suggested a bipolar model for Earth's transition of 'green house' to 'ice house', indicating a greater control of global cooling to changes in greenhouse gases in contrast to tectonic forcing.

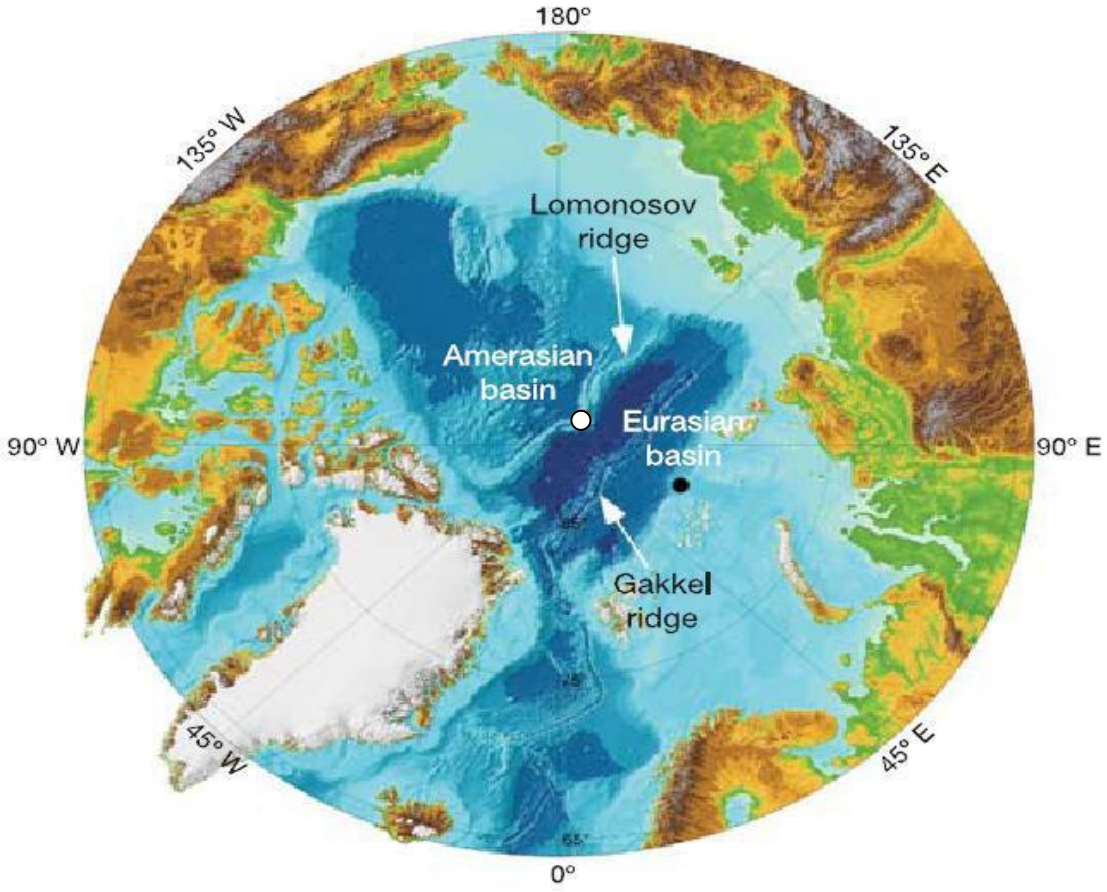

Figure 6: Present location of Lomonosov ridge (From Moran et al., 2006)

3.1 Paleocene Eocene Thermal Maximum (PETM)

The Paleocene Eocene Thermal Maximum (PETM), also referred to as "Late Paleocene Thermal Maximum" (Zachos et al., 2001) and "Initial Eocene Thermal Maximum" (Svensen et al., 2004) is the largest known climatic warming of the Cenozoic (Brinkhus et al., 2006) which occurred around 55 Ma (Kennett et al., 1991; Zachos et al., 2000; Tripati and Elderfield, 2005; Svensen et al., 2004; Brinkhus et al., 2006 Moran et al., 2006,). More recently, the age of PETM is estimated to around 56.3 Ma based on dating of Carbon Isotope Excursion (CIE) onset (Westerhold et al., 2009; Jaramilo et al., 2010; Mclnerney and Wing, 2011). Astronomical cyclostratigraphy suggests PETM duration of 150-220 ka (Röhl et al., 2003 and 2007; Aziz et al., 2008), whereas the study of extraterrestrial ^{3}He depicts a span of 120-220ka (Farley and Eltgroth, 2003; Murphy et al., 2010). There occurred a rise in temperature of the deep seas by 5-6^{o}C (Zachos et al., 2001) and surface temperatures of the Arctic Ocean increased to 24^{o}C, which was

18°C immediately before and after the PETM. This indicates that there was no ice covering the poles at that time and a lower temperature gradient existed between the poles and the equator (Sluijs et al., 2006). The onset of this event was geologically instantaneous (Cramer and Kent, 2005) and around 2000 Gt. of carbon was added to the atmosphere in a short time interval (Kennet et al., 1991; Thomas and Shackleton, 1996; Katz et al., 1999). The progress in resolving the rates and scales of Cenozoic climate change can be attributed to the development of high-resolution deep-sea oxygen (^{18}O) and carbon (^{13}C) isotope records. Kennett and Stott (1991) presented the primary evidence of PETM in terms of rapid shifts in stable carbon and oxygen ratios observed in species-specific foraminiferal carbonate from Ocean Drilling Program (ODP). Zachos (2001) compiled the oxygen and carbon isotope data for bottom dwelling, deep-sea foraminifera from 40 different locations representing various intervals of the Cenozoic (Figure 7). A negative excursion is visible in both ^{18}O and ^{13}C close to the PETM interval.

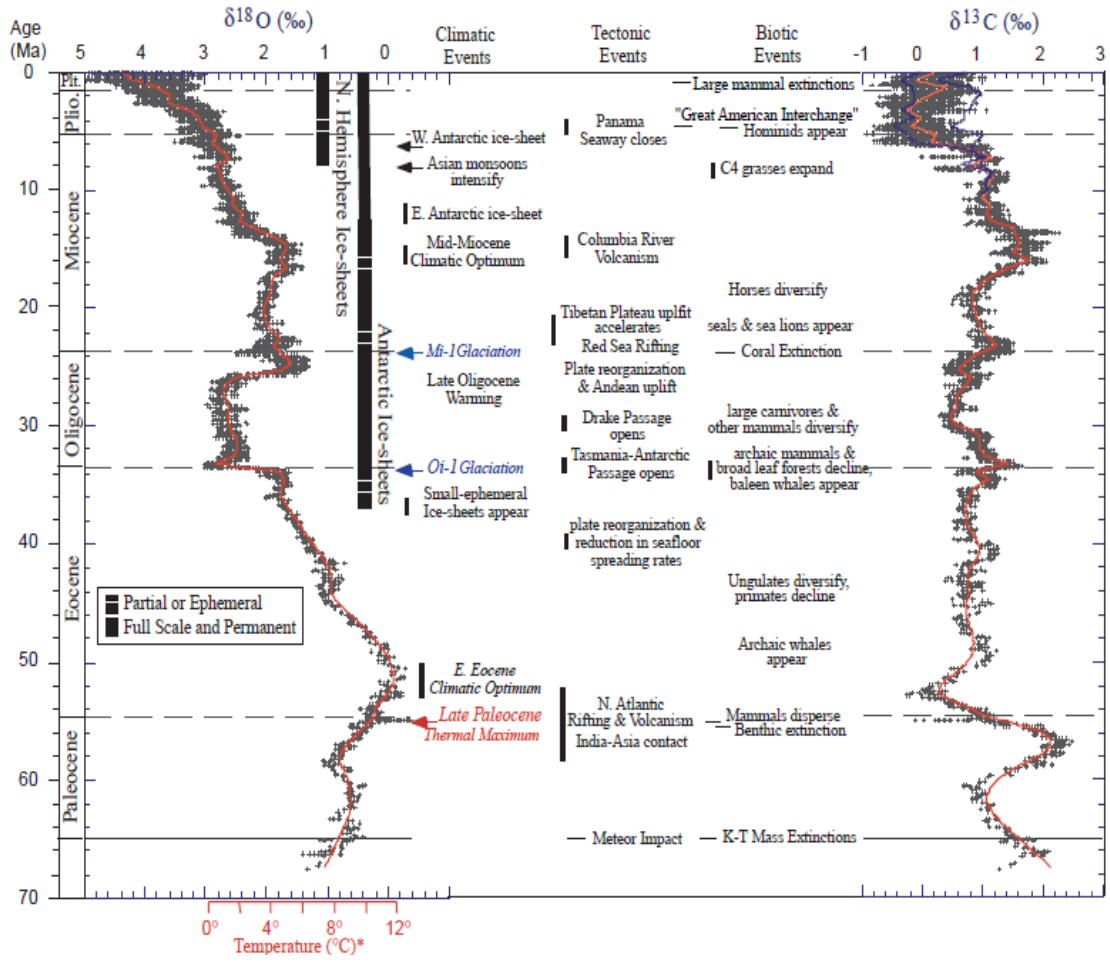

Figure 7: Isotopic oxygen and carbon excursions of Tertiary (Zachos et al., 2001)

3.2 Environmental impact of PETM

The consequence of this event was on a global scale (Zachos et al., 1993). The sedimentary succession has preserved severe repercussions of sudden increase in global temperature. A spatial variation exists in the amount of warming during the PETM (Mclnerney and Wing, 2011). The temperature increase in the Arctic (Lomonosov Ridge) was determined from biomarker paleothermometers (TEX_{86}' and GDGT) (Sluijs et al., 2006, Weijers et al., 2007). Development of photic euxinia, coincident with bottom water anoxia occurred at the PETM interval (Sluijs et al., 2006; Harding et al., 2011). This anoxia could have formed due to increased stratification of water mases as a result of increased precipitation and enhanced melting of glacial ice (Dypvik et al., 2011). Widespread evidence is present to indicate increased precipitation on the continents which caused changes in the runoff (Pagani, 2006; Mclnerney and Wing, 2011), but this precipitation did not occur in mid-latitude regions (Mclnerney and Wing, 2011). Many marginal marine sections also show an increase in kaolinite content at the Paleocene-Eocene boundary, which is a product of weathering in warm and wet climates (Robert & Kennett, 1994; Gibson et al., 2000; Bolle and Adatte, 2001). However, abundance of kaolinite probably reflects erosion of previously formed clay, rather than weathering and erosion during the PETM (Thiry and Dupuis, 2000; Schmitz et al., 2001). In a more recent study of Paleogene basin of Svalbard, Dypvik et al., has concluded that increased kaolinite content and high kaolinite/chlorite ratio are an indication of improved chemical weathering in terrestrial soils. The hypothesis of increased precipitation on land is also supported by the abrupt increase in the eutrophic dinoflagellate populations in coastal marine sections during the PETM (Crouch et al., 2001 and 2003).

Although the geographical and environmental extent of the PETM was global, no significant biotic changes have been observed in macroinvertebrate fossils (Ivany and Sessa, 2010). PETM effects on the marine ecosystem are observed entirely through microfossils study (Mclnerney and Wing, 2011). For benthic fauna, the extent of rapid changes in composition and extinction was minor at shallower depth and it occurred dominantly at middle bathyal and greater depths (Algeret et al., 2009a,b; Aref and Youssef, 2004; Thomas, 1989). Benthic Foraminifera suffered most severe extinction (30-50%) (Kennett and Stott, 1991). Planktic forams show a shift in geographic ranges during the PETM (Mclnernay and Wing, 2011). For terrestrial fossils, a burst of mammalian first species is reported at the boundary of Paleocene-Eocene (Gingerich, 1989, 2003, 2006; Hooker 1998; Rose, 1981).

3.3 Factors of climatic warming

Release of large amount of ^{13}C-depleted carbon in the atmosphere is widely accepted at the onset of PETM (Mclnerney and Wing, 2011), probably in the form of CO_2 and CH_4 (Sluijs et al., 2008). The source and mass of this carbon is unclear and widely debated. Mclnerney and Wing (2011) have listed five sources, postulated over the last two decades from different researches:

Methane Clathrates: These compounds are a potentially large source of$\delta^{13}C$ (≈60‰ $\delta^{13}C$ values) (Katz et al., 1999) and are stored in the deep sea sediments. Their destabilization through global warming (Dickens et al., 1995 and 1997) or decrease in pressure through slope failure (Katz et al., 1999) can cause massive release of methane.

Wildfires: Increase in atmospheric O_2, dryer climates and/or uplift of coal basins formed during the Paleocene could have resulted in the large scale burning of peat and coal (≈22‰ $\delta^{13}C$) values deposits (Kurtz et al., 2003). Evidence of this phenomenon was not observed in Atlantic or Pacific (Moore and Kurtz, 2008).

Thermogenic Methane: Release of tremendous amount of thermogenic methane (≈30‰ $\delta^{13}C$ values) could have occurred from magmatic injection into organic rich sediments (Svenen et al., 2004 & 2010; Westerhold et al., 2009)

Drying Epicontinental Seas: Rapid desiccation and oxidation of organic matter (≈22‰ $\delta^{13}C$ values) in an isolated epicontinental sea during the PETM could be a plausible reason (Higgins and Schrag, 2006). However drying up of shallow seas is not much documented coincident with the PETM (Gavrilov, 2003).

Permafrost: Since ice free poles are proposed in the Paleogene, enormous quantities of carbon stored as permafrost and peat in the ice caps of Antarctica could have been rapidly thawed and oxidized. Thus, releasing gigantic amounts (≈22‰ $\delta^{13}C$ values) of ^{13}C depleted carbon (DeConto et al., 2010).

Evaluating these hypotheses through mass balance calculations, Mclnerney and Wing (2011) suggested the Antarctic peat and permafrost as the most promising candidate for the carbon released at PETM and the consequent hyperthermals.

4 Materials and methods

This chapter discusses the methods used for different types of analyses done on the well cores during this master thesis. Several methods (XRD, TOC, TC, TIC, CaCO3, Thorium and Uranium analyses) have been used to elucidate the paleoenvironment of the lower Frysjaodden Formation (Gilsonryggen member), particularly the Paleocene Eocene Thermal Maximum (PETM). Materials from the sedimentological logging and sampling have been used to observe the mineralogical changes across the PETM.

4.1 Sedimentological core logging

Core logging of three wells BH 7/08 (40m), BH 9/06 (35m) and BH 10/06 (45m) was carried out in August 2010 during field trip to Longyearbyen, Svalbard. A standard logging sheet (included in appendices) was used for logging at a scale of 1:20. Store Norske Spitsbergan Kulkampani's core storage unit, situated in Gruve 6 was provided for this purpose. Units of one meter length cut and a stored in a core box which enclosed 5 such units. Observations were made using hand lens and entire length of the logged core was photographed both in general (whole core box) and close-ups of some identified areas.

BH 7/08 was logged from 95m to 55m depth, BH 9/06 from 135m to 100m and BH 10/06 from 520m to 125m by the writer and Dwarika Maharjan under the supervision of Professor Henning Dypvik and Professor Jeno Nagy, assisted by Jonathan.

4.2 Sampling

During core logging, 116 samples were collected for further investigative analyses. 29 samples were collected from BH 7/08, 42 samples from BH 9/06 and 45 from BH 10/06 by Professor Henning Dypvik and Professor Jeno Nagy with assistance from by Jonathan. The initial sample density was 1m, but samples were also collected at certain intervals on the indication of the writer and Dwarika Maharjan.

4.3 Facies description and facies analyses

Sedimentary strata in the cores have been divided into respective facies on the basis of observed structures, texture and lithology. Recognition of different facies was done through the observations of thin sections, core photos and sedimentary logs prepared during the field work. Seven facies have been recognized and Boggs (2006) classification of shales and siltstones

according to Potter, Mynard and Pryor has been followed. Successive facies representing certain depositional environments have been grouped into facies associations.

4.4 Geochemical analyses

Different geochemical analyses (Total organic carbon, Total Carbon, Total inorganic Carbon, Calcium carbonate, Uranium and Thoriu) of the rock samples have been done to aid in inferring the depositional environment of sediments, and to predict the bottom water conditions (oxic or anoxic) at the time of deposition of these sediments (Uranium and Thorium).

4.3.1 Thorium and Uranium

Different trace elements can be used as proxies for the reconstruction of paleoproductivity and paleoredox conditions (McManus et al., 1998; Tribovilard et al., 2006; Dean et al., 1997). Thus, variation in trace element concentrations in sedimentary rocks is useful for reconstruction of paleodepositional conditions (Stüben et al., 2002). Enrichment of Uranium in sediments has been used as proxy for anoxic conditions.11 samples were selected from BH 7/08 and sent to Activation Laboratories LTD (ACT LAB, Canada) for determination of Uranium and Thorium content.

4.3.2 Total organic carbon and calcium carbonate

These analyses were done at the University of Oslo and were carried out by Mofak S. Naoroz. A total of 49 samples were selected, out of which 17 samples were chosen from BH 9/06 and 16 samples each from BH 7/08 and BH 10/06 to determine the total carbon (TC), total organic carbon (TOC) and total inorganic carbon (TIC). A CR-14 Carbon Analyzer has been employed for carbon analyses (TC, TOC, and TIC). Accuracy of measured values is ±1%.

For this process, pulverized and weighed (0.35g) rock samples are treated with hydrochloric acid (HCl) to dissolve the inorganic carbon. The washed and dried residue is then heated in the instrument to 1350˚C in the presence of free oxygen, so that the carbon is released and oxidized to CO_2. This released CO_2 is measured, which give the measure of TOC. Similar procedure is repeated without HCl treatment to yield the TC. Based on these two values, TIC can be determined from the following equation:

$$TIC = TC - TOC \quad (1)$$

Assuming all the inorganic carbon to be calcium carbonate ($CaCO_3$), it can be calculated by using the molecular weights of $CaCO_3$ (Mw $CaCO_3$) and carbon (Mw C):

$$CaCO_3\ (\%) = TIC * Mw\ CaCO_3/Mw\ C = TIC * 8.333 \quad (2)$$

4.3.3 Rock-Eval pyrolysis

For this analyses, the samples (which had previously undergone geochemical analyses: TOC, TC, TIC) were sent to the Geolab Nor. in Trondheim. Rock-Eval pyrolysis was conducted on 17 samples. **7** samples were selected from BH 7/08 and 6 samples each form BH 9/06 and BH10/06 to represent the core sections.

Rock-Eval pyrolysis provides a swift estimation of potential source rock by characterizing quantity, type and thermal maturation of the associated organic matter (Espitaliè et al, 1977; Peters, 1986). The process starts by gradually heating a pulverized sample under an inert atmosphere. The free organic compounds are distilled by this heating, and then pyrolytic products are cracked from the insoluble organic matter (kerogen) (Peters, 1986). The key parameters measured in this process, are (Tissot and Welte, 1984):

S1: the amount of free hydrocarbons (gas and oil) that can be volatilized out of the rock (mg HC/gm Rock) without cracking the kerogen.

S2: the amount of hydrocarbons generated through thermal cracking of kerogen. It is measures the quantity of hydrocarbon that the rock has potential of producing if the burial and maturation continues. It gives a more realistic measure of source rock potential than the TOC, which includes dead carbon.

Production index (PI), S1/(S1+S2): generally increase with depth and coupled together with Tmax can be used as a maturation parameter.

Hydrogen index (HI), S2/TOC [HC/g Corg]: specifies the amount of hydrogen in the kerogen and provides vivid information on the potential of a rock to generate oil.

Oxygen index (OI), S3/TOC [CO2/g Corg]: indicate the amount of oxygen in the kerogen. HI vs. OI plots (modified van Krevelen diagram) can be used to determine kerogen type in the sample.

T_{max}: refers to the pyrolysis oven temperature at maximum S2 generation, and is used as a thermal maturity indicator.

4.4 Sequence Stratigraphy

Sequence stratigraphy is the recognition and correlation of changes in depositional environments represented by stratigraphic surfaces. Factors responsible for generating these changes are the interplay of sediments, erosion and oscillating base level and are determined by sedimentological analysis and geometric relationships (Embry, 2001). The T-R sequence corresponds to the orignally used T-R cycle unit (Johnson et al., 1985) and a subaerial unconformity and its correlative transgressive surface forms the boundary of this sequence (Embry and Podruski, 1998; Embry, 1998, 1993, 1995).

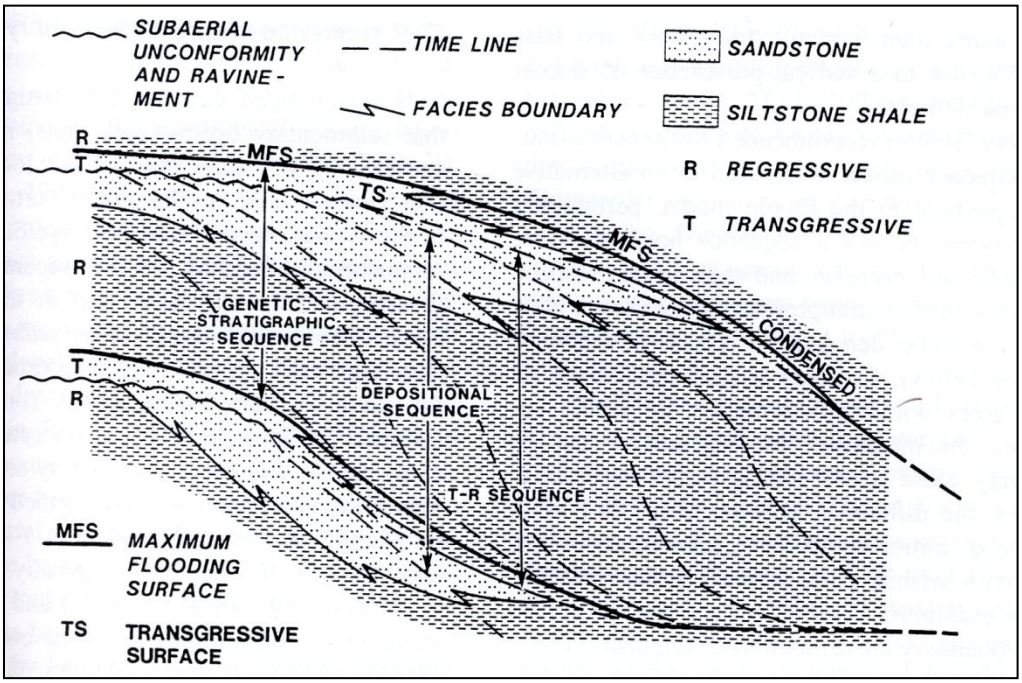

Figure 8: The Embry model, the T-R sequence (From Embry, 1993). The schematic stratigraphic section shows the boundaries of the T-R sequence compared with the boundaries of the Exxon depositional sequence and Galloway's genitic stratigraphic sequence.

A T-R sequence comprises of two systems tracts (Figure 8). The strata from the lower boundary to the maximum flooding surface (MFS) is termed as the transgressive systems tract (TST),

while the regressive systems tract (RST) constitutes strata from the maximum flooding surface to the upper boundary (Embry, 1993). The conformable surface differentiating the transgressive systems tract from the regressive systems tract is termed as the transgressive surface (Embry, 1995). The transgressive systems tract of a T-R sequence is equivalent to the transgressive systems tract of the Exxon model and the regressive systems tract of a T-R sequence is comparable to the highstand systems tract and lowstand or shelf margin systems tract of the Exxon model (Nystuen, 1998). Recognition or interpertation of Embry's T-R sequences can be done both in silt and clay dominated epcontinental basins and in sand rich, basin margin environments with distinct shelf/slope settings. In this study, Embry's T-R sequences will be used to define the sequence architecture of different formations

4.5Mineralogical and petrographical analyses

Mineralogical and petrographical analyses of collected rock samples was carried out using XRD (X-ray diffraction) analyses and optical study of thin sections.

4.5.1 X-Ray diffraction (XRD) analyses

The qualitative and semi-quantitative analyses of the minerals present in the well cores is done using bulk XRD analyses technique.

Table 1: Bulk XRD samples with depth and XRD plate number.

BH 9/06				BH 10/06				BH 7/08			
XRD no.	Depth	XRD no.	Depth	XRD no.	Depth	XRD no.	Depth	XRD no.	Depth	XRD no.	Depth
6958	104,50	6967	125,45	6975	475,55	6983	505,15	6991	57,45	6999	77,50
6959	106,73	6968	126,50	6976	479,50	6984	508,95	6992	58,80	7000	80,45
6960	109,35	6969	128,05	6977	482,35	6985	511,20	6993	59,90	7001	83,50
6961	112,20	6970	129,10	6978	485,45	6986	511,90	6994	62,25	7002	86,90
6962	115,05	6971	130,70	6979	488,50	6987	512,90	6995	66,50	7003	87,73
6963	118,00	6972	131,60	6980	492,50	6988	514,90	6996	70,40	7004	87,90
6964	118,90	6973	132,50	6981	496,85	6989	516,25	6997	72,20	7005	90,95
6965	122,50	6974	135,00	6982	501,80	6990	518,05	6998	74,80	7006	91,55
6966	123,65										

Bulk Analyses

Samples were crushed using an agate mortar to fine powder (1-2 mm) and then filled in aluminum holders using a compaction machine. These prepared samples were then run on X-ray diffractometer (XRD) for bulk analyses. B Crushing and sample preparation was done in the sedimentology lab at the University of Oslo. 49 samples were selected from the three cores, 17 samples from BH 9/06 and 16 samples each from BH 10/06 and BH 7/08 (Table 1).

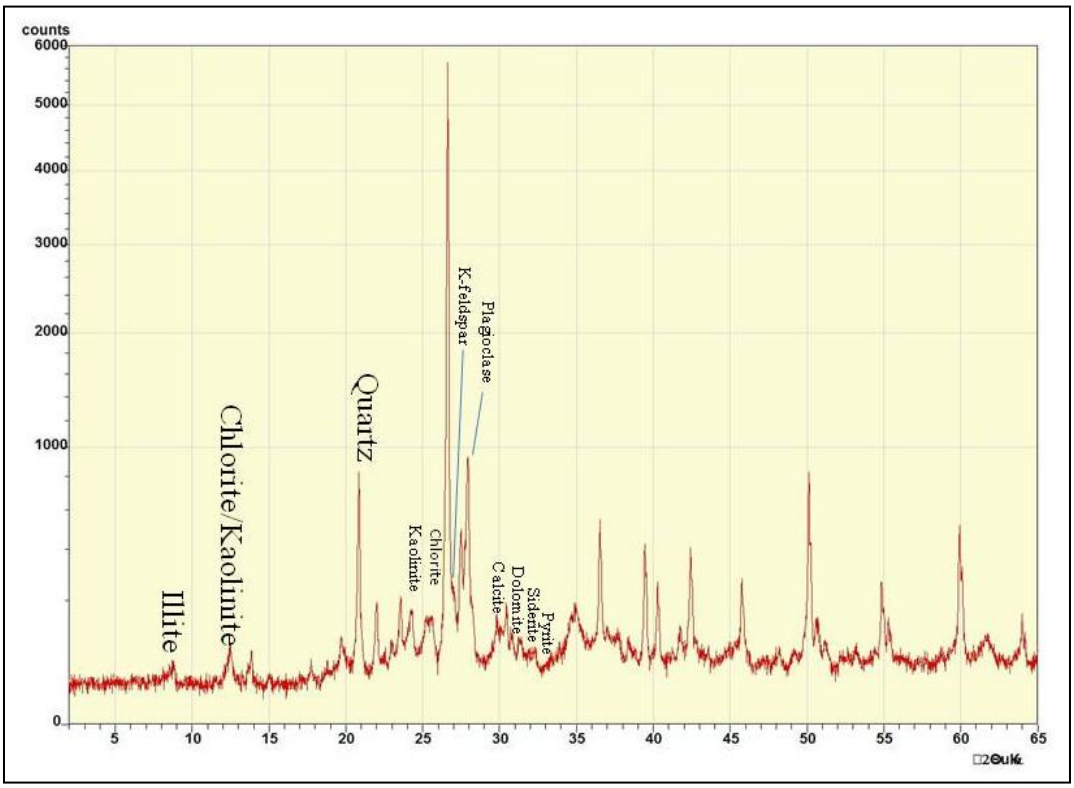

Figure 9: Diffractigram for bulk XRD analyses from 57.45m in BH 7/08 (Macdiff. Software).

Qualitative XRD analyses

The X-ray diffractometer identifies the minerals based on X-rays reflection by characteristic atomic lattice planes within the mineral crystals (Thorez, 1976). Thus, the resulting diffraction patterns enhance the basal (001) reflection and aid in identification of different minerals (Moore and Reynolds, 1989). By Xray diffractometer analyses, it is possible to analyse all the constituent minerals. Following minerals have been identified and quantified (Also shown in Figure 9).

- ***Clay minerals:***
  - *Illite:* 001 reflection identified at 10,0 Å.

- *Kaolinite/Chlorite:* The 001 reflection for kaolinite and 002 reflection for chlorite overlap at 7,00 Å. Therefore, the kaolinite 002 reflection at 3,58 Å and chlorite 004 reflection at 3,54 Å are identified and their internal ratio is applied on the reflection at 7,00 Å to obtain a semi-quantification of kaolinite and chlorite.

- ***Quartz**:* The 002 reflection at 4,26 Å is used instead of the 001.

- ***Feldspars:***
  - *K-feldspar:* The 001 reflection at about 3,24 Å is used.
  - *Plagioclase:* The 001 reflection at about 3,19 Å is used.

- ***Carbonates**:*
  - *Calcite:* 3,03 Å reflection is used.
  - *Dolomite:* 2,89 Å reflection is used.
  - *Siderite:* 2,79 Å reflection is used.

Pyrite: Reflection at 2,71 Å is used.

Semi quantitative XRD analyses

For this master's thesis, Macdiff software has been used for quantitative analyses of the bulk analyses. Maximum intensities for the representative mineral reflections were used for the semi quantification.

4.5.2 Thin Sections

Optical thin section study was done in order to support the data obtained from XRD analyses and to yield information about the texture and mineralogy of the rock samples. Small slabs of rocks were cut from the core samples and sent to the Naturhistorisk Museum for thin section preparation. Impregnation with stained epoxy was done befor thin section waer perpared.

Thin section description:

A total of 25 thin sections were prepared, out of which 9 thin sections were selected as representative of the core from BH10/06 and 8 sections each from BH7/08 and BH 9/06. The purpose of this study is to acquire detailed information of lithology, grain shape, grain size, framework configuration. Appendix 1 contains the summarized results.

Table 2: Analysed Thin sections. Point counted sections are given in italic bold.								
Core	Thin section no.	Depth	Core	Thin section no.	Depth	Core	Thin section no.	Depth
7\08	1	***57,45***	9\06	9	***100,00***	10\06	18	***479,55***
7\08	2	***70,40***	9\06	10	***112,00***	10\06	19	501,80
7\08	3	***83,50***	9\06	11	***118,00***	10\06	20	***505,20***
7\08	4	87,.73	9\06	12	***118,90***	10\06	21	511,20
7\08	5	***87,90***	9\06	13	***129,10***	10\06	22	***511,.90***
7\08	6	88,73	9\06	14	130,70	10\06	23	512,90
7\08	7	***90,95***	9\06	15	***131,60***	*10\06*	24	***514,90***
7\08	8	91,55	9\06	16	132,50	10\06	25	516,25
				17	135,00	10\06	26	***518,05***

Mineral Counting

Manual counting of the mineral content has been done to support the XRD results using a swift automatic counter. A Nikon Optiphot-Pol petrographic microscope was employed and 16 of the prepared thin sections were point-counted to 400 points using both X-Nicol and Plane Poalrized light (PPL) lenses. Mineral point counting was conducted on 16 thn sections. Appendix 3 contains the results of mineral point counting. This procedure was done in the sedimentology lab at the University of Oslo.

5 Sedimentological description

This chapter presents the results of different sedimentological analyses done during this master thesis. These include the sedimentological core logging, mineralogical and petrographical description and geochemical analyses results. Sedimentological core logs of 3 wells BH 7/08, BH 9/06 and 10/06 were collected in the last week of August 2010. Study of upper part of Grumantbyen Formation and lower Gilsonrygen Member of Frysjaodden Formation was the prime objective. In addition, Marstranderbreen Member and Hollendardalen Member were also observed in core BH 7/08 and BH 9/06. The sedimentological features identified on the basis of field logs, supported by photographs will be presented in this sub chapter.

5.1 Facies description

This chapter presents the main characteristics of the seven identified facies. The results have been summarized in Table 3 and Figure 13.

i. Highly bioturbated sandstone/siltstone (Figure 10b-11c)

The highly bioturbated sandstone facies is observed in all three cores BH 7/08, BH 9/06 and BH 10/06. Sandstones of Grumantbyen Formation and Hollendardalen Member contain this facies. This facies is characterized by the high levels of bioturbation evident from intense burrowing and has resulted in complete destruction of sedimentary structure. These sandstones are fairly well sorted with occasional rip up mud clasts and chert concretions.

In BH 7/08, two upwards finning units (95,00-94,55m, 94,45-93,70m) of Grumantbyen Formation represent this facies. It consists of silty sandstone of very fine size in which bedding and other sedimentary structures are completely destroyed by heavy bioturbation.

Similarly, in BH 9/06 this facies is observed in two sandstone units of Grumantbyen which are fining up (135,00-132.10m and132.00-128,80m). High levels of bioturbation has occurred resulting in intensive burrowing. Plant fragments and rip-up clast are regularly encountered.

This facies is present in BH 10/06 in the form of two upwards finning and one smaller upwards coarsening unit (520,00-513,00m).The Hollendardalen member is not present in this core. This sandstone displays similar characteristics as the other two sections with burrows and Chert concretion present in this sandstone.

Table 3: Sedimentary facies in cores BH 7/08, BH 9/06 and BH10/06

Facies No.	Facies	Grain Size	Physical/biological structures	Occurence	Figures
(i)	Highly boiturbated Siltstone / Sandstone	Silt to very fine sand	Heavy bioturbation, bedding absent, well sorting, plant fragments, burrows, rip up mudclasts, chert.	**7/08:** 95,00-94,55m . 94,45-93,70m **9/06:** 135,00-132.10m . 132,00-128,80m **10/06:** 520,00-513,05m	10b-11c
(ii)	Plane parallel laminated Sandstone	Silt to very fine sand	Parallel laminations, bioturbation absent or low, moderate sorting, pyrite concretions	**7/08:** 90,60-90,35m . 89,70-89,40m **9/06:** 121,10-119,10m . 118,50-116.20m	10f
(iii)	Low angle ripple laminated Sandstone	Very fine sand	Ripple marks, moderate bioturbation	**7/08:** 90,95-90,15 . 90,00-89,70m . 89,40-88,20m **9/06:** 122,70-121,10m . 120,10-119,40m . 119,10-118,50m .	11b
(iv)	Laminated siltstone	Clay to silt	Liminated shaly siltstone, moderate bioturbation,	**9/06:** 128,75-127,50m **10/06:** 513,00-511,40m	10d
(v)	Conglomerate	Pebble to Gravel	Well rounded to subangular grain,average framework is grain supported, matrix content increses at places.	**7/08:** 94,55-94,45m . 93,70-91,55m . 90,15-90,00m **9/06** 132,10-132,00m . 128.80-128,75m . 126,50-126,35m . 119,15-119,10m **10/06** 513,05-513,00m	10c-10e
(vi)	Claystone	Clay to silt	Light grey color, moderate bioturbation, moderate to poor sorting, pyrite and siderite present, lamination absent.	**7/08:** 91,55-90,95m . 88,20-85,10m . 79,10-75,90m **9/06:** 127,50-126,50m . 125.10-122,70m . 16.20-115-60m . 112,25-110,10m. **10/06:** 511,40-509,50m . 484,60-475,00m	9c
(vii)	Clayshale	Clay	Parallell lamination, bioturbation absent or low, moderate sorting, minor silty sequences,siderite layers and pyrite present. plant fragments,slikensides.	**7/08** 85,10-79,10m . 75,90-55,00m **9/06** 126,35-125,10m . 115,60-112,25m . 110,10-100,00m **10/06** 509,47-484,60m	11d-11e and 9b

ii. Plane parallel laminated sandstone (Figure 11f)

Very fine grained parallel laminated sandstone facies is present in BH 7/08 at level 90,60-90,35m and 89,70-89,40m. This non bioturbated unit belongs to the lower and middle parts of Hollendardalen Member.The sandstone units present in this facies are moderate to well sorted. Core BH 9/06 also contains this facies in the Hollendardalen Member at the middle and upper levels (121,10-119,15).

iii. Low angle ripple laminated sandstone (Figure 12b)

Low angle ripples are observed in the Hollenderdalen member present in the two cores BH 7/08 and BH 9/06. Three units (90,95-90,15m, 90,00-89,70m. 89,40-88,20m) which are moderately bioturbated and very fine grained are present in BH 7/08. Bioturbation levels are negligible in these units. Four successions of relatively clean sand appear in BH 9/06 characterized by ripple laminated sandstone. Coal fragments are also scattered in these sandstones.

iv. Laminated siltstone (Figure 11d)

A laminated siltstone, 1m thick (128,50-127,50m) is present at the base of Marstranderbreen Member in BH 9/06. This siltstone contains Planolities plant fossils and low bioturbation. In BH 10/06, a finig up sequence containing two siltstone units display the characteristics of this facies at levels 513.00-511,40m. These units represents a gradual transition form the underlying sandstone of Grumantbyen Formation to the overlying shales of Gilsonryggen Member.

v. Conglomerate (Figure 11c-e)

Two different types of conglomerates have been observed during core logging. Rounded pebble sized conglomerates with varying composition and larger gravel sized subangular conglomerates with relatively high amount of matrix content. Both types have been grouped together into conglomerates facies. These conglomerates are mostly clast supported.

The top Grumantbyen conglomerate forms a thick unit in BH 7/08 (93.70-91.55m). A 10cm thick conglomerate layer is also present separating two beds of Grumantbyen Formation (94,55-94,45m). The Hollendardalen Member in BH 7/08 also contains a 15cm thick conglomerate layer (90,15-90.00m). In BH 9/06, this facies marks the top of Grumantbyen Formation with a 5cm

thin layer (129,80-128,75m). A thicker 15cm layer is found in the Marstranderbreen Member at interval 126,50-126,35m. One such layer is also present within the Hollenderdalen Member (119,15-119,10) in this core . A prominent pebble sized conglomerate with a non-erosional base marks the top of Grumantbyen sandstone in BH 10/06 (513,05-513,00m).

vi. Claystone (Figure 10c)

This facies has been characterized by absence of lamination and its light grey color. Moderate bioturbation has been noticed within this facies..

The entire thin unit of Marstranderbreen Member in BH 7/08 constitutes the claystone facies (91.55-90.95m) which forms an upwards finning sequence. This unit is bounded by the Grumantbyen conglomerate at the base and Hollendardalen Formation is present at its upper boundary.This facies reappears twice: as another finning up unit close to the base (88,20-85.10m) and as a homogenous clay unit in the middle (79,10-75,90m) of Gilsonryggen Member. In BH 9/06, this facies is present at the lower middle part of Marstranderbreen Member (127,50-126,50m, 125,10-123,20) and within shales of Gilsonryggen Member (112,25-110,10m) in the form of a coarsening up unit. The presence of this facies has been noticed in BH 10/06 in the 110cm shale interval present at the base of Gilsonryggen Member (511,40-509,50m) and in its upper part also (484,60-475,00m).

vii. Clayshale (Figure 10b)

All three cores contain the clayshale facies in the Gilsonryggen Member shales. This shale is parallel laminated can be recognized by its dark grey color. High pyrite content is present in some intervals along with some sidrite rich zones. Two intervals in BH 7/08 (85,10-79,10m) and 75.90m-55.00m), a large homogenous interval in BH 10/06 (509,47-484.60m) and three smaller units in BH 9/06 (126,35-125,10m, 115,60-112,25m, 110,10-100,00m) show characteristics of this facies. These shales are generally well sorted with some disturbances due to increase in silt content at certain intervals.

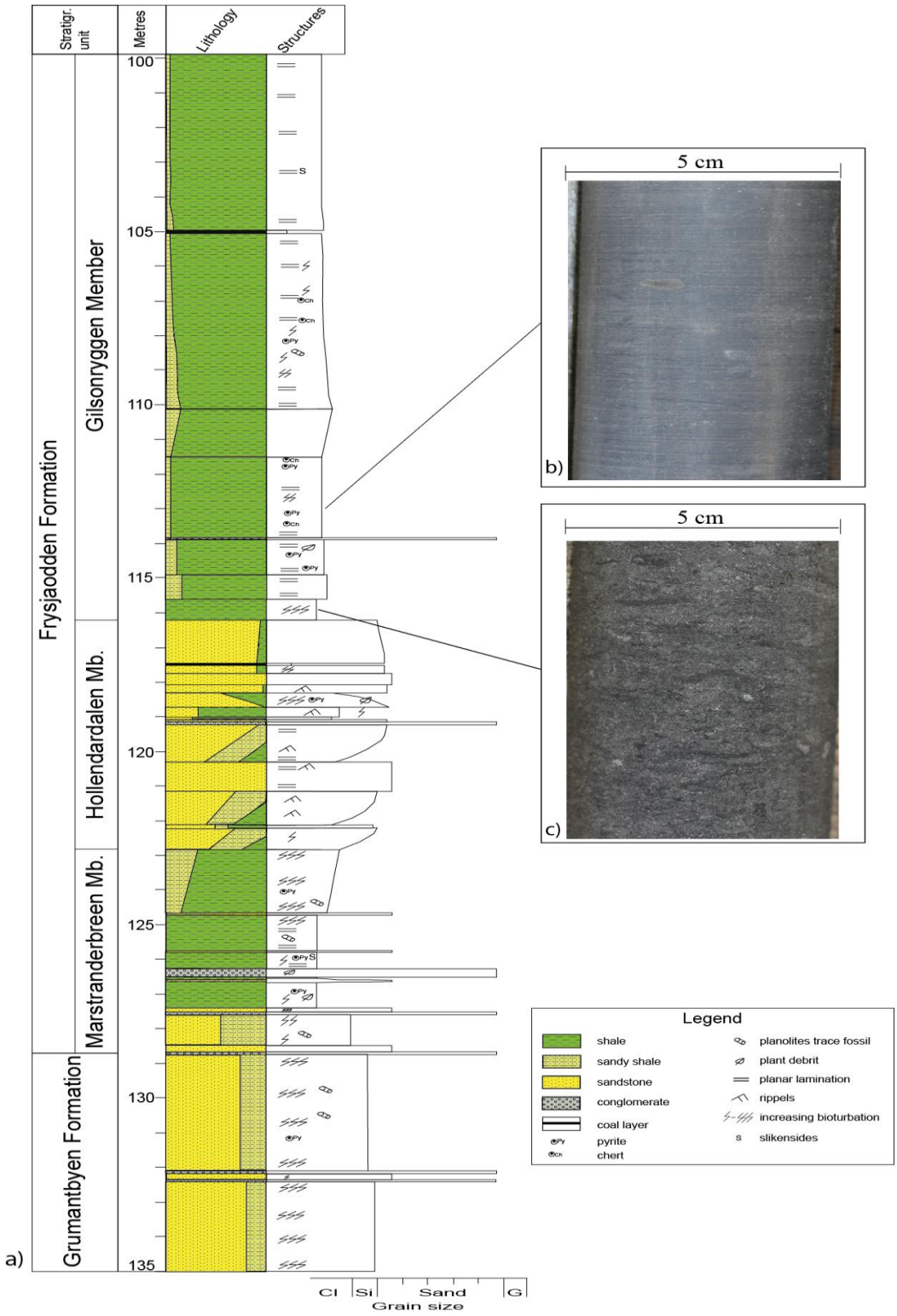

Figure 10: a) Sedimentological log of core BH 9/06 showing lithology and observed sedimentary structures. b) Clayshale at level 113,35m with pyrite concretion. c) Claystone at level 115,70m.

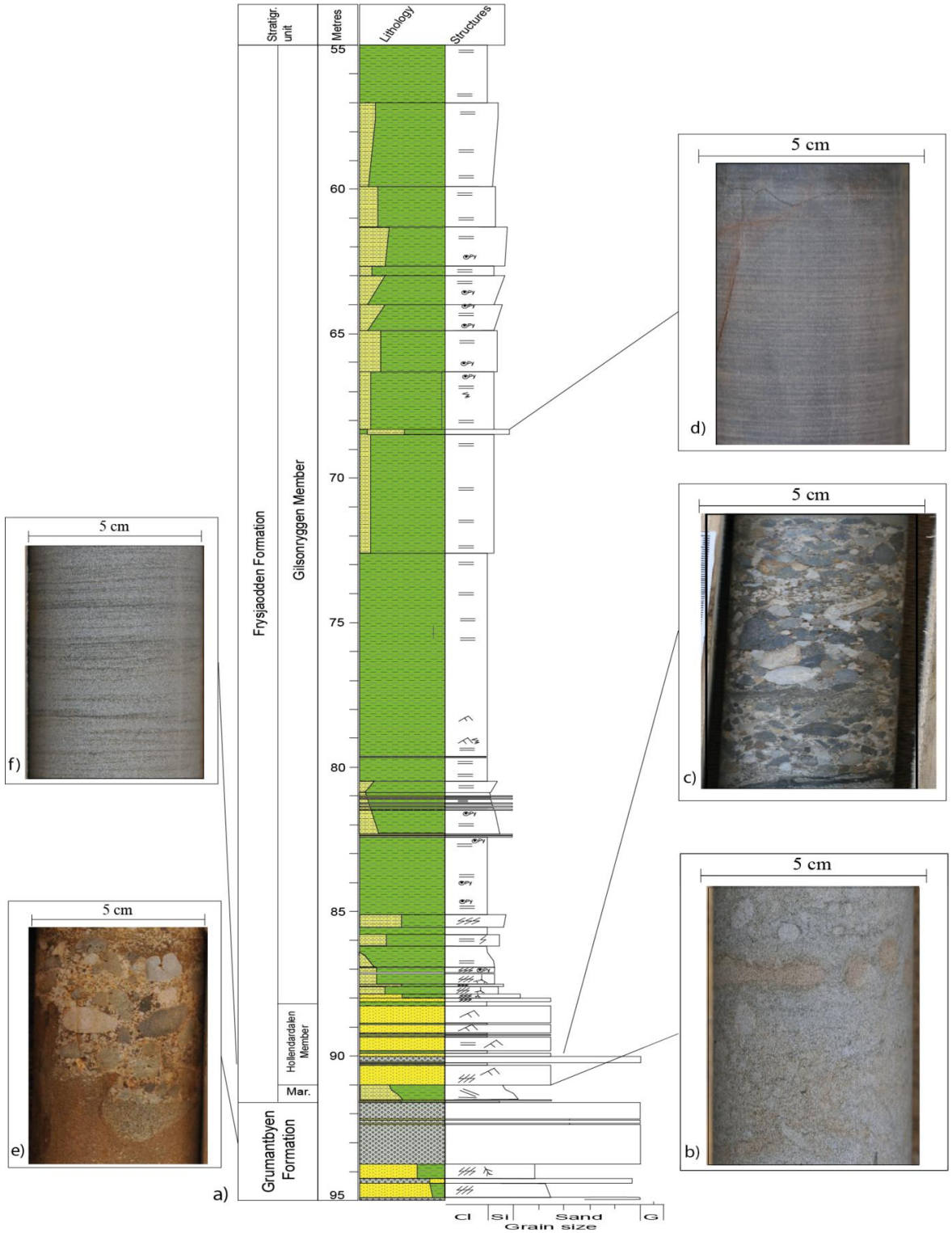

Figure 11: a) Sedimentological log of core BH 7/08 showing lithology and observed sedimentary structures. b) Bioturbated sandstone at level 90,90m. c) Conglomerate layer at level 90,25m. d) laminated siltstone at level 67,49m. e) Conglomerate layer at level 94,50m. f) Parallel laminated sandstone at level 88,60m.

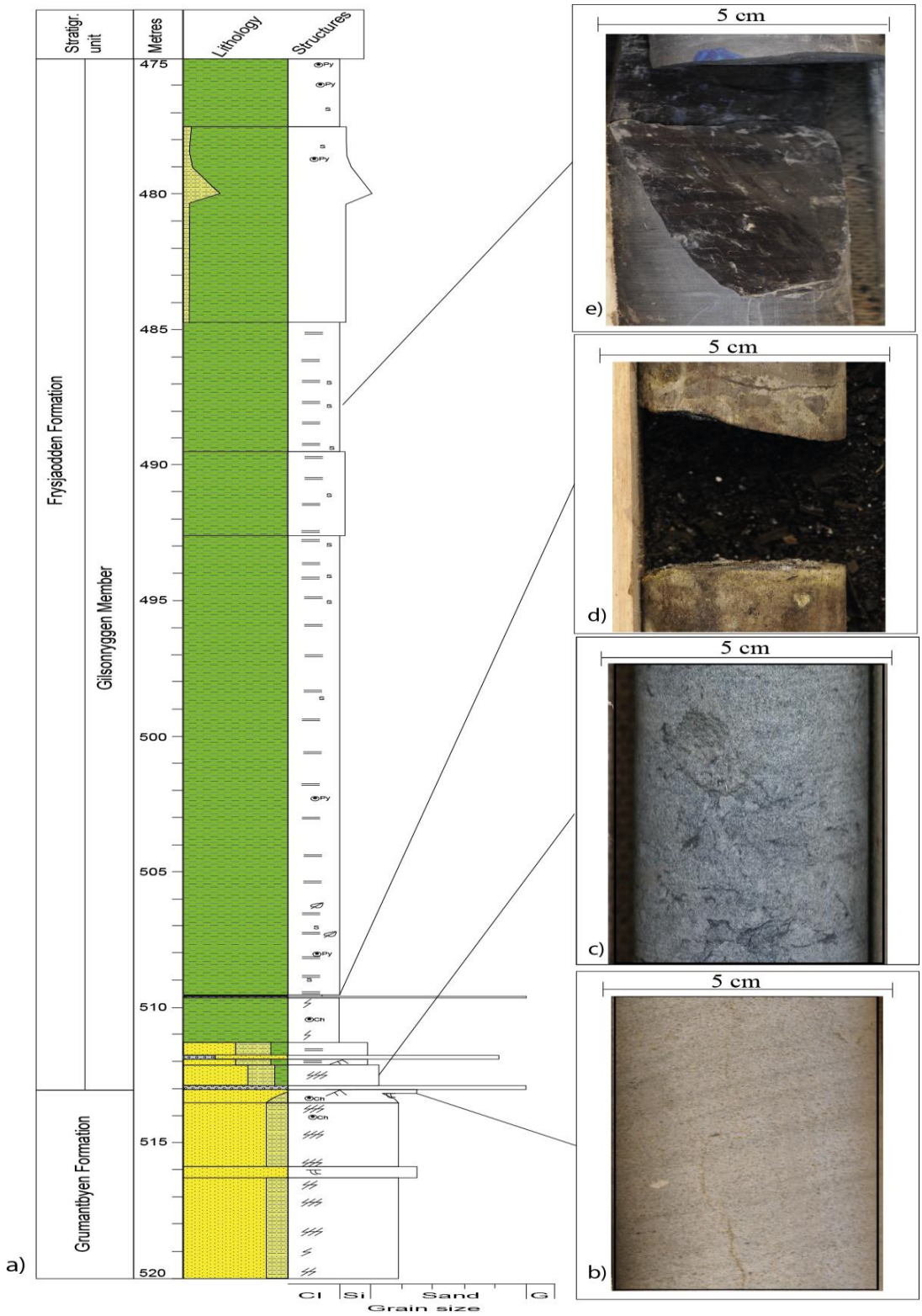

Figure 12: a) Sedimentological log of core BH 9/06 showing lithology and observed sedimentary structures. b) Low angle ripple laminated sandstone at level 513,40m. c) Highly bioturbated siltstone at level 512,40m. d) Plant fragment (black) at level 509,65m. e) Slicken side at level 488.10m.

5.2 Facies associations

- **FA1:** Sandstone of upper Grumanttbyen Formation (Figure 13)
    - *Highly bioturbated sandstone (i), Ripple laminated sandstone (iii), Conglomerates (iii)*
- **FA2:** Shales of Marstranderbreen Member (Figure 13)
    - *Laminated siltstone (iv), Claystone (vi), Clay shale (vii), Conglomerates (v)*
- **FA3:** Sandstone of Hollendardlaen Member (Figure 13)
    - *Highly bioturbated sandstones (i), Parallel laminated Sandstones (ii), Low angle ripple laminated sandstone (iii). Conglomerate (v)*
- **FA4:** Shales of lower Gilsonryggen Member (Figure 13)
    - *Claystone (vi), Clayshale (vii,) Laminated siltstone (iv)*

5.2.1 FA1: Upper Grumantbyen Formation sandstone association

This facies association embodies the lowermost part in all three cores. It includes highly biturbated sandstone facies (i). These sandstone units form two upward finning sequences in BH 7/08 and BH 9/06, while two thick homogenous silty sandstone units overlain by one thin coarsening up sand sequence containing ripple laminations (iii) has been observed in BH 10/06. A conglomerate layer (v) representing the transition between the Grumantbyen Formation sandstones and the overlying Gilsonryggen Member (BH 10/06) or Marstranderbreen Member shales (BH 7/08 and BH 9/06) marks the top of Grumatbyen Formation in all three cores.

5.2.2 FA2: Shales of Marstranderbreen Member

The Marstrandebreen Member is represented by a thin (50cm) claystone unit in BH 7/06. This member begins with laminated siltstone (iv) interval (128,50-127,50m) in BH 9/06 which is moderately bioturbated overlying the top Grumantbyen Formation conglomerate. This member then shows finning up into alternating claystone (vi) and clayshale units (vii) before ending in a coarsening up shaly sequence. A conglomerate layer (v) is also present in this member.

5.2.3 FA3: Hollendardalen Member sandstone

This facies association consists of ripple laminated and moderately bioturbated sandstone (iii) in the lower part of Hollendardalen member (BH 9/06). Alternating units of parallel laminated sandstone (ii) and ripple laminated sandstone are found in the middle of this member. An upward

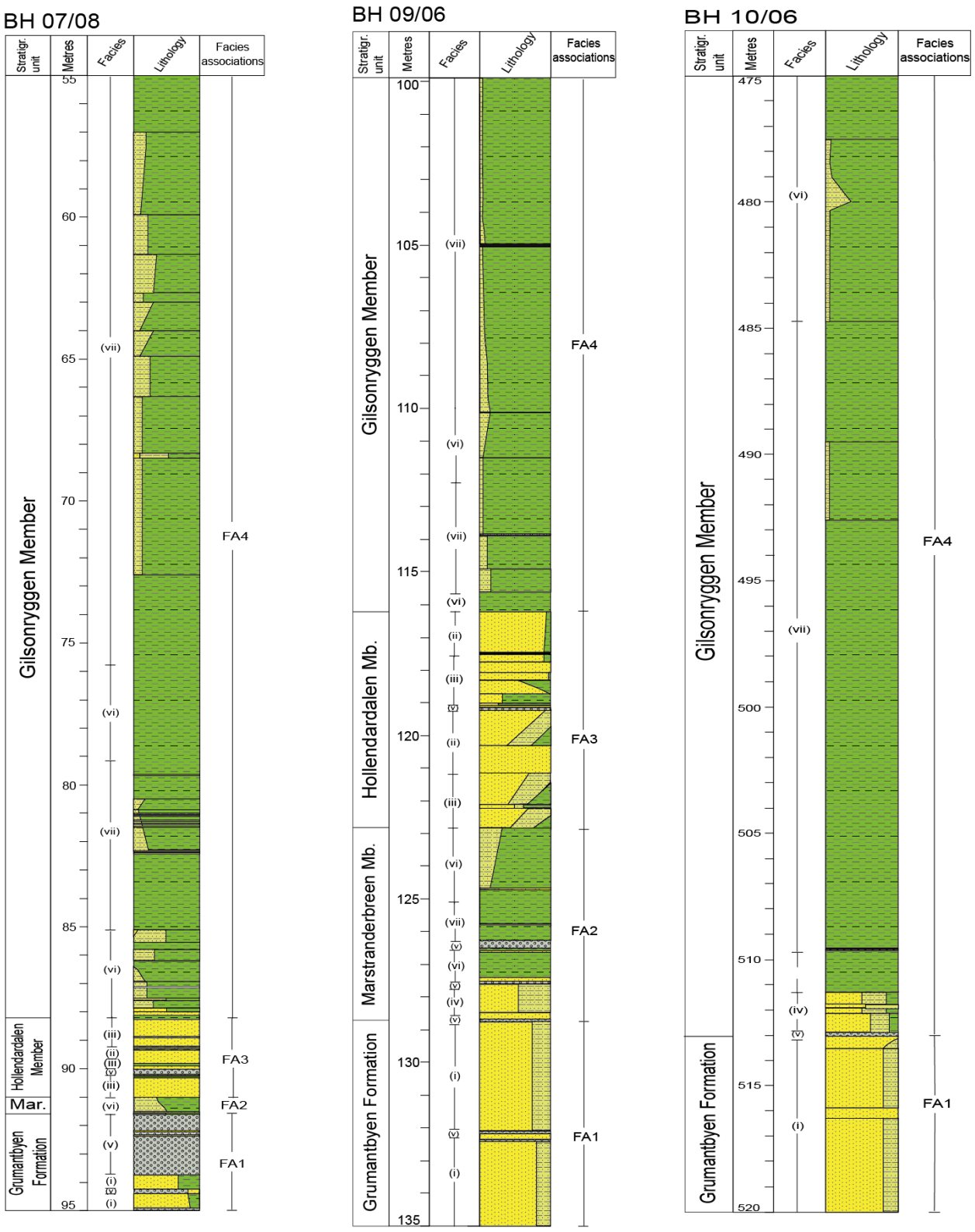

Figure 13: Facies and Facies association of core BH 7/08, BH 9/06 and BH 10/06

finning unit of highly bioturbated sandstone (i) has been observed at the upper middle level containing wood fragments. A thinner Hollendardalen member is present in BH 7/08 (Figure13) with heavily bioturbated sandstone in its lowest part. Other facies recognized in this member are low angle ripple laminated sandstone, parallel laminated sandstone and a thin conglomerate layer.

5.2.4 FA4: Shales of Lower Gilsonryggen

Shales of the lower Gilsonriggen Member begin with small finning upward laminated siltstone (iv)overlying the conglomerate of upper Grumantbyen Formation in BH 10/06 (Figure 13), while clayshale (vii) and claystone (vi) intervals exist at the basal parts of Gilsonryggen Member in BH 7/08 and BH9/06 respectively (Figure 13). The shale gets homogenous and laminated towards shallower depths. Relatively coarser quartz and feldspar grains are scattered in clay matrix. Lower parts of Gilsonryggen Member shows moderate to low bioturbation tracks. Pyrite and siderite is present in large amount towards the middle part of this member, both in the form of formaboids and continous layers.

6 Mineralogy and Petrography

The results from mineralogical and petrographical description will be presented in this sub chapter. These observations were carried out by thin section studies and XRD analyses, according to the procedure explained in chapter 4.

6.1 Thin section analyses

This sub chapter will present the results of thin section analyses. Lithological characteristics and petrographical properties of the formations will be presented together.

6.1.1 Sandstones of Grumantbyen Formation:

Thin sections of this formation were observed from cores BH 9/06 and BH 10/06. Five thin sections were studied from BH 9/06 and four from BH 10/06 including a thin section of the conglomerate at top of the Grumantbyen Formation. These conglomerates have a non erosive boundaries both at the top and bottom.

In general, the upper Grumantbyen Formation consists of very fine grained sandstone which is devoid of sedimentary structures due to high levels of bioturbations (Figure 14a). These sandstones also contain some silt content in them. The framework is majorly grain supported and clay matrix is present in between the sand grains. Grain shape varies between subangular to angular. Concave o convex and long grain to grain contacts are commonly identified between the grains with some tangential contacts. Tiny fractures have been observed within in the grains. Porosity of these sandstones is low because the sand grains are packed with clay and few pores are observed with no interconnection between them (Figure 14b). From point counting, quartz appears to be the dominant mineral in samples from BH 10/06 (Appendix 3). However, feldspar dominates the two thin sections from BH 9/06. This difference is probably due to the position of samples in the two cores. Quartz is mostly monocrysralline but several polycrystalline quartz minerals are also present. Quartaz overgrowth has also been noticed, although not in large quantities. Little alteration of feldspar into clay minerals has occurred in both core sections. Among the micas, muscovite is dominant and appears randomly oriented in the thin sections. Larger flakes of mica are deformed between the sand grains. Mudclasts are also visible in some thin sections (Figure 14 c). Low quantities of organic matter are present and fossils are scarce. The mineral glauconitie is present in considerable quantities (3% in mineral counting) and is

frequently observed in the sections. Chlorite and some heavy minerals were also encountered during the analyses.

a)

b)

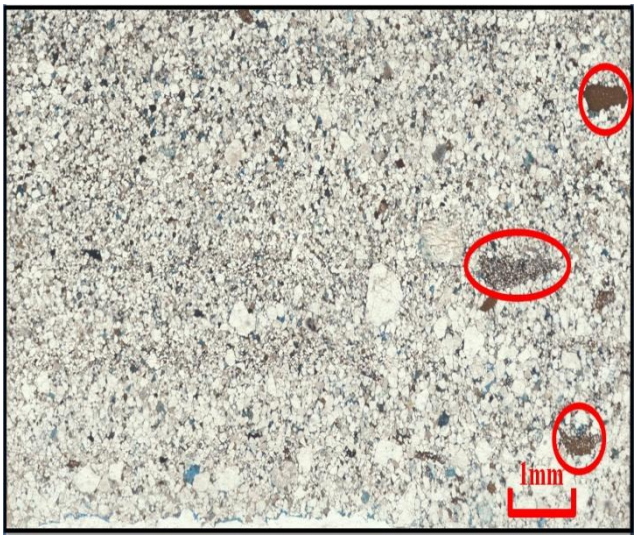

c)

Figure 14:Thin sectin scanned pictures a) Highly bioturbated sandstone, tracks marked with brown lines (516,25m, BH 10/06). b) Low porosity(blue) visible in sandstone (135,0m, BH 9/06). c) Three examples of mudclasts marked with red circles (514,90m, BH 10/06).

The top of Grumantbyen Formation sandstone is overlain by a conglomerate layer in BH 10/06. This conglomeratic horizon is the transistional zone between Grumantbyen Formation and overlying Gilsonryggen Member. These conglomerates have an erosional base with the

underlying sandstone The average grain size is medium. This unit is poorly sorted as it contains pebble size grains (seven) in it. The matrix of this zone contains angular grains of chert, feldspar and quartz. Glauconite is present and mud clasts are also observed in this core.

6.1.2 Hollendardalen Formation siltstone/sandstone

Two thin sections have been studied from this formation in BH 9/06. First thin section is from the clay rich unit (118.90m). The framework of this thin section is matrix supported with well sorting. Illitic clay is present. Bioturbation is moderate and very little lamination is preserved at this level (Figure 15a). Organic matter is scattered throughout the thin section but in low quantities.

The second thin section belongs to the very grained fine sandstone in the upper part of the Hollendardalen Member. This unit is moderately bioturbated and some lamination is also preserved (Figure 15b). The grain size is very fine with sub angular to angular grains and moderate sorting. Mineral counting results show quartz to be the dominant mineral which mainly consists of monocrystaline quartz. Alternating intervals of fine grained and coarse grained beds are present. Clasts of clay are observed in and presence of glauconite is also noticed in this thin section.

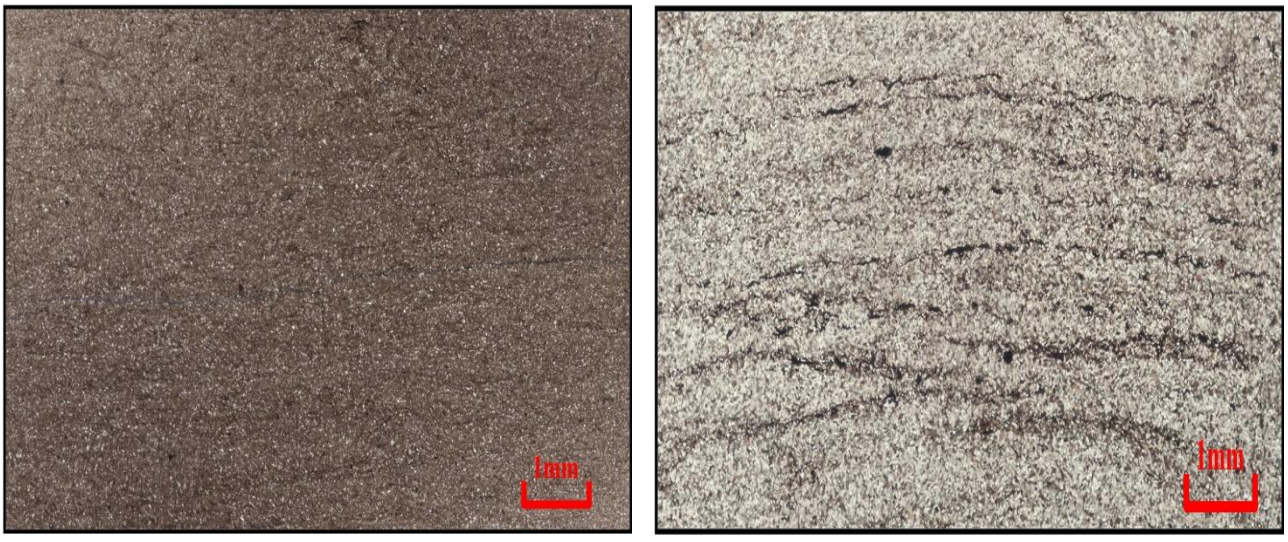

a) **b)**

Figure 15: Thin sectin scanned pictures. a) Clay rich homogenous unit with low bioturbation (118,90m BH 9/06). b) Moderately bioturbated sandstone with some lamination preserved (118,0m, BH 9/06).

6.1.3 Lower Gilsonryggen shales

Shales of the lower Gilsonryggen member have been studied through twelve thin sections. Five thin sections from BH 7/08, two thin sections from BH 9/06 and four thin sections were selected from BH 10/06 to represent the Formation.

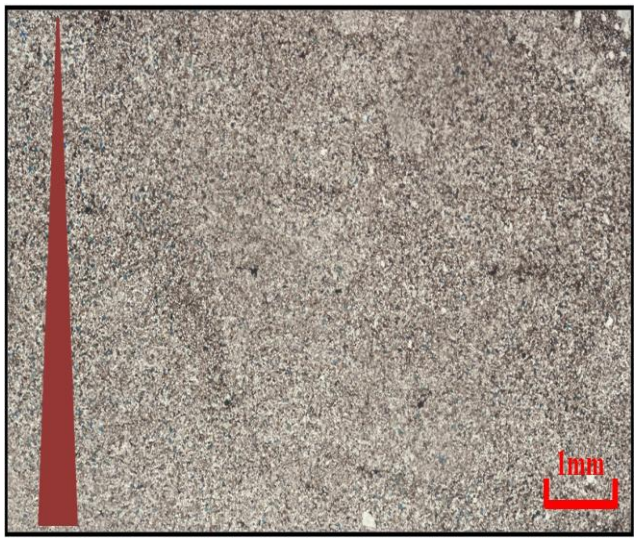

a)

b)

c)

Figure 16: a) Thin sectin scanned pictures.Upwards finning silt (511,90m, BH 10/06). b) Dispersed quartz and feldspar grains in clay with some bioturbation tracks (505,15m BH 10/06. c) Dark color shale with organic matter and pyrite formaboids (118,90m BH 9/06).

The Gilsonryggen member is overlying Hollendardalen Member in two cores (BH 7/08 and BH 9/06) and Grumantbyen Formation in BH 10/06. In all three cores, the transistion occurs from sandstones to shales through upwards finning silty units (Figure 16a). In general, the shales of lower Gilsonryggen Member display a matrix supported framework with alternating silty and shaly beds at the base. Moving up, the clay gets homogenous and laminated. On average, more than 60% of the thin section consists of dark brown to black color clay matrix. Quartz and feldspar grains are observed dispersed in the matrix (Figure 16b). Besides the matrix, other non-clay mineral observed is pyrite in the form of framboids and bands (Figure 16c). Moderate bioturbation has been noted in some thin sections. Small amounts of organic matter have also been identified.

6.2 X-Ray Diffraction (XRD) analyses

This subchapter presents the results of XRD analyses. Bulk analyses was carried out and both clay and non-clay minerals have been identified and semi-quantified. The purpose of this analyses is to study the mineralogical variation across the studied cores. Method of simple peak height percentage calculation of each mineral was employed for semi-quantification on Macdiff. software. It should be noted that the XRD% do not represent true volume percentages. Results of this analyses are displayed in Appendices 4,5 and 6 and Figures 17, 21 and 22.

Upper Grumantbyen Formation sandstones

Bulk XRD analyses of the samples from upper Grumantbyen Formation was done in BH 9/06 and BH 10/06. Feldspar is the dominating mineral in BH 9/06 with an average content of 52,0 XRD%, of which 31,7XRD% is plagioclase and K-feldspar makes 20,3 XRD%. The quartz content has an average of 40,09 XRD% making the average quartz/feldspar ratio of 0,41. Chlorite is the most prominent clay mineral with 1,7 average XRD%, while the concentrations of illite and kaolinite are 0,8 XRD% and 0,3 XRD% respectively. Pyrite content is low (0,2 XRD%). The carbonates contitute 4,8 XRD% of the rock samples, where dolomite (2,4 XRD%) is the abundant mineral.

In BH 10/06, quartz has the highest concentration of an average 60.4 XRD%, followed by feldspar (31,5 XRD%). Clay minerals show 2,7 average XRD%, while dolomite is dominant

(2,4XRD%) among the carbonates mineral group (4,8 XRD%). The average pyrite content in the well core is 0,62XRD%.

Marstranderbreen Member siltstone

One sample (128,5) has been analysed from the lower siltstone unit of Marstranderbreen Member in BH 9/06 (Appendix 5). Bulk XRD of this sample shows average plagioclase and feldspar content to be 44 XRD% and 21 XRD% respectively, making a total feldspar content of 64.9 XRD%. Quartz comprises 26,5 XRD% which yields a quartz to feldspar ratio of 0.29. Chlorite (2,3 XRD%) is the most abundant clay mineral. The carbonate minerals (4 XRD%) are dominated by dolomite (1,8 XRD%). Pyrite concentration in this siltstone is low (0,53 XRD%).

Marstranderbreen Member shales

The Marstranderbreen Member shales mineralogy has been studied through the analyses of 3 samples in BH 9/06 at the middle and upper shale unit. Highest values are of quartz (39,1 XRD%), followed by feldspar (31,6 XRD%). Siderite content is highest (8,6 XRD%) of the carbonates with calcite and dolomite absent in some samples. Pyrite content in one of the samples is 6,7 XRD%.

Hollendardalen Member sandstone

Three samples (118,00m, 118,90m and 122,50m) have been selected from BH 9/06 to represent Hollendardalen Member mineralogy. Quartz is the dominating mineral of this interval with an average of 47,2 XRD% values. Feldspar follows with 29 XRD% and the ratio of quartz to feldspar is 0,60. The clay minerals iIllite, chlorite and kaolinite have 4,5 XRD%, 8,26 XRD% and 2,.4 XRD% values respectively. Carbonate mineral content (7,23 XRD%) is led by siderite (4,77 XRD%).

Shales of Lower Gilsonryggen Member

The Gilsonryggen Member is the most extensively studied unit in this thesis due to the presence of PETM. 32 Samples of this unit were studied from cores BH 7/08 (14 samples), BH9/06 (5 samples) and 10/06 (14 samples). In BH 7/08, bulk analyses reveals quartz to be the dominant mineral of this interval with an average of 45,7 XRD%. Feldspar minerals make up 30,7 XRD%,

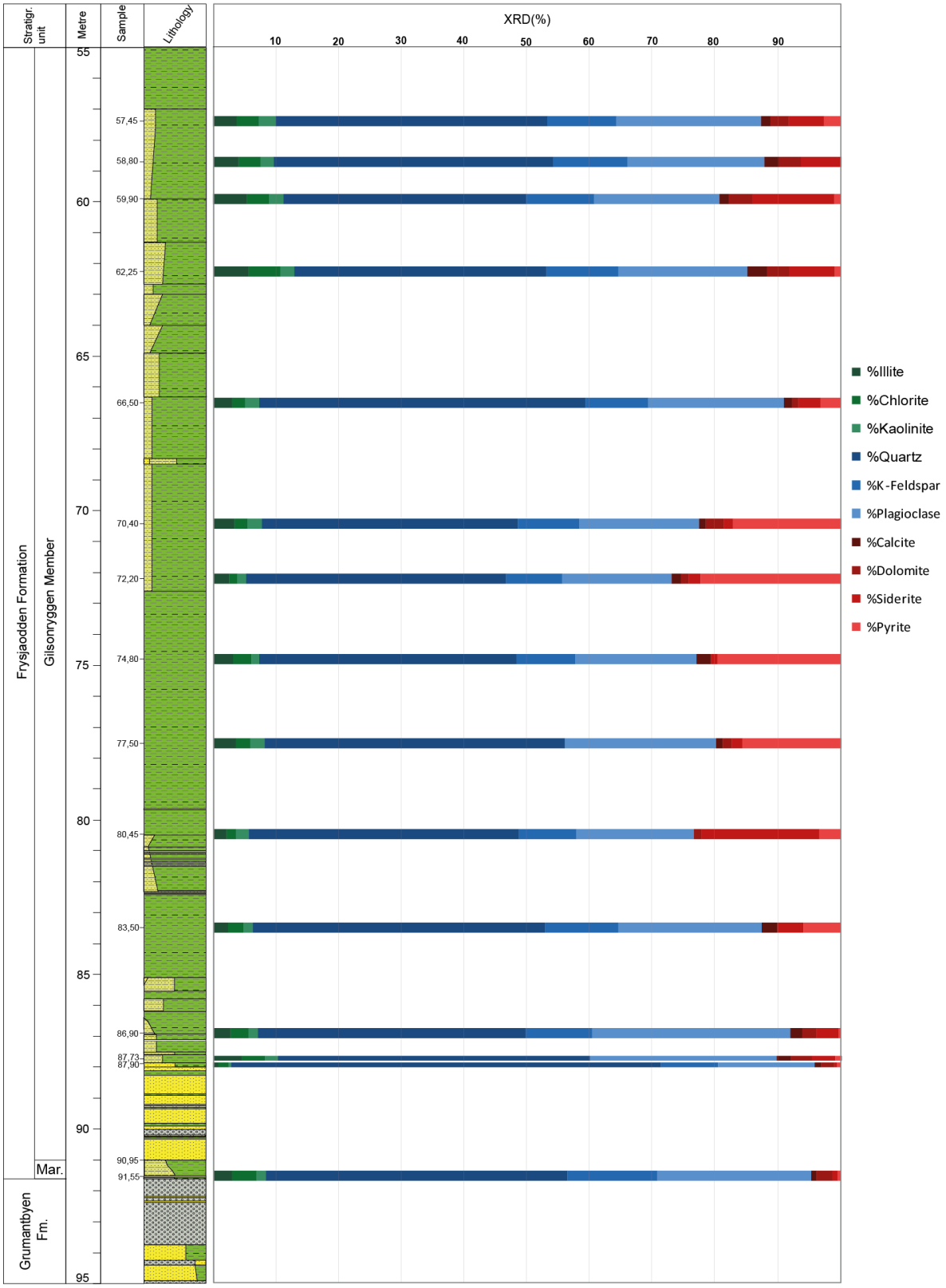

Figure 17: Minerals estimation bulk analyses plotted against the lithological column at respective depths of samples in BH 7/08.

21,8 XRD% of which is plagioclase and 8,8 XRD% comprises k-feldspar. Among the clay minerals, illite is most common with an average of 3,2 XRD%. Chlorite content is 2,7 XRD% and kaolinite forms 1,9% of the total clay portion.

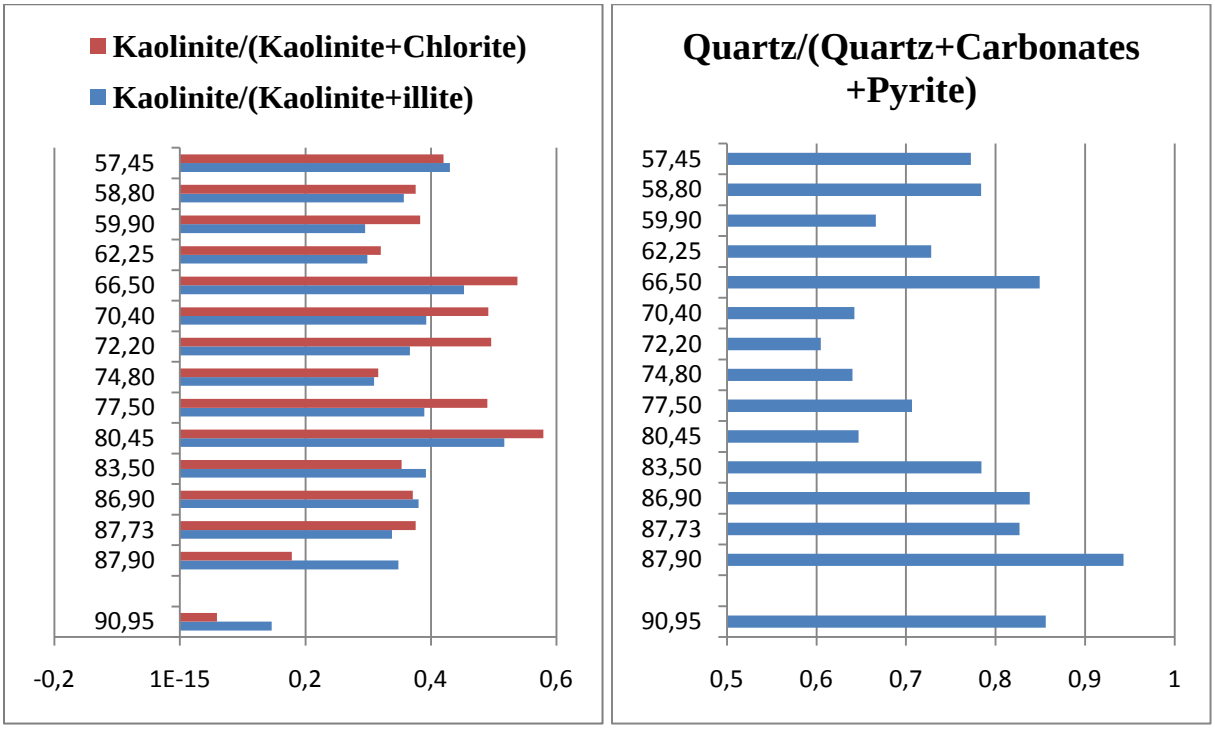

a) **b)**

Figure 18: a) Kaolinite/(Kaolinite+Chlorite) and Kaolinite/(Kaolinite+Illite) ratios in the lower Gilsonryggen member in BH7/08. b) Quartz/(Quartz+Carbonates+Pyrite) ratio of same interval as a measure of allogenic vs. authigenic minerals. Lowermost sample belongs to the sadstone of Hollenderdallen and is added for comparision.

Samples from BH 9/06 yield similar mineralogical characteristics with an average 41,2 XRD% quartz and 31.9 XRD% feldspar (25 XRD% plagioclase and 6,9 XRD% feldspar). Illite remains the most frequently occurring clay mineral with an average of 4,8 XRD%. Chlorite portion varies between 3,13 XRD% and 4,58 XRD% forming an average of 3,4 XRD%. The kaolinite content shows fluctuation between 1,9 XRD% and 6,5 XRD%, resulting in an average of 3,7 XRD% across the interval.The mineralogical analyses of BH 10/06 also coincides with the results from BH 7/08 and BH 9/06 with the commonly occurring mineral being quartz (42,51 XRD%). Average feldspar content of 25,3 XRD% is distributed between plagioclase and K-feldspar as 16,25 XRD% and 9,04 XRD% respectively. In clay minerals, Illite is prominent with 3,55

XRD% and chlorite portion is 3,21 XRD%. Kaolinite has the lowest concentration in the clay minerals (2,24 XRD%).

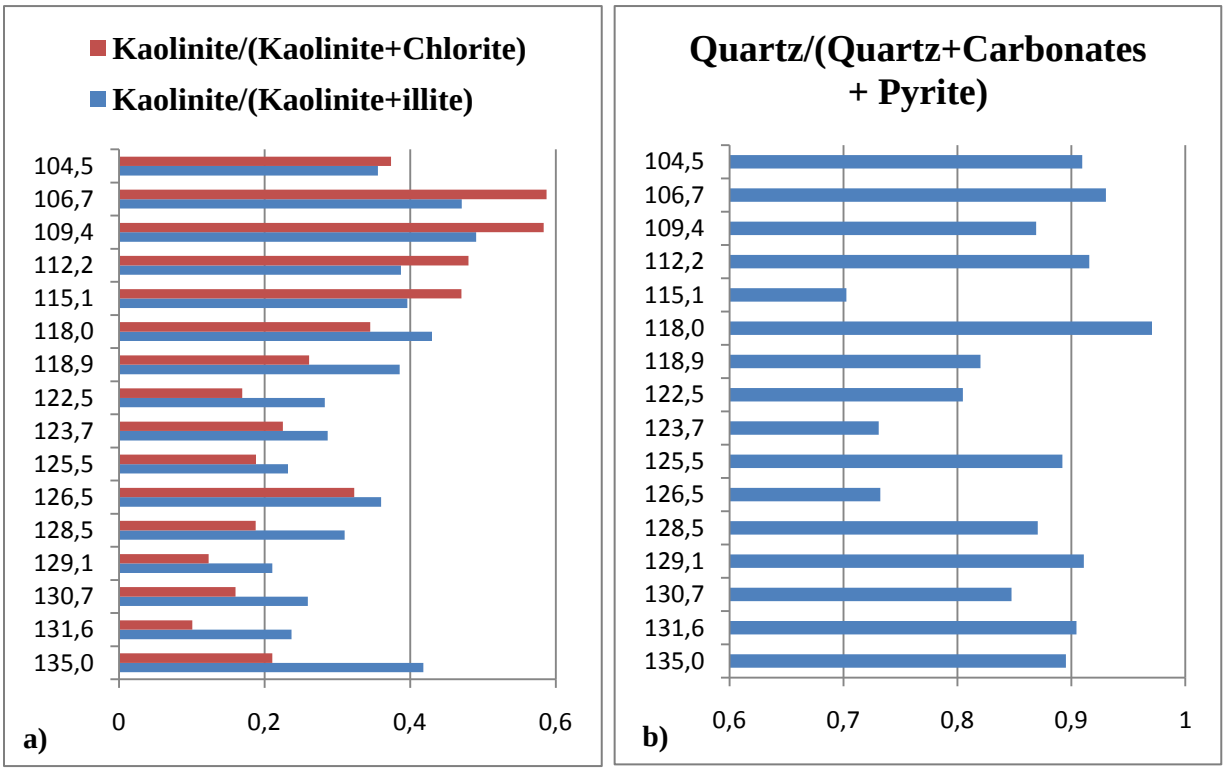

Figure 19: a) Kaolinite/(Kaolinite+Chlorite) and Kaolinite/(Kaolinite+Illite) ratios in the upper Grumatbyen sandstone, Marstranderbreen member, Hollendardalen member and lower gilsonryggen member in BH9/06. b) Quartz/(Quartz+Carbonates+Pyrite) ratio of same interval as a measure of allogenic vs. authigenic minerals.

As already mentioned in chapter 1, clay mineralogy is the important factor in studying the paleoclimatic and paleoenvironmental conditions especially around the PETM region. Therefore, trends of the kaolinite/illite and kaolinite/Chlorite have been studied (Figures 18a,19a and 20a). A similarity is observed in the trends of both ratios. These trends are most prominent in BH 7/08 (Figure 18a), where an increase is observed from lowest readings of around 0,2 in both ratios at the base of Gilsonryggen Member (87,90m) to the highest values of 0,55 at 80,45m.. Moving stratigraphically up, both ratios depict a decreasing trend to lower values of 0,3 at 74,80m. One sample from the Hollendardalen member (90,95m) is included for comparision. Similarly in BH 10/06, values of kaolinite/illite and kaolinite/chlorite are close to 0,3 near the base of Gilsonryggen Member at 511,20m (Figure 20a). Then these values increase to around 0,5 at 492,90m depth before decreasing once again to around 0,3 at 485,45m. Two exceptionally high

values are encountered at depths 49,85m and 482,35m (Figure 20a). Detailed analyses of these samples shows that these samples are from siderite rich zones (Appendix 7). Therefore, these values are excluded when observing the trends of kaolinite/kaolinite+illite and kaolinite/ kaolinite +chlorite ratios The 5 samples analysed from the 15m interval of Gilsonryggen Member in BH 9/06 show ratio of around 0,4 at the base of this unit (115,05m), increasing to around 0,54 at the middle (Figure 19a). Decreased values to around 0,35 are observed at the top level of the core (104,50m).

The measure of allogenic minerals against the authigenic minerals is done by determining the quartz/ (quartz+qarbonates+pyrite). This ratio is close to 0,8 at the bottom of the succession in BH 7/08 (Figure 18a) and decreases to around 0,6 at 72,20m before rising once again to 0,85 at 66,50m. Likewise, higher values are encountered at the bottom of the Gilsonryggen Member (0,8) with a decreasing (0,45 at 492,90m) and then increasing trend (0,70 at 475,55m). These trends have also been disturbed by the values samples from the two siderite layers which makes the Quartz / (quartz+carbonates+pyrite) ratio close to zero at these two depths..

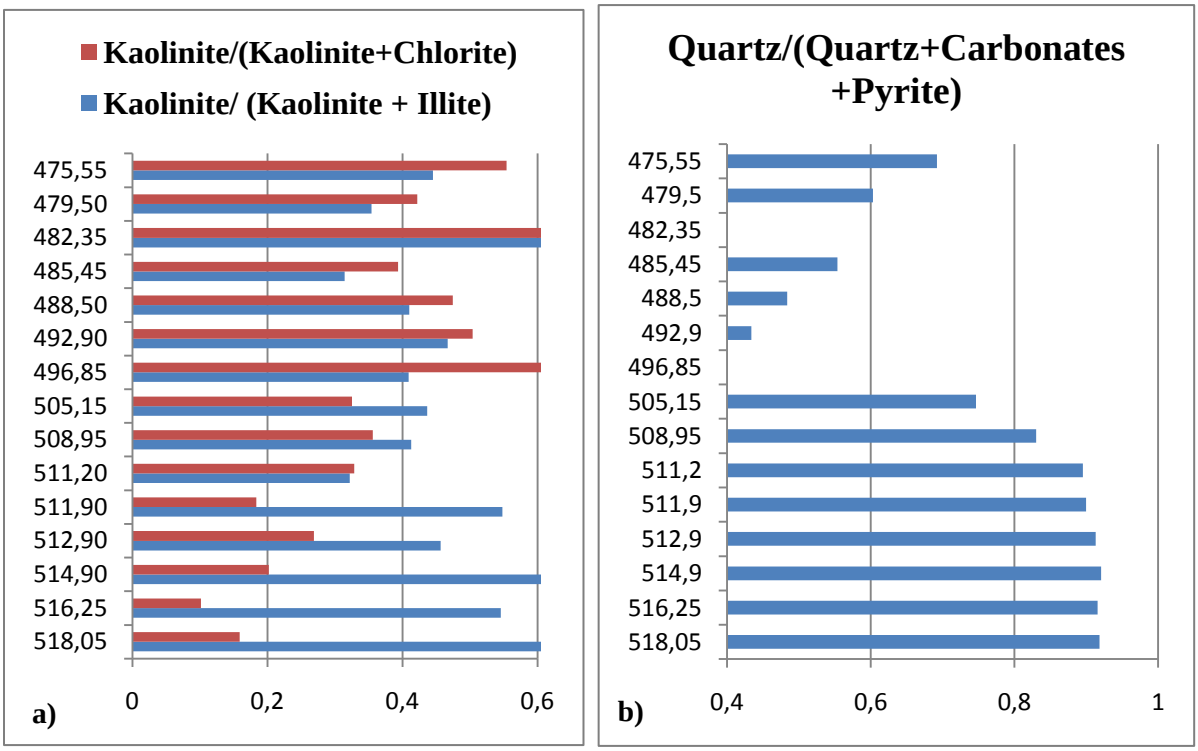

Figure 20: a) Kaolinite/(Kaolinite+Chlorite) and Kaolinite/(Kaolinite+Chlorite) ratios of the upper Grumantbyen and lower Gilsonryggen member in BH 10/06. b) Quartz / (Quartz + Carbonates + Pyrite) ratio of same interval as a measure of allogenic vs. authigenic minerals.

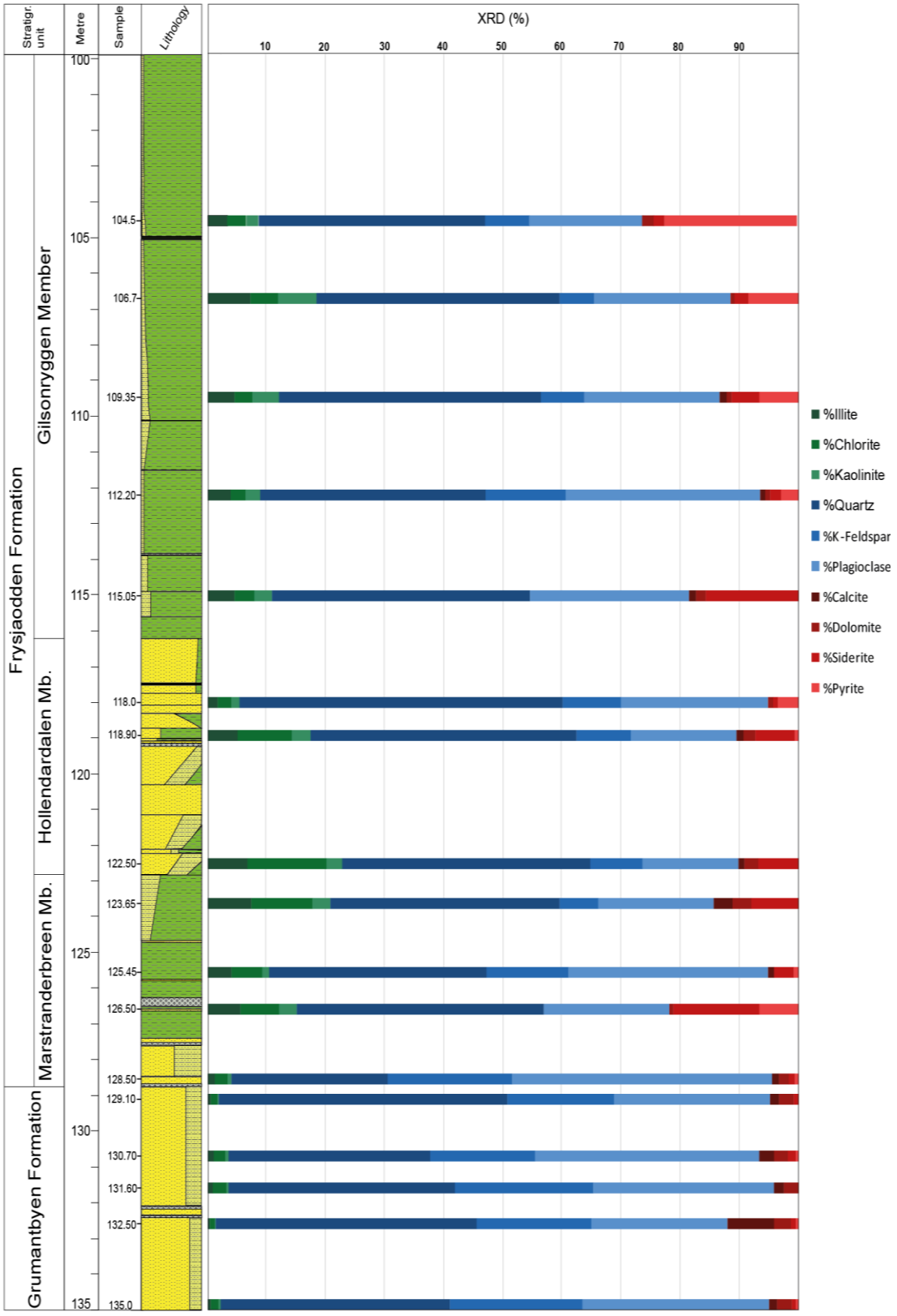

Figure 21: Minerals estimation bulk analyses plotted against the lothological column at respective depths of samples in BH 9/06.

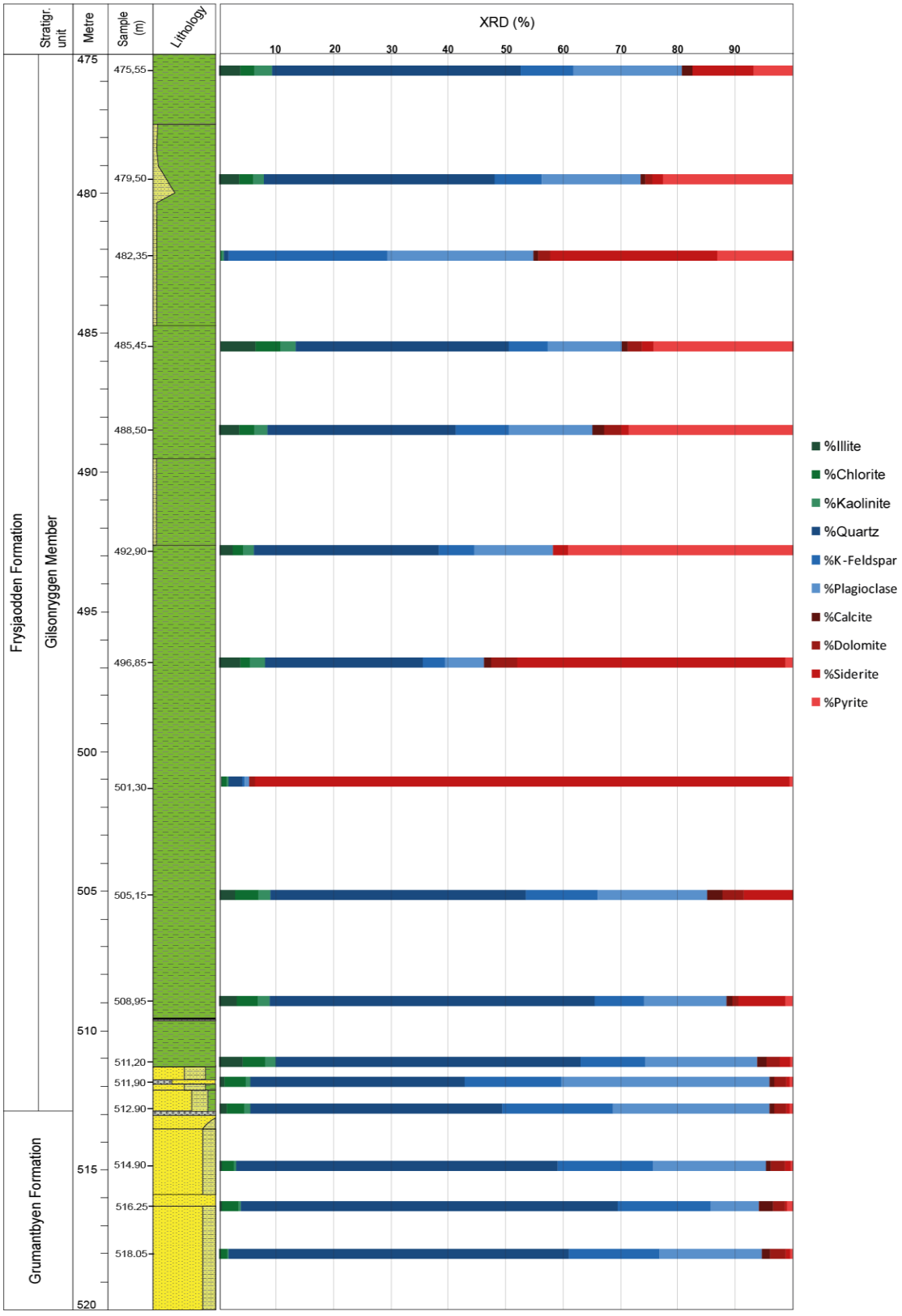

Figure 22: Minerals estimation bulk analyses plotted against the sedimentary log at respective depths of samples in BH 10/06.

7 Geochemistry

This chapter presents the geochemistry of the three cores based on the Rock-Eval, TOC, $CaCO_3$ and Th/U analyses. These parameters will be used to determine the amount of organic matter, evaluation of bottom water depositional conditions and Characterization of Kerogen type.

7.1 TOC, CaCO3 and Th/U analyses

7.1.1 TOC

In general, TOC data throughout the three cores shows relatively low values for all the formations present (Figure 25). In BH 7/08, average values of TOC are 1,37%. Highest values are attained at 86,90m and 83,50m (1,84% and 2,70% respectively). Similar increase in TOC is observed in BH 10/06 from depths 505,5m (2,26%) to 501,80 (3,28%). This trend is also visible in BH 9/06 where relatively high values are recorded at 115,05m (3,03%) and 112,20m (2,37%) than the average values for this core (1,17%) (Appendix 7).

7.1.2 $CaCO_3$

The $CaCO_3$ distribution does not display any proper trends in any of the cores. Overall values are low with lowest values in Grumantbyen formation. Abnormally high values are recorded the in BH 10/06 at 501,80m (41,80%). XRD analyses of this sample reveals this to be a siderite sample.

7.1.3 Th/U

The Th/U ratio is close to 7 at the base of Gilsonryggen member (87,90m) and then drops to 4 at 83,50m (Figure 25). This ratio remains constant when we move stratigraphically up in the well core. At 63,40m, the ratio increases once again to around 6 and the top most sample (58,80m) display similar value to the deepest sample.

7.1.4 Rock-Eval Analyses

Temperature is the most subtle parameter in the generation of hydrocarbons. Reconstruction of temperature history and kerogen characterization is roughly estimated through Rock-Eval analyses (Tissot et al., 1987). Paleotemperatures cannot be determined through direct conversion of measureable parameters. Different maturation indices are used as an indirect method. Among these indices, T_{max} is rapidly becoming the most widely used (Tissot et al., 1987). Rock-Eval analysis has been done as described in chapter 4.3 in order to determine the kerogen type and thermal maturation history of the studied cores. Modified van Krevelen diagram with T_{max} vs

hydrogen Index diagram (Figure 23) and production index vs depth (Figure 24) from Peters (1986) have been used to determine the thermal maturation and kerogene typification. The samples from all three core polt as a mixture of type II and III. Therefore, a mixture of organic matter with both marine and terristrial origin is present in these sediments. Highest observed HI and S_2/S_3 values are 194 and 20 and these indicate coal since typical values for coal are below 300 HC/g C_{org} and S_2/S_3 greater than 5 (Peters (1986).

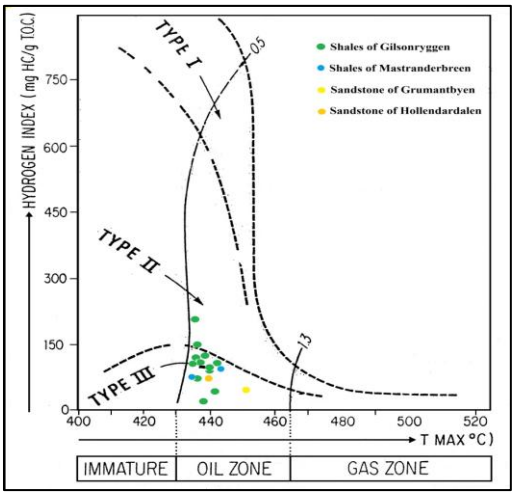

Figure 23: Tmax vs Hydrogen index (Orignal diagram was reproduced from Espitalie et al., 1984)

Both diagrams show good correspondence in terms of temperatures and imply the existance of all the samples within the oil zone. The PI vs Depth diagram shows that the samples from shallower cores (BH 7/08 and BH 9/06) have been subjected to temperatures between 70°- 90 °C and the deepest core (BH 10/06) has experienced higher temperatures (90°-120 °C). One sample from lowermost part of BH 10/06 belonging to the Grumantbyen Formation plots out the normal trend. This is because it shows a high hydrogen index resulting in a high production index.

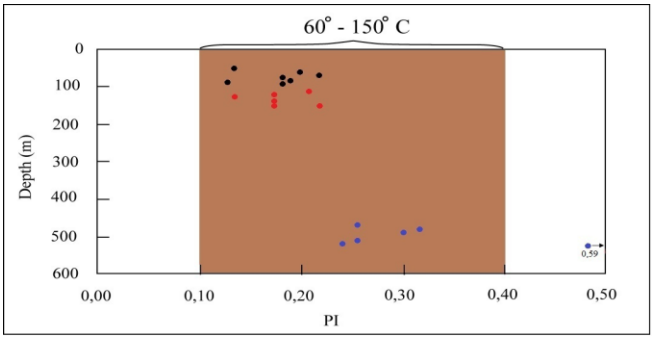

Figure 24: Production Index vs Depth as thermal maturation indicator. Temperatures from Peters (1986). Samples from BH 7/08 (Black dots), BH 9/06 (Red dots) and BH 10/06 have been plotted.

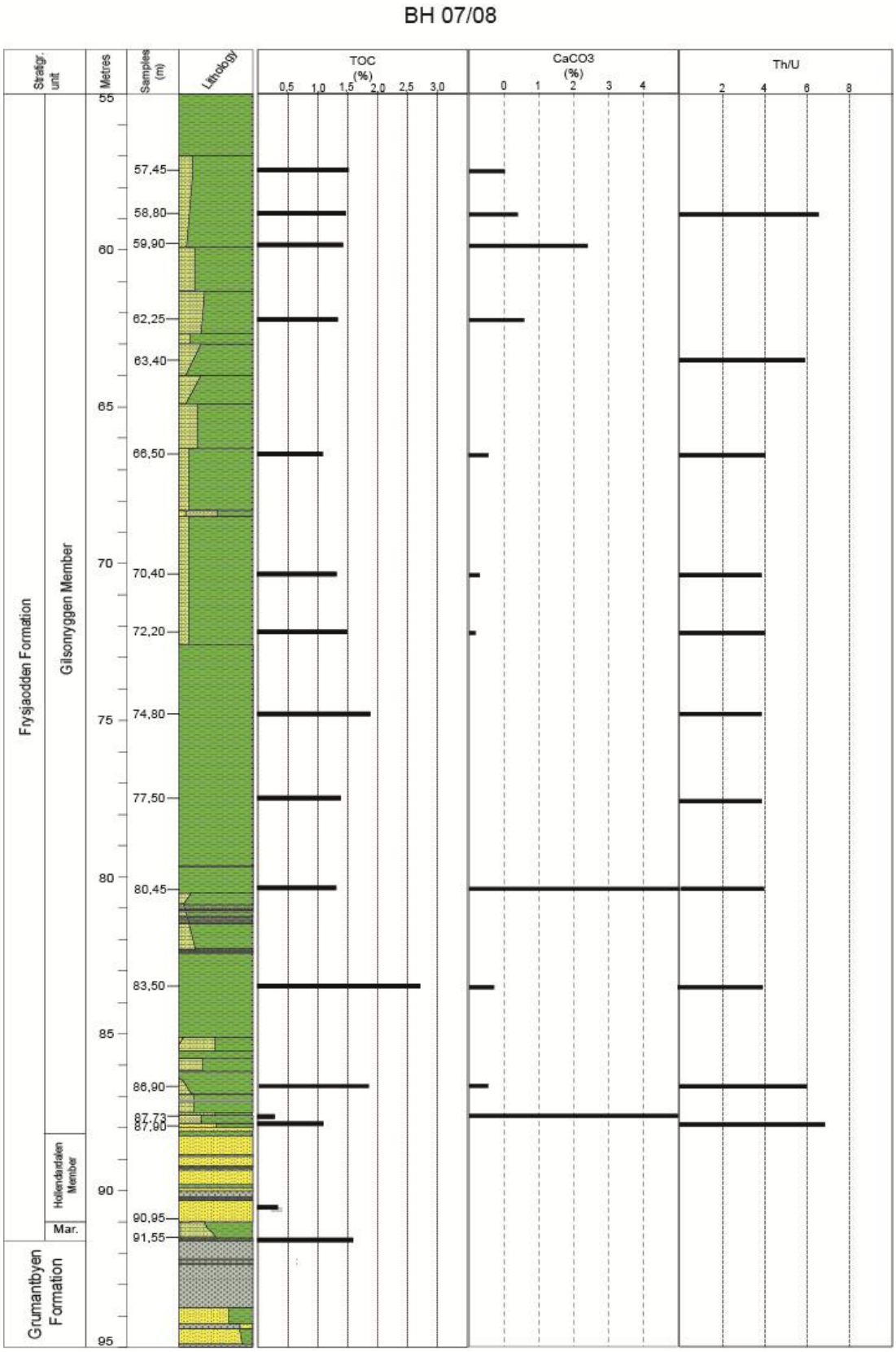

Figure 25: TOC and CaCO3 content and U/Th ratio of BH 7/08

8 Discussion of data and reconstruction of depositional environments

"Sedimentation results from the interaction of supply of sediments, its reworking and modification by physical, chemical and biological processes, and accommodation space-that is, the space available for potential sediment accumulation" (Reading, 2009). The physical disintegration and chemical decomposition of already formed rocks to produce stable minerals and rock fragments is termed as weathering (Boggs, 2006). Weathering can occur from thermodynamic difference in ambient conditions and mineral formation conditions (chemical weathering) (White, 1995), or through the mechanical disintegration (physical weathering) of rocks through various causes with minimal alteration in chemical and mineralogical composition. The studied core consist mostly of shales, with a small portion of sandstones, therefore emphasis will be on the study of argelaceous rocks. Bottom water O_2 conditions determine the lithological characteristics of shales and factors such as lamination, color, bioturbation, organic matter quantity and type, pyrite content and U/Th ratio control these conditions (Potter et al., 2005).

Changes in climatic conditions prevailing in the continental source areas has been interpreted in terms of the variations in the vertical clay mineral distribution in deep-sea sediments (Chamley, 1967, 1975; Singer, 1984). Numerous studies have also recunstructed the paleoclimate and continental paleoenvironment by using the inheritance relationship between marine clay and soil clay as fully demonstrated, even obvious (Chamley, 1989; Robert and Kennett, 1992;Gibson et al., 1993; Chamley, 1997). XRD analysis of deep see clay minerals in the Atlantic ocean by Thiry (2000) has shown abundance of kaolinite between the tropics while illite and chlorite prevail at high lattitudes. This led to the conclusion that marine clay minerals are in general inhertied. Clay minerals present at this level are considered to be of detrital origin (Riber,2010).

Formation of kaolinite, a typical clay mineral, occurs primarily through weathering in humid climates. The reaction is given as: K(Na)AlSi3O8 + 2H+ + 9H2O = Al2Si2O5(OH)4 + 4H4SiO4. The threshold for this reaction to continue is the constant removal of reaction products K^+ and N^+ and supply of new fresh (meteoric) water (Byørlykke, 2010). Kaolinite can also be directly precipitated (neoformation) in sandstone pores during diagenisis (Bergaya et al., 2006) . Other clay minerals such as illite and chlorite are deposited in cold climates where chemical weathering is low due to scarcity of rainfall (Robert and Kennett, 1994). Proposed mechanism

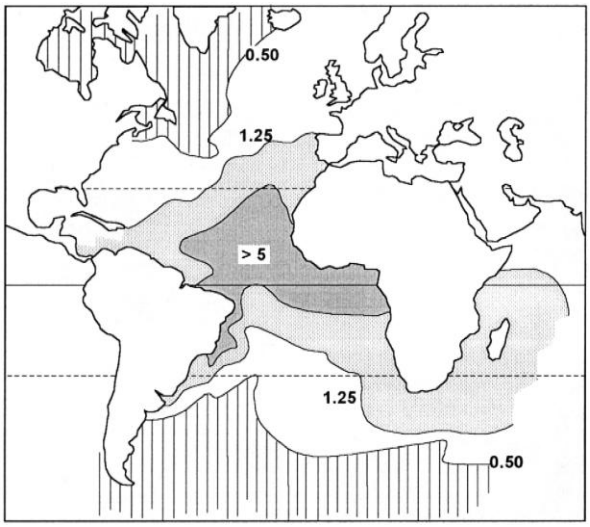

Figure 26: Kaolinite/chlorite ratios peak areas in recent deep sea clays in the Atlantic Ocean (from Biscaye, 1965).

for authegenic illite formation is through replacement of dissolve kaolinite (Bjørlykke, 1998) and burial diagenisis (Bergaya et al., 2006).. Other clay minerals such as illite and chlorite are deposited in cold climates where chemical weathering is low due to scarcity of rainfall (Robert and Kennett, 1994). Proposed mechanism for authegenic illite formation is through replacement of dissolve kaolinite (Bjørlykke, 1998) and burial diagenisis (Bergaya et al., 2006).

When analyzing shale, it is important to identify the origin of clay minerals as detrital or authigenic. Presence of mostly detrital illite has been proposed in an earlier study by Ribers (2009) through SEM analyses. Thin section analyses done by this study also reveals presence of detrital clay minerals as little feldspar dissolution has been noted. Rock-Eval results show highest Tmax to be 452^{o} C, and it is inferred that the lowest part of this core has suffered deeper burial then the suggested 1500 m depth by Throndsen (1982). Yet, the burial depth was not sufficient to cause illitization of kaolinite.

The following sub chapter contains the discussion for reconstruction of depositional environment in terms of T-R sequence stratigraphy (Figure 27) as discussed in. PETM is discussed separately and candidate interval for this event is proposed for each core. All three cores have been correlated by integrating the sedimentary data with geochemical and biofacies analysis of the same cores by Maharjn (2011). A base line formed at the extinction event of benthic foramnifera.

8.1 Sandstones of upper Grumantbyen Formation (Regression and Transgression):

Deposition of the upper part of this sandstone is interpreted to have occurred first as a result of a regressive cycle and then a transgressive cycle, The regressive systems tract (RST) terminates in a conglomerate layer observed in all three cores in the lowermost part of the sections. The transgressive systems tract (TST) is defined by the finning up sandstone sucession composing the upper part of Grumantbyen Formation in cores BH 9/06 and BH 7/08 (Figure 27) . High glauconite content is observed in these sandstones during petrographic analyses. Shallow marine environments (shoreface to shallow shelf) support the formation and enrichment of glauconite (McRae, 1972; Boggs 2006). Rock eval analyses reveals the common occurrence of type III kerogen (Figure 23) in this formation which originates mainly from land plants (Peters and Cassa, 1994). Coal fragments and wood particles have been observed both during core logging and thin section study. Average grain size very fine sand has also established through thin section analyses. High bioturbation in the form of large burrows has destroyed all the physical sedimentary structures in this sandstone. All these evidences are sufficient to assign a shallow marine depositional environment to the upper Grumantbyen Formation.

Petrographic analyses shows low porosity in these sandstones (Figure 14b). Observation of grain to grain contacts displays dominance of concave-convex and long contacts which indicates that these sandstones have suffered mostly physical compaction. Nominal chemical compaction is also interpreted in thin sections by low degree dissolution of feldspar grains. Factors controlling the maturity of sandstones are grain shape, grain size, grain sorting and quartz/feldspar ratios (Boggs, 2006). Observation of these factors in thin sections suggests that the Grumantbyen sandstones display the character of immature sandstone.

Bulk XRD analyses results indicate quartz to feldspar ratio of 0.4, with dominant feldspar being the plagioclase. Boggs (2006) provides two possible explanations for the presence of high feldspar content in sandstones: 1) A plagioclase rich source area which probably is of volcanic origin (high plagioclase content). Existence of volcanic rocks is known in the source region of this formation. 2) A short transportation distance from source to the deposition area which prevents less resistant minerals like feldspar from weathering. A small source distance is probable in the depositions of these sands. Another possibility could be the absence of meteoric

water flushing. In that case, dissolution of plagioclase into kaolinite would have occurred resulting in precipitation of kaolinite (Lanson, 2002). These sandstones contain 0.7% kaolinite indicating little dissolution of plagioclase. Distal shelf settings are the areas safe from this phenomenon (Bjølykke, 1998). Impermeable rocks can also resist meteoric water flushing (Lanson, 2002). Permeability and porosity of Grumatbyen sandstones is moderate to poor but the initial conditions could have been much better since mechanical compaction of these sands has occurred over time. Therefore the scarcity of authigenic kaolinite cannot be used as an indication of distal depositional area as these sandstones are poorly sorted, which would resist meteoric water flushing due to reduced permeabilities.

An exception exists in the core BH 7/08, where a 2 m thick conglomerate layer has been observed at the top of Grumantbyen Formation. The characteristic of these conglomerates point towards the erosion of these sandstones due to subaerial exposure. The explanation for this comes from the location of this core. It lies on the peripheral buldge in the east, and this region was subject of erosion while sands were being deposited in areas of other two cores.

8.2 Marstranderbreen Member (Maximum flooding Interval and Regression)

The transgression initiated in the upper Grumantbyen formation ends in a maximum flooding interval within the Marstrandebreen member (Bruhn and Steel, 2003). This unit is well developed in BH 9/06, while in core BH 7/08 its thickness is only arount 0.5m. This member consists of siltstone unit at the base overlying the top Grumantbyen conglomerates which continues into shales towards the middle part, and ends into the overlying Hollendardalen member. XRD analyses show an increase in quartz/(quartz+feldspar ratio) which can be explained by the change in either provenance area or transportation mechanism. It has been suggested by Steel et al., (1981) that the initial deposits of Frysjaodden Formation were formed during as shift from transtension-transpression tectonic regime. During this period, the source area was present probably in the western or north-western regions. The change in thickness in the two cores also points towards the shift in tectonic regimes.

XRD of a sample at 126,50m depth in BH 9/06 shows high levels of siderite and pyrite (Appendix 5). Formation of siderite is authigenic (Pearson, 1979) and it existance is is interpreted as an indication of decreasd levels of oxygen in bottom waters, representing the intermediate stage between glauconite enrichment (oxic environments) and pyrite enrichment

(anoxic environments) (Potter et. al., 1980). On the contrary, presence of pyrite has also been reported in homogenous bioturbated shales indicating less reducing bottom waters (Moris 1979). Sedimentary logs show absence of bioturbation at this level (Figure 10a). Combining this evidence with XRD indicates the presence of this sample within or at the base of maximum flooding zone.

An upward coarsening development about 3m below the top of Marstrandebreen menber shows the deposition of a regressive systems tract which follows into the overlying Hollenderdallen member sands. In general, a distal shelf deposition in restricted basin environment during transgression is concluded for this member by Burca (2008). Increase in quartz/(quartz+feldspar) ratio coupled with increased siderite and pyrite content and decrease in grain size to shales supports this interpretation.

Well defined conglomerate layers has been observed within Marstranderbreen Member. The basal contacts of these thin conglomerates are non-erosive and it shows mainly subaqueous deposition without subaerial exposure. Sharp contacts for this conglomerate have been observed during sedimentary logging. Non-erosive conglomerate base suppresses the idea of deposition by density currents (Dalland 1976). Probable transport mechanisms of these pebble and gravel rich conglomerates have been discussed by Dalland (1976) and transportation of material by ice rafting has been postulated as the suitable candidate. This model apparently fits the deposition of coarse material in such thickness without eroding the underlying layer. On the contrary, greenhouse environment has been widely accepted during Tertiary (Schweitzer, 1982; Moran et al., 2006) which contradicts the existence of ice during this time period. To coup wit this, Dalland (1976) proposes another mechanism which states transport by algal mats or kelps. A conglomerate bed similar to the one observed in this study has been observed by Burca (2008) in the marstranderbreen member, which was suggested to be formed through fluid flow process. Winnowing of clays containing dispersed clasts of pebble and gravel size could have occured over time, resulting in the removal of clays. Therby, concentrating these pebbles and gravels in well defined layers.This mechanism is likely to be the most probable reason (Personal com. Nagy).

8.3 Hollendardalen Member (Regression)

The Hollenderdallen member represents the regressive systems tract continuing form the upper part of Marstranderbreen shales. This regression is observed in the form of three coarsening up units (Figure 27). These sandstones are ripple laminated with moderate bioturbation. Plant fragments have also been observed in these sandstones. Plant rootlets have been reported in the top massive sandstone unit in Nordenskioldfjellet (Harding et al., 2011). These observations imply a terristrial deposition. Quartz/(quartz+feldspar) ratio similar to other members of Frysjaodden Formation and are higher than the Grumantbyen sandstones. Similar relationship exists in other parts of The Central Basin (pers. com. Sætre).This supports the idea of change in the sediment source area. On the basis of measurments of ripples and cross bedding direction Sætre (2001) concluded that the source of Hollendardalen Member was situated somewhere in the north to north-western region. Correlation of the three cores (Figure 27) shows thinning of Hollendardalen Member from BH 9/06 towards BH 7/08 and its complete absence in BH 10/06. This observation supports the idea of a north to north-western source.

8.4 Shales of the Gilsonryggen Member: (Transgression, Maximum flooding and Regression)

The boundary of Gilsonryggen Member is identified on the basis of conglomerate. It is underlain by the Grumantbyen Formation in one core and Hollenderdallen member in two cores BH 7/08 and BH 9/06. The lower part of this formation is moderatly bioturbated and light grey in color. The XRD analyses shows low amounts of pyrite which indicate well-oxygenated environments (Wignal, 2005) in the lower parts of this shale. This pyrite content increases upwards indicating the approaching of Maximum flooding interval. Above this, decrease in pyrite content and increased amounts of silt indicates the the initiation of a regressive systems tract (Figure 27) .

Quartz/(quartz+feldspar) ratios are higher than in the Grumantbyen Formation. This draws to a similar conclusion as Marstranderbreen Member of change in provenance area or the transportation mechanism. Lithological logs show an abrupt change from sands to shales which is interpreted as rapid transgressions up to the siderite and pyrite rich zone. A distal shelf setting fit the deposition of these shales.

Maximum flooding zone

Precise identification of a maximum flooding surface is difficult through the analyses of cores. Therefore, a maximum flooding zone (MFZ) has been proposed, containing probably several suitable candidates for the maximum flooding surface (MFS). A trangressive systems tract terminates at the base of this zone while a regressive systems tract initiates from its top. This zone is characterized by the existence severely hypoxic conditions and laminated homogenous shales, which are common features of maximum flooding event according to Emery and Myers (2006). In all three cores, prominent zones have been identified containing finely laminated dark color shales with high siderite and pyrite content as compared to the rest of the core. Presence of these units can be seen in the sedimentological logs (Figure 27). Other evidences are also present to support the hypothesis of low oxygen bottom water conditions during the deposition of this unit. These intervals are: 77.50-70.40m in BH 7/08, 492.90-479.55m in BH 10/06 and from 109.35-104.50m in BH 9/06. The presence of pyrite in large amounts has been observed both in bulk XRD analyses and thin section study. Th/U ratio from the elemental analyses of 7/08 shows a rather ambiguous trend, but a decrease is observed few meters below these levels which increase to previous high values moving sitatigraphically up from the top of this unit (Figure 25). Low TOC content has been observed throughout all the three cores, but highest values are present within and few meters below these intervals. Integrating this data with the biostratigraphic observations of Maharjan (pers. Com. 2011), suggest narrower MFZ's in the three cores (i.e. 82.12-78.36m in BH 7/08, 106.73-104.05m in BH 9/06 and 492.50-485.45m in BH 10/06).

Paleocene Eocene Thermal Maximum

The base PETM boundary is recognized by the onset of negative Carbon Isotopic excursion (CIE) and has been defined globally by the assignment of a global stratotype and section Point (GSSP) in Dababiya Quarry section of Egypt (Luterbacher et al. 2000). Existence of PETM candidate in the Tertiary shales of the Central Basin of Svalbard has been established by Dypvik et al.,(2011), Harding et al., (2011) and Cui et al.,(unpiublished data) with an approximate age of 55.6 Ma (Ribers, 2010). Recent studies have placed the PETM onset at 56.3 Ma (McInerney and Wing, 2011).

One of the objectives in this thesis is to observe if the climatic change during the PETM can be recognized by the variation in clay mineral assemblages. Kaolinite/(kaolinite+illite) and kaolinite/ (kaolinite+chlorite) ratios are used as the proxies for changing humidity and subsequent precipitation, although a number of environmental conditions are liable to the formation of detrital clay minerals such as illite chlorite and kaolinite in sediments. Similar trends have been observed in these ratios from bulk XRD analyses. Highest values in the kaolionite/ (kaolinite+Illite) and kaolinite/ (kaolinite+chlorite) are attained in the form of a well-defined peak at depths 80.45m in BH 7/08,close to 496.85m in BH 10/06 and around 106.70m in BH 9/06 (Figure18a, 19a, 20a). Extinction of benthic foramnifera, extremely low diversity of foramnifera and surficial formnifera in vicinity of these intervals has been reported by Maharjan (2011, unpublished master thesis). Therefore suitable candidate for PETM interval are the zones in the vicinity of these depths are proposed.

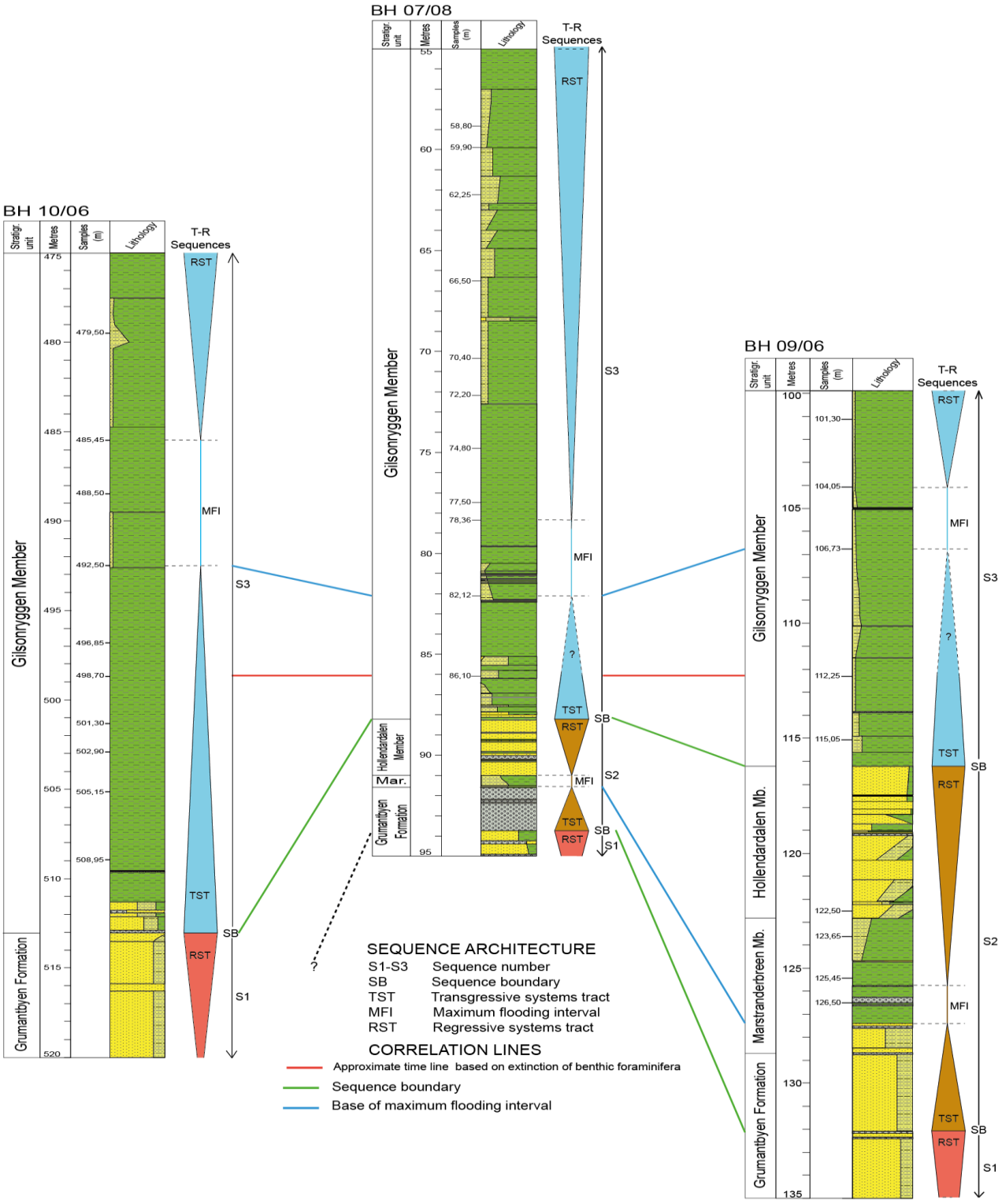

Figure 27: Sequence architecture and correlation of BH 7/08, BH 9/06 and BH 10/06. Approximate timeline has been established on the basis of biotic facies extinction.

9 Conclusions

Recunstruction of depositional environments during the Paleocene-Eocene sedimentation and the changes in paleoclimate conditions across the PETM in the Central Tertiary Basin has been done on the basis of results from sedimentary core logging, mineralogical analyses (Thin sections and XRD), geochemical analysis (Rock-Eval, TOC, TC, $CaCO_3$ and U/Th). Following conclusions are postulated:

1) The upper Grumantbyen Formation is interpreted as finning up sandstone which was deposited during the maximum regression from east to west and the consequent transgression. High levels of bioturbation resulting in destruction of sedimentary structures and a very fine grain size imply a shallow marine depositional environment.Mineralogical characteristics also reveal a proximate source area. Presence of a thick conglomerate in the eastern most core indicates exposure of these sandstones due to uplift from prepheral bulge.

2) The Marstranderbreen Member represents a general shallowing upward sucesion into the overlying Hollendardalen Member. This member comprises of clayshale, claystone and siltstone facies. The maximum flooding is identified in it lower part on the basis of siderite and pyrite content and lithological characteristics. In terms of sequence stratigraphy, a maximum flooding interval initial part of a regressive systems tract has been identified in the Marstranderbreen Member.

3) Shallowing up sequences in Hollendardalen Member coupled with occurrence of terrestrial vegitation leads concludes a terrestrial depositional environment. This unit completes the regressive systems tract which initiated in Marstranderbreen Member. Thinning out of Hollendardalen member and Marstranderbreen members from core 9/06 towards core 7/08 and its absence in Core BH 10/06 confirms the existance of western to north-western source area for these sediments.

4) The lower part of Gilsonryggen shales marks the initiation of an abrupt transgression from the underlying sandstones. A second maximum flooding interval has been identified in the basal parts of these shales on the basis of similar identification characteristics as the first one.

5) Candidate PETM intervals are identified in all three cores based on kaolinit/(kaolinite +chlorite) and kaolinite/(kaolinite+illite) ratios and shale characteristics such as pyrite content,

color and lamination. Increased ratios lead to conclude that these sediments were deposited during humid climatic conditions. By integrating these results with previous studies in Svalbard, it is also concluded that PETM anomaly is a regional phenemenon in The Central Basin.

5) Sequence stratigraphic analyses reveals the presence of one complete sequencs and two incomplete sequences in the studied cores:

- S1: A regressive systems tract represents this sequence consists the upper part of Grumantbyen formation in all three cores.
- S2: This complete sequence is represented by topmost part of Grumantbyen Formation, the Marstranderbreen Member and the Hollendardalen Member and is present two cores.
- S3: Contains transgressive systems tract, maximum flooding interval and part of regressive systems tract and is recognized in the lower Gilsonryggen Member of all thee cores.

References

Alegret, L., Ortiz S., Molina E., 2009a. Extinction and recovery of benthic foraminifera across the Paleocene-Eocene Thermal Maximum at the Alamedilla section (Southern Spain). Palaeogeographical. Palaeoclimatology. Palaeoecology. v. 279, p. 186–200.

Alegret, L., Ortiz S., Orue-Etxebarria. X., Bernaola G., Baceta, J.I., et al. 2009b. The Paleocene-Eocene thermal maximum: new data on microfossil turnover at the Zumaia section, Spain. Palaios. v. 25, p. 318–28.

Aref, M., Youssef, M., 2004. The benthonic foraminifera turnover at the Paleocene/Eocene Thermal Maximum Event (PETM) in the southwestern Nile Valley, Egypt. Neues Jahrb. Geol. Pal¨aontol.-Ab, v. 234, p. 261–89.

Aziz, H. A., Hilgen, F. J., Van luijk, G. M., Sluijs, A., Kraus, M. J., Pares, J. M. & Gingerich, P. D. 2008. Astronomical climate control on paleosol stacking patterns in the upper Paleocene-lower Eocene Willwood Formation, Bighorn Basin, Wyoming. Geology, v. 36**,** p. 531-534.

Berger, A., 1988, Milankovitch theory and climate: Reviews of Geophysics, v. 26, p. 624-657.

Bergaya, F., Theng, B.K.G., and Lagaly, G., 2006, Handbook of clay science: Amsterdam, Elsevier, XXI, 1224 s. p.

Biscaye, P.E., 1965. Mineralogy and sedimentation of recent deep-sea clay in the Atlantic ocean and adjacent seas and oceans. Geological Society of America Bulletin, v.76, p. 803–832.

Bjørlykke, K.. 1998. Clay mineral diagenesis in sedimentary basins - a key to the prediction of rock properties. Examples from the North Sea Basin: Clay Minerals, v. 33, p. 15-34.

Bjørlykke, K. 2010 and Jaren, H. 2010. "Sandstones and Sandstone reservoir". In Bjørlykke, K. 2010. PetroleumGeoscience: From Sedimentary Environment to Rock Physics, Berlin, Heidelberg, Springeræ-Varalg Berlin Heidelberg. p, 113-140.

Boggs, S., 2006, Principles of sedimentology and stratigraphy: Upper Saddle River, N.J., Pearson Prentice Hall, XIX, 662 s. p.

Bolle, M.P., and Adatte, T. 2001. Palaeocene early Eocene climatic evolution in the Tethyan realm: clay mineral evidence. Clay Mineral, v. 36, p. 249–261.

Brinkhuis, H., Schouten, S., Collinson, M.E., Sluijs, A., Sinninghe Damsté, J.S., Dickens, G.R., Huber, M., Cronin, T.M., Onodera, J., Takahashi, K., Bujak, J.P., Stein, R., van der Burgh, J., Eldrett, J.S., Harding, I.C., Lotter, A.F., Sangiorgi, F., van Konijnenburg-van Cittert, H., de Leeuw, J.W., Matthiessen, J., Backman, J., Moran, K. and the Expedition 302 Scientists. 2006. Episodic fresh surface waters in the Eocene Arctic Ocean. Nature, v. 441 (1), p. 606-609.

Bruhn, R. & Steel, R. 2003. High-Resolution Sequence Stratigraphy of a Clastic Foredeep Succession (Paleocene, Spitsbergen): An Example of Peripheral-Bulge-Controlled Depositional Architecture. Journal of Sedimentary Research, v. 73**,** p. 745-755.

Burca, F. 2008. Palaeogene depositional environments of the Frysjaodden and Hollendardalen formations in central Spitsbergen, University of Oslo.(unpublished master thesis).

Chamley, H., 1967. Possibilite´s d'utlisation de la cristallinite´ d'unmine´ral argileux _illite. comme te´moin climatique dans lesse´diments re´cents. C.R. Acad. Sci. Paris v.265, p. 184–187, Se´r.D.

Chamley, H., 1997. Clay mineral sedimentation in the ocean. In: Paquet, H., Clauer, N. _Eds.., Soils and Sediments. Mineralogy and Geochemistry. Springer, Berlin, p. 269–302.

Cramer, B. S., and Kent, D. V. 2005. Bolide summer: The Paleocene/Eocene thermal maximum as a response to an extraterrestrial trigger, Palaeogeography. Palaeoclimatology. Palaeoecology., v. 224, p. 144– 166.

Chamley, H., 1975. Se´dimentation argileuse en Mer Tyrrhe´ne´enneau Plio-Ple´istoce`ne d'apre`s l'e´tude du forage JOIDES 132. Bull. Groupe Fr. Argiles 27, Strasbourg, p. 97–137.

Singer, A., 1984. The paleoclimatic interpretation of clay minerals in sediments — A review. Earth-Science Reviews, v. 21, p 251–293.

Chamley, H., 1989. Clay Sedimentology. Springer, Berlin, p. 623.

Crane, K., Eldholm, O., Myhre, A. M. & Sundvor, E. 1982. Thermal implications for the evolution of the spitsbergen transform fault. Tectonophysics, v. 89, p. 1-32.

Sætre, C. 2011. Development of Hollendardalen Formation (Svalbard); with emphasis on sedimentological and petrographical analysis, University of Oslo. (unpublished master thesis).

Crouch, E.M., Dickens, G.R., Brinkhuis H., Aubry MP., Hollis, C.J, et al. 2003. The Apectodinium acme and terrestrial discharge during the Paleocene-Eocene thermal maximum: new palynological, geochemical and calcareous nannoplankton observations at Tawanui, New Zealand. Palaeogeography. Palaeoclimatoogy. Palaeoecology. v. 194, p. 387–403.

Crouch, E.M., Heilmann-Clausen. C,Brinkhuis .H, Morgans. H.E.G,Rogers. K.M,et al. 2001. Global dinoflagellate event associated with the Late Paleocene Thermal Maximum. Geology, v. 29, p. 315–18.

Dalland, A., 1976. Erratic clasts in the Lower Tertiary deposits of Svalbard-evidence of transport by winter ice. Årbok - Norsk Polarinstitutt 1976, p. 151 - 165.

Dallmann, W.K.1999. Lithostratigraphic lexicon of Svalbard: review and recommendations for nomenclature use : Upper Palaeozoic to Quaternary bedrock: Tromsø,Norsk polarinstitutt, 318 s. p.

De Boer, P. L. & Smith, D. G. 2009. Orbital Forcing and Cyclic Sequences, International Association of Sedimentologists, Special Publication Number, v 19, P 1-14.

DeConto R, Galeotti S, Pagani M, Tracy DM, Pollard D, Beerling DJ. 2010. Hyperthermals and orbitally paced permafrost soil organic carbon dynamics. Presented at AGU Fall Meeting., Dec. 13–17, San Francisco (Abstract # PP21E-08)

Dickens, G.R., Castillo, M.M., Walker, J.C.G. 1997. A blast of gas in the latest Paleocene: simulating first-order effects of massive dissociation of oceanic methane hydrate. Geology, v. 25, p. 259–62.

Dickens, G.R, Oneil JR, Rea DK, Owen RM. 1995. Dissociation of oceanic methane hydrate as a cause of the carbon-isotope excursion at the end of the Paleocene. Paleoceanography. v. 10, p.965–71.

Maharjan, D. 2011. Stratigraphy with biotic responses to the Paleocene-Eocene Thermal Maximum (PETM) in The Central Basin, Unversity of Oslo, unpublished master thesis.

Dypvik, H., et al., The Paleocene-Eocene thermal maximum (PETM) in Svalbard-clay mineral and geochemical signals, Paleogeogr. Paleoclimatol. Paleoecol. (2011), doi:10.1016/j.paleo.2010.12.025.

Embry, A.F, Catuneanu, O., 2001. Practical Sequence Stratigraphy: Concepts and Applications, short course notes. Canadian Society of Petroleum Geologists. p, 167.

Emery, D., Myers, K., and Bertram, G.T., 1996, Sequence stratigraphy: Oxford, Blackwell Science, V, 297 s. p.

Embry , A.F. 1988. Triassic sea-level changes: Evidence from the Canadian Arctic Archipelago. In: Wilgus, C.K. Hastings, B.S.Kendall C.G.St.C. Posamentier, H.W. Ross, C.A. and Van Wagnor, J.C. (Editors), Sea-Level changes: An integrated approach. Society of Econology, Paleontology, Mineralogy., Special publication, v. 42, p. 249-259.

Embry, A.F. 1993. Transgrassive-regressive (T-R) sequence analysis of Jurassic sucession of Sverdrup Basin, Canadian Arctic Archipelago. Canadia Journal of Earth Science, v.30, p. 301-320.

Embry, A.F. 1995. Sequence boundaries and sequencs hierarchies: problems and proposals. In: Steel, R.J. Felt, V.L. Johannessen, E.P. and Mathieu (Editors), Sequence stratigraphy on the North west European Margin. Norwegian Petroleum Society (NPF), Special publication 5, Elsevier, Amsterdam, p. 121-146.

Embry, A.F. 2001b. Sequence Stratigraphy: what it is, why it works and how to use it. Reservoir. Canadian Society of Petroleum Geologist, v. 28 (8), p. 15.

Embry, A.F. and Podruski, J.A. 1998. Third order depositional sequences of the Mesozoic sucessions of Sverdrup Basin. In: James, D.P. and Leckie, D.A. (Editors). Sequences, Stratigraphy, Sedimentology: Surface and Subsurface. Canadian Society of Petroleum Geologists Memoirs, v.15, p. 73-84.

Farley, K. A. & Eltgroth, S. F. 2003. An alternative age model for the Paleocene-Eocene thermal maximum using extraterrestrial 3He. Earth and Planetary Science Letters, 208**,** 135-148. Gibson TG, Bybell LM, Mason DB. 2000. Stratigraphic and climatic implications of clay mineral changes around the Paleocene/Eocene boundary of the northeastern US margin. Sedimentary Geology, v. 134, p. 65–92.

Gavrilo, Y. O., Shcherbinina, E. A. & Oberhänsli, H. 2003. Paleocene-Eocene boundary events in the northeastern Peri-Tethys. Geological Society of America Special Papers, v.369, p 147-168.

Gibson TG, Bybell LM, Mason DB. 2000. Stratigraphic and climatic implications of clay mineral changes around the Paleocene/Eocene boundary of the northeastern US margin. Sedimentary Geolog,v. 134,p. 65–92.

Gibson, T.G., Bybell, L.M., Owens, J.P., 1993. Latest Paleocenelithologic and biotic events in neritic deposits of southwestern New Jersey. Paleoceanography, v. 8 (4), p 495–514.

Gingerich PD. 1989. New earliest Wasatchian mammalian fauna from the Eocene of northwesternWyoming: composition and diversity in a rarely sampled high-floodplain assemblage. Univ. Mich. Pap. Paleontol. v. 28, p. 1–97.

Gingerich PD. 2003. Mammalian responses to climate change at the Paleocene-Eocene boundary: Polecat Bench record in the northern Bighorn Basin, Wyoming. Geol. Soc. Am. Spec. Pap. v. 369, p. 463–478.

Gingerich PD. 2006. Environment and evolution through the Paleocene-Eocene thermal maximum. Trends Ecol. Evol.v. 21, p. 246–253.

Harding, I. C., Charles, A. J., Marshall, J. E. A., Pälike, H., Roberts, A. P., Wilson, P. A., Jarvis, E., Thorne, R., Morris, E., Moremon, R., Pearce, R. B. & Akbari, S. 2011. Sea-level and salinity fluctuations during the Paleocene-Eocene thermal maximum in Arctic Spitsbergen. Earth and Planetary Science Letters, v. 303**,** p 97-107-

Harland, W. B., 1965, The tectonic evolution of the Arctic-North Atlantic region. Philosophical Transactions of the Royal Society., v. 258, p. 59-75.

Harland, W.B. 1969. Contribution of Svalbard to the evolution of the North Atlantie region.- In: MCKAY (ed.), North Atlantic Geology and Continental Drift. Am. Ass. Petrol. Geol. Mern. v. 12, p. 817-857.

Helland-Hansen, W., 1990, Sedimentation in Paleogene foreland basin, Spitsbergen, Aapg Bulletin-American Association of Petroleum Geologists, v. 74, p. 260-272.

Higgins, J. A. & Schrag, D. P. 2006. Beyond methane: Towards a theory for the Paleocene-Eocene Thermal Maximum. Earth and Planetary Science Letters, v. 245**,** p. 523-537.

Hooker, J.J., 1998, Mammalian faunal change across the Paleocene-Eocene transition in Europe. In M.-P. Abury, S.G. Lucas and W.A. Berggren (eds.): Late Paleocene-early Eocene climatic and biotic events in the marine and terrestrial records, p. 428-450. Columbia University Press.

Ivany, L.C. Sessa, J.A. 2010. Effects of ocean warming and acidification during the Paleocene-Eocene ThermalMaximum on deep and shallow marine communities. Presented at Ecol. Soc. Am. Annu. Meet., Pittsburgh, PA

Jaramillo, C., Ochoa, D., Contreras, L., Pagani, M., Carvajal-Ortiz, H., Pratt, L. M., Krishnan, S., Cardona, A., Romero, M., Quiroz, L., Rodriguez, G., Rueda, M. J., De La Parra, F., Morón, S., Green, W., Bayona, G., Montes, C., Quintero, O., Ramirez, R., Mora, G., Schouten, S., Bermudez, H., Navarrete, R., Parra, F., Alvarán, M., Osorno, J., Crowley, J. L., Valencia, V. & Vervoort, J. 2010. Effects of Rapid Global Warming at the Paleocene-Eocene Boundary on Neotropical Vegetation. Science, v. 330, p. 957-961.

Johnson, J.G, Klapper, G. and Sandberg, C.A. 1985. Devonian eustatic fluctuation in Euramerica. Geological Society os America, Bulletin, v. 82, p. 567-587.

Katz, M.E., Pak, D.K., Dickens, G.R., Miller, K.G. 1999. The source and fate of massive carbon input during the Latest Paleocene Thermal Maximum. Science, v. 286, p. 1531–1533.

Kellogg, H.E. 1975, Tertiary Stratigraphy and Tectonism in Svalbard and Continental drift: Aapg Bulletin-American Association of Petroleum Geologists, v. 59, p. 465-485.

Kennett, J. P. and Stott, L. D. 1991. Abrupt deep-sea warming, palaeoceanographic changes and benthic extinctions at the end of the paleocene. Nature, v. 353, p. 225-229.

Kurtz, A.C., Kump, L.R., Arthur, M.A., Zachos, J.C., Paytan, A. 2003. Early Cenozoic decoupling of the global carbon and sulfur cycles. Paleoceanography, v. 18, p . 1090.

Luterbacher H, Hardenbol J, Schmitz B. 2000. Decision of the voting members of the International Subcommission on Paleogene Stratigraphy on the criterion for the recognition of the Paleocene/Eocene boundary. Newsl. Int. Subcomm. Paleogene Stratigr. v.9, p.13.

Major, H., and Nagy, J., 1972, Geology of the Adventdalen map area: Oslo, Norsk polarinstitutt, 58 s. p.

Manum, S.B. and Throndsen, T. 1978a. Rank of coal and dispersed organic matter and its geological bearing in the Spitsbergen Tertiary. Norsk Polarinstitutt Årbok 1977, p. 159-177.

Manum, S.B. and Throndsen, T. 1978b. Dispersed organic matter in the Spitsbergen Tertiary. Norsk Polarinstitutt Årbok 1977, p. 179-187.

Mcinerney, F. A. & Wing, S. L. 2011. The Paleocene-Eocene Thermal Maximum: A Perturbation of Carbon Cycle, Climate, and Biosphere with Implications for the Future. Annual Review of Earth and Planetary Sciences, v. 39**,** p. 489-516.

McRae, S.G., 1972, Glauconite: Earth-Science Reviews, v. 8, p. 397-440.

Moore, E.A and Kurtz, A.C. 2008. Black carbon in Paleocene-Eocene boundary sediments: a test of biomass combustion as the PETM trigger. Palaeogeography. Palaeoclimatology. Palaeoecology, v. 267, p.147–52.

Moran, K., Backman, J., Brinkhuis, H., Clemens, S.C., Cronin, T., Dickens, G.R., Eynaud, F., Gattacceca, J., Jakobsson, M., Jordan, R.W., Kaminski, M., King, J., Koc, N., Krylov, A., Martinez, N., Matthiessen, J., McInroy, D., Moore, T.C., Onodera, J., O'Regan, M., Palike, H., Rea, B., Rio, D., Sakamoto, T., Smith, D.C., Stein, R., St John, K., Suto, I., Suzuki, N., Takahashi, K., Watanabe, M., Yamamoto, M., Farrell, J., Frank, M., Kubik, P., Jokat, W. and Kristoffersen, Y. 2006. The Cenozoic palaeoenvironment of the Arctic Ocean. Nature. v. 441 (7093), p. 601-605.

Morris, K.A., 1979, Classification of Jurassic marine shale sequences - Example from the Toarcian (Lower Jurassic) og Great-Britain Palaeogeography Palaeoclimatology Palaeoecology, v. 26, p. 117-126.

Mörner, N.-A. 1976. Eustacy and geoid changes. The journal of geology, v, 84 no- 2, p. 123-151.

Mörner, N.-A. 1980. The Fennoscandian uplift: Geological data and their geodynamic implications. Earth Rheology, Isostasy and Eustacy, p. 251-284.

Murphy, B. H., Farley, K. A. & Zachos, J. C. 2010. An extraterrestrial He-3-based timescale for the Paleocene-Eocene thermal maximum (PETM) from Walvis Ridge, IODP Site 1266. Geochimica Et Cosmochimica Acta,,v. 74**,** p. 5098-5108.

Myhre, A. M., Eldholm, O. & Sundvor, E. 1982. The margin between Senja and Spitsbergen fracture zones: Implications from plate tectonics. Tectonophysics, v. 89**,** p. 33-50.

Müller, R.D., and Spielhagen, R.F., 1990, Evolution of the Central Tertiary Basin of Spitsbergen – Towards a Synthesis of Sediment and Plate Tectonic History: Palaeogeography Palaeoclimatology Palaeoecology, v. 80, p. 153-172.

Nagy, J., Kaminski, M.A., Kuhnt, W. and Bremer, M.A. 2000. Agglutinated Foraminifera from Neritic to Bathyal Facies in the Palaeogene of Spitsbergen and the Barents Sea. *In* Hart, M.B., Kaminski, M.A. and Smart, C.W. (eds). Proceedings of the Fifth International Workshop on Agglutinated Foraminifera: Grzybowski Foundation Special Publication, v.7, p. 333-361

Nagy, J., 2005, Delta-influenced foraminiferal facies and sequence stratigraphy of Paleocene deposits in Spitsbergen: Palaeogeography Palaeoclimatology Palaeoecology, v. 222, p. 161-179.

Nystuen, J.P. 1998. History and development of sequence stratigraphy. In Sequence Stratigraphy- Concepts and applications.Norwegian Petroleum Institute (NPF), v.8, p. 316

Pearson, M.J., 1979, Geochemistry of the Hepworh Carboniferous sediment sequence and origin of the diagenetic iron minerals and concretions: Geochimica Et Cosmochimica Acta, v. 43, p. 927-941.

Peters, K.J., 1986, Guidelines for evaluating petroleum source rock using programmed pyrolysis: Guidelines for evaluating petroleum source rock using programmed pyrolysis, v. 70, p. 318.

Peters, K., and Cassa, M., 1994, Applied source rock geochemistry, *in* Magoon, L.B., and Dow, W.G., eds., 1994, The petroleum system from source to trap: AAPG Memoir 60, p. 93-117.

Plink-Björklund, P. 2005. Stacked fluvial and tide-dominated estuarine deposits in high-frequency (fourth-order) sequences of the Eocene Central Basin, Spitsbergen. Sedimentology, v, 52, p 391-428.

Potter, P.E., Maynard, J.B., and Pryor, W.A., 1980, Sedimentology of shale: study guide and reference source: New York, Springer, x,306 s .p.

Reading, H.G., 2009, Sedimentary environments: processes, facies and stratigraphy: Oxford, Blackwell Science, XIV, 688 s. p.

Robert, C., Kennett, J., 1992. Paleocene and Eocene kaolinite distribution in the South Atlantic and Southern Ocean: Antarctic climatic and paleoceanographic implications. Marine. Geology, v.103, p. 99–110.

Robert C, Kennett JP. 1994. Antarctic subtropical humid episode at the Paleocene-Eocene boundary—claymineral evidence. Geology, v.22, p, 211–214.

Rose KD. 1981. The Clarkforkian Land-Mammal Age and Mammalian Faunal Composition Across the Paleocene-Eocene Boundary. University of Michigan Papers on Paleontology, v. 26, p. 1-197.

Röhl, U., Bralower, T.J., Norris, R.D., and Wefer, G., 2000, New chronology for the late Paleocene thermal maximum and its environmental implications: Geology, v. 28, p. 927-930.

Röhl, U., Westerhold, T., Bralower, T. J. & Zachos, J. C. 2007. On the duration of the Paleocene-Eocene thermal maximum (PETM). Geochemistry Geophysics Geosystems, 8.

Rüther, C. D. 2007. Delta influenced Paleogene depositional environments of the Frysjaodden and Hollendardalen formations, University of Oslo (Unpublished Master Thesis).

Savin, S.M., Douglas, R.G., and Stehli, F.G. 1975, Tertiary Marine Paleotemperatures: Geological Society of America Bulletin, v. 86, p. 1499-1510.

Schmitz, B,, Pujalte, V., Nunez-Betelu, K. 2001. Climate and sea-level perturbations during the initial Eocene thermal maximum: evidence from siliciclastic units in the Basque Basin (Ermua, Zumaia and Trabakua Pass), northern Spain. Palaeogeography. Palaeoclimatology. Palaeoecology, v. 165, p. 299–320.

Schülter and Hinz, K. The continental margin of West Spitsbergen, Polarforschung, v, 48, p 151-169.

Schtweizer, H.J. 1980. Environment and climate in the early Tertiary of Spitsbergen Palaeogeography Palaeoclimatology Palaeoecology, v. 30, p. 297.

Sluijs, A., Röhl, U., Schouten, S., Brumsack, H.-J., Sangiorgi, F., Sinninghe Damsté, J. S. & Brinkhuis, H. 2008. Arctic late Paleocene–early Eocene paleoenvironments with special emphasis on the Paleocene-Eocene thermal maximum (Lomonosov Ridge, Integrated Ocean Drilling Program Expedition 302). Paleoceanography, v.23, p. PA1S11.

Spencer A. M., Home P. C., Berglund L. T.1984. In Petroleum Geology of the North European Margin, Tertiary structural development of the western Barents Shelf: Troms to Svalbard, ed SpencerA. M., et al. (Graham & Trotman, London), pp 199–209.

Steel, R.J., Dalland, A., Kalgraf, K., Larsen, V., 1981. The central Tertiary basin of Spitsbergen—sedimentary development in a sheared margin basin. In: Kerr, J.W.,Fergusson, A.J. (Eds.), Geology of the North Atlantic Borderlands, Memoir Canadian Society of Petroleum Geologists, v. 7, p. 647– 664.

Steel, R.J., Gjelberg, J., Helland-Hansen, W., Kleinsphen, K., Noettvedt, A., Rye larsen, M., 1985. The Tertiary strike-slip basins and orogenic belt of Spitsbergen. In: Biddle, K.T., Christie- Blick, N. (Eds.), Strike-Slip Deformation, Basin Formation and Sedimentation, Special Publication Society of Economic Paleontologists and Mineralogists, v. 37, p. 339– 359.

Sundvor, E and Eldhom. 1977. Marine geophysical survey on the continental margins from Baer Island to Hornsund, Spitsbergan, Univ. Bergen Seismol. Obs., Sci. Rep. **3**, p. 28.

Sundvor, E. Eldholm. 0.. Giskehaug. A. and Myhre. A.. 1977. Marine geophysical survey of the western and northern continental margin of Svalbard. Univ. Bergen Seismol. Obs. Sci. Rep.. No. 4: 35 pp.

Svensen H, Planke S, Corfu F. 2010. Zircon dating ties NE Atlantic sill emplacement to initial Eocene global warming. Journal of Geological Society, v.167,p.433–36.

Svensen H, Planke S, Malthe-Sorenssen A, Jamtveit B, Myklebust R, et al. 2004. Release of methane from a volcanic basin as a mechanism for initial Eocene global warming. Nature, v.429, p.542–45.

Talwani, M., and Eldholm, O., 1977, Evolution of the Norwegian-Greenland Sea: Geological Society of America Bulletin, v. 88, p. 969-999.

Thiry, M. 2000. Palaeoclimatic interpretation of clay minerals in marine deposits: an outlook from the continental origin. Earth-Science Reviews, v. 49**,** p. 201-221

Thiry, M. and Dupuis, C. 2000. Use of clay minerals for paleoclimatic reconstructions: Limits of the method with special reference to the Paleocene—lower Eocene interval. *GFF*, v. 122**,** p. 166 - 167.

Thomas, E., Shackleton, N.J. 1996. The Paleocene-Eocene benthic foraminiferal extinction and stable isotope anomalies. In Correlation of the Early Paleogene in Northwest Europe Correlation of the Early Paleogene in Northwest Europe, Special Publication. 101, ed. RWOB Knox, R Corfield, RE Dunay, pp. 401–41. Washington, DC: Geol. Soc.

Throndsen, T. 1982: Vitrinite reflectance studies of coals and dispersed organic matter in Tertiary deposits in the Adventdalen area, Svalbard. Polar Research v. 2, p. 77-91.

Tissot, B.P, Pelet, R and Ungerer. P.H. 1987. Thermal history of sedimentary basins, Maturation indices and kinetic of Oil and Gas generation. The American Association of Petroleum Geologist Bulletin, v. 71, p. 1445-1466.

Tissot, B.P and Welte, D.H. 1984. Petroleum formation and occurrence, 2nd ed: New York, Springer Verlag, p. 699.

Tripati, A. & Elderfield, H., 2005. Deep-sea temperatures and circulation changes at the Paleocene-Eocene thermal maximum. Science, v. 308, p. 1894–-1898.

Vogt, R.K. Perry, R.H. Feden, H.S. Fleming and N.Z. Cherkis. The Greenland-Norwegian sea and Iceland environment: geology and geophysics, The Ocean Basins and Margins, v. 5, p. 493-598.

Vonderbank, K, 1970. Geologie und Fauna der tertiären Ablagerungen Zentral-Spitzbergens, Nor. Polarinst. v. 153, p. 1–119.

Westerhold, T., Röhl, U., Mccarren, H. K. & Zachos, J. C. 2009. Latest on the absolute age of the Paleocene-Eocene Thermal Maximum (PETM): New insights from exact stratigraphic position of key ash layers + 19 and - 17. Earth and Planetary Science Letters, v. 287**,** p. 412-419.

White, A.F. & Brantley, S. L, 1995. Chemical weathering rates of silicate minerals: an overview. In Chemical weathering rates of silicate minerals. Reviews in mineralogy v. 31, p 1-22.

Worsley, D. 2008. The post-Caledonian development of Svalbard and the western Barents Sea. Polar Research, v. 27**,** p. 298-317.

Zachos, J. C, Lohmann, K.C., Walker, J.C.G. and Wise, S.W. 1993. Abrupt climate change and transient climates during the Paleogene: A marine prespective. Journal of Geology,v. 101, p. 191-213.

Zachos, J. C. & Dickens, G. R. 2000. An assessment of the biogeochemical feedback response to the climatic and chemical perturbations of the LPTM. GFF v.122, p188–189.

Zachos, J. C, Pagani, M., Sloan, L., Thomas, E., and Billups, K., 2001, Trends, rhythms, and aberrations in global climate 65 Ma to present: Science, v. 292, p. 686-693.

Appendices

Appendix 1: Logging sheet used for the current study

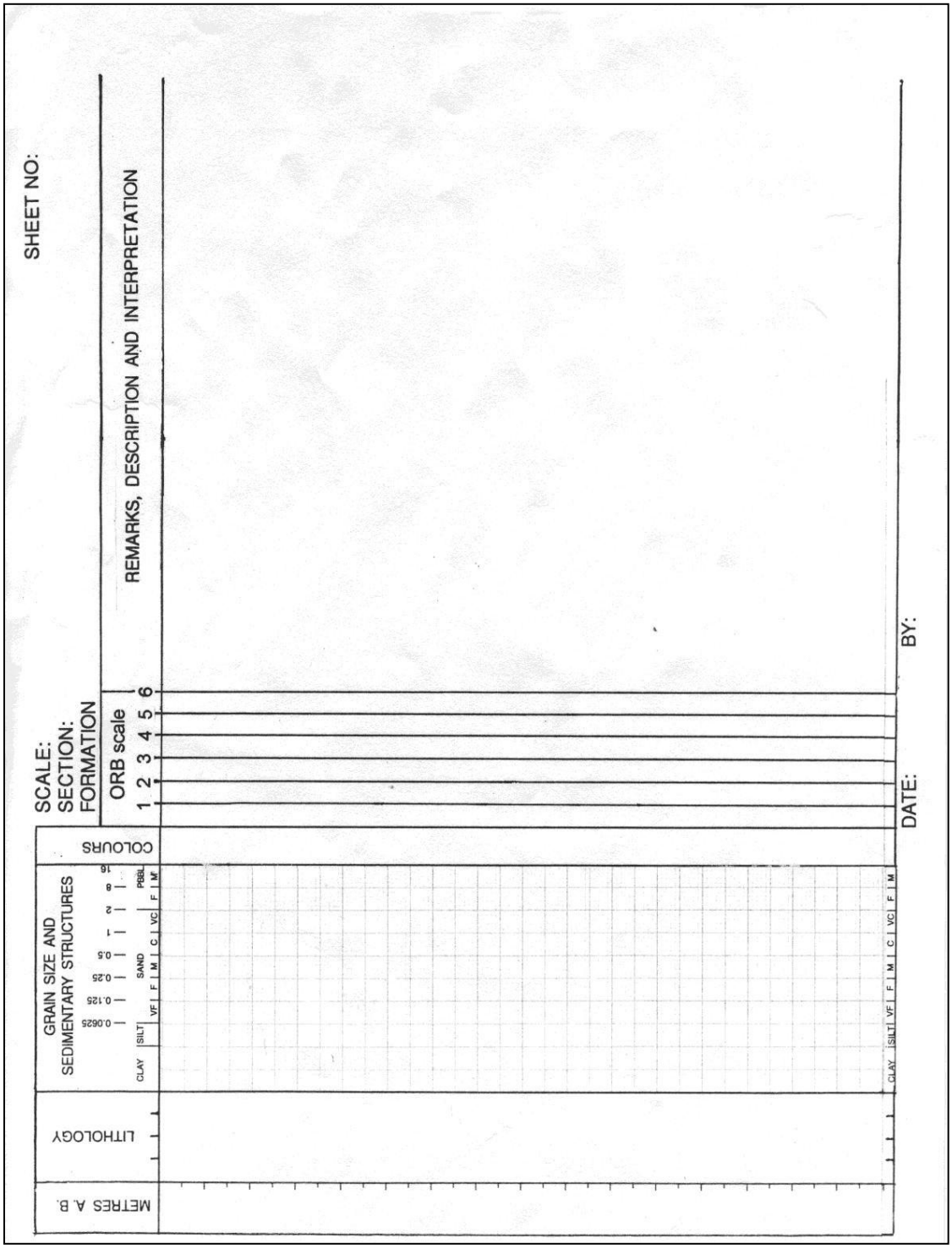

Appendix 2: Thin sections description

BH 9/06							
Formation/Member	**Depth**	**Lithology**	**Framework Configuration**	**Observed Structures**	**Grain Size**	**Grain Shape**	**Sorting**
Gilsonryggen Mb.	112,20	Silty Shale	Matrix Supported	Moderate bioturbation	Clay	Sub rounded	Poor sorting
Hollendardalen Member	118,00	Sandstone	Matrix Supported	ripple lamination	Silt to very Fine	Sub angular	Moderate Sorting
	118,90	Silty shale	Matrix Supported	laminationn	Clay to Silt	Sub angular	Moderate Sorting
Grumantbyen Formation.	129,10	Sandstone	Grain Supported	high bioturbation	Fine	Sub angular	Well sorted
	130,70	Silty Sandstone	Matrix Supported	high bioturbation	Fine	Sub angular	poor sorting
	131,60	Sandstone	Grain Supported	Moderate bioturbation	Medium	Sub angular	Moderate Sorting
	132,50	Sandstone	Grain Supported	Moderate bioturbation	Fine to Medium	Subrounded	Well sorted
	135,00	Sandstone	Grain Supported	High bioturbation	Fine	Subangular	Well sorted
BH 7/08							
Formation/Member	**Depth**	**Lithology**	**Framework Configuration**	**Observed Structures**	**Grain Size**	**Grain Shape**	**Sorting**
Gilsonryggen Member.	57,45	Shale	Matrix Supported	Parallel Lamination	Clay	Sub rounded	Moderate
	70,40	Shale	Matrix Supported	Parallel Lamination	Clay	Subrounded	Moderate
	83,50	Siltstone	Matrix Supported	Bioturbation	Silt	Subrounded	poor
	87,73	Siltstone	Matrix Supported	Bioturbation	Silt	Subrounded	poor
	87,90	Sandstone	Matrix Supported	Bioturbation	Fine	Sub angular	poor
Hollenderdallen Member	88,73	Sandstone	Grain supported	Hummocks??	Fine	Sub angular	Well sorted
	90,95	Glauconitic Sandstone	Grain supported	Lamination	Fine	Sub angular	Moderate
Marstrandebreen Mb.	91,55	Conglomerate	Grain supported	Hetrogenity	Coarse	Sub angular	Moderate
BH 10/06							
Formation/Member	**Depth**	**Lithology**	**Framework Configuration**	**Observed Structures**	**Grain Size**	**Grain Shape**	**Sorting**
Gilsonryggen Mb	479,55	Shale	Matrix Supported	Moderate bioturbation	Clay	Angular	Moderate sorting
	501,80	Shale (Siderite)	Matrix Supported	None	Clay	Angular	Well sorted
	505,15	Shale	Matrix Supported	High bioturbation	Clay	Angular	Well sorted
	511,20	Siltstone	Matrix Supported	Moderate bioturbation	Silt to clay	Angular	Poor
	511,90	Silty sandstone	Grain Supported	High bioturbation	Very Fine	Angular	Well sorted
Grumantbyen Fm.	512,90	Conglomerate	Matrix Supported	Hetrogenity	Medium to Coarse	Sub angular	Poor
	514,90	Sandstone	Grain Supported	High bioturbation	Very fine	Sub angular	Poor
	516,25	Sandstone	Grain Supported	Moderate bioturbation	Fine to Medium	Sub rounded	Poor
	518,05	Sandstone	Grain Supported	Moderate bioturbation	Fine	Sub rounded	Well sorted

Appendix 3: Thin section mineral counting results

BH 9/06														
	Depth (m)	Quartz (M) (%)	Quartz (P) (%)	Feldspar (%)	Mica (M) (%)	Mica (B) (%)	Organic Matter (%)	Pyrite (%)	Chlorite (%)	Matrix		Glauconite (%)	Fossils (%)	FeO (%)
										Clay (%)	Illitic Clay(%)			
Gilsonryggen Member	100,0	1,5	0,0	6,2	0,0	0,0	6,0	21,2	0,5	57,2	3,5	0,0	0,0	0,0
	112,2	16,6	3,2	29,0	2,7	0,0	16,1	2,0	3,0	15,4	10,1	0,2	0,0	0,0
Hollendardalen Member	118,0	46,0	5,0	23,0	1,5	0,5	5,0	3,0	2,0	1,2	10,0	2,8	0,0	0,0
	118,9	25,7	0,0	11,0	4,2	0,0	15,0	0,5	0,7	9,5	32,0	1,2	1,0	0,1
Grumantbyen Formation	129,1	28,5	6,5	48,0	2,5	0,0	1,5	0,0	1,2	3,7	4,0	2,5	0,0	0,0
	131,6	30,7	5,7	50,0	0,2	0,0	1,2	0,0	2,2	4,0	2,7	3,0	0,0	0,0
BH 10/06														
	Depth (m)	Quartz (M) (%)	Quartz (P) (%)	Feldspar (%)	Mica (M) (%)	Mica (B) (%)	Organic Matter (%)	Pyrite (%)	Chlorite (%)	Matrix		Glauconite (%)	Fossils (%)	FeO (%)
										Clay (%)	Illitic Clay(%)			
Gilsonryggen Member	479,5	1,7	0,2	4,5	1,7	0,2	2,2	1,2	0,0	77,0	11,0	0,0	0,0	0,0
	505,2	2,2	0,0	2,2	0,0	0,2	1,5	0,5	0,2	68,0	25,0	0,0	0,0	0,0
	511,9	31,7	10,5	30,0	8,0	0,2	1,2	0,7	3,0	6,7	5,5	2,2	0,0	0,0
Grumantbyen Formation	514,7	63,2	0,0	30,0	0,5	0,0	0,7	0,0	2,0	1,5	5,5	2,5	0,0	0,0
	518,0	43,0	11,2	26,0	4,7	0,0	0,5	2,0	1,7	2,7	6,7	1,2	0,0	0,0
BH 7/08														
	Depth (m)	Quartz (M) (%)	Quartz (P) (%)	Feldspar (%)	Mica (M) (%)	Mica (B) (%)	Organic Matter (%)	Pyrite (%)	Chlorite (%)	Matrix		Glauconite (%)	Fossils (%)	FeO (%)
										Clay (%)	Illitic Clay(%)			
Gilsonryggen Menber	57,5	1,7	0,0	4,2	1,0	0,2	1,0	3,5	0,2	78,2	9,7	0,0	0,0	0,0
	70,4	0,5	0,0	5,5	1,5	0,0	2,5	6,7	0,0	72,0	11,2	0,0	0,0	0,0
	83,5	10,0	0,0	15,0	2,2	0,7	11,7	3,0	2,0	36,7	17,7	0,5	0,0	0,0
	87,9	43,3	1,3	23,0	1,6	0,0	4,0	0,3	1,3	5,0	18,6	1,3	0,0	0,0
Hollendardalen Member	90,95	41,0	3,0	27,7	1,0	0,0	2,7	0,0	1,7	2,7	14,7	5,2	0,0	0,0

Appendix 4: Mineral estimation from bulk XRD in BH 7/08

BH 7/08														
Depth	Illite %	Chlorite %	Kaolinite %	Quartz %	K-feldspar %	Plagioclase %	Feldspar %	Calcite %	Dolomite %	Siderite %	Pyrite %	Kaolinite/ Chlorite	Kaolinite/ Illite	Quartz/ Feldspar
Shales of Lower Gilsonryggen														
57,45	3,6	3,7	2,7	43,2	11,1	23,1	34,2	1,4	3,0	5,7	2,7	0,72	0,75	0,56
58,80	3,8	3,5	2,1	44,5	11,8	21,9	33,8	2,2	3,6	6,5	0,0	0,60	0,56	0,57
59,90	5,3	3,6	2,2	38,6	10,9	20,0	30,9	1,3	3,8	13,1	1,2	0,62	0,42	0,56
62,25	5,5	4,9	2,3	40,2	11,4	20,6	32,0	3,2	3,4	7,3	1,1	0,47	0,43	0,56
66,50	2,9	2,0	2,4	51,9	10,0	21,6	31,6	1,3	1,1	3,5	3,4	1,16	0,83	0,62
70,40	3,3	2,2	2,1	40,9	9,7	19,1	28,8	1,0	3,0	1,6	17,2	0,97	0,65	0,59
72,20	2,3	1,4	1,4	41,4	8,9	17,6	26,5	1,4	1,3	2,0	22,5	0,98	0,58	0,61
74,80	3,0	2,9	1,3	41,1	9,2	19,4	28,6	2,2	0,0	1,1	19,7	0,46	0,45	0,59
77,50	3,5	2,3	2,2	48,0	0,0	24,1	24,1	1,0	1,5	1,7	15,8	0,96	0,64	0,67
80,45	1,9	1,5	2,1	43,2	9,1	18,6	27,7	0,0	1,3	18,6	3,7	1,38	1,07	0,61
83,50	2,2	2,6	1,4	46,5	11,7	22,8	34,5	2,6	0,0	4,2	6,1	0,55	0,65	0,57
86,90	2,7	2,8	1,6	42,6	10,6	31,4	42,1	1,9	2,3	3,7	0,4	0,59	0,61	0,50
87,73	4,3	3,7	2,2	49,7	0,0	29,8	29,8	2,3	3,3	3,9	1,0	0,60	0,51	0,63
87,90	0,7	1,7	0,4	68,5	9,3	15,4	24,6	1,0	2,0	0,6	0,6	0,22	0,53	0,74
Average	***3,2***	***2,8***	***1,9***	***45,7***	***8,8***	***21,8***	***30,7***	***1,6***	***2,1***	***5,2***	***6,8***	***0,70***	***0,62***	***0,60***
Hollendardalen Member Sandstone														
90,95	0,5	1,5	0,1	45,6	17,4	27,3	44,7	1,5	4,2	1,3	0,6	0,06	0,17	0,51
Conglomerate														
91,55	2,7	4,0	1,4	48,2	14,2	24,5	38,7	0,9	2,4	0,9	0,6	0,36	0,52	0,55

Appendix 5: Mineral estimation from bulk XRD in BH 9/06

BH 9/06														
Depth	**Illite %**	**Chlorite %**	**Kaolinite %**	**Quartz %**	**K-feldspar %**	**Plagioclase %**	**Feldspar %**	**Calcite %**	**Dolomite %**	**Siderite %**	**Pyrite %**	**Quartz/ Feldspar**	**Kaolinite /Illite**	Kaolinite/ Chlorite
Shales of lower Gilsonryggen														
104,50	3,5	3,2	1,9	38,3	7,6	19,4	27,0	0,0	2,0	1,8	22,3	0,59	0,36	0,37
106,73	7,3	4,6	6,5	41,2	5,9	23,0	28,9	0,0	0,8	2,3	8,4	0,59	0,47	0,59
109,35	4,6	3,1	4,4	44,4	7,3	23,0	30,2	1,1	0,8	4,8	6,6	0,60	0,49	0,58
112,20	3,9	2,6	2,4	38,2	13,5	33,0	46,5	0,8	0,9	1,9	2,9	0,45	0,39	0,48
115,05	4,6	3,4	3,0	43,7	0,0	26,8	26,8	1,2	1,7	15,6	0,0	0,62	0,40	0,47
Average	***4,8***	***3,4***	***3,7***	***41,2***	***6,9***	***25,0***	***31,9***	***0,6***	***1,2***	***5,3***	***8,0***	***0,60***	***0,42***	***0,50***
Sandstones of Hollendardalen														
118,00	1,7	2,4	1,3	54,8	9,8	25,0	34,8	0,0	0,7	0,9	3,4	0,61	0,43	0,35
118,90	5,1	9,1	3,2	45,0	9,1	17,9	27,0	1,2	2,1	6,6	0,6	0,62	0,39	0,26
122,50	6,8	13,2	2,7	41,9	8,9	16,2	25,1	1,0	2,4	6,8	0,0	0,63	0,28	0,17
Average	***4,6***	***8,3***	***2,4***	***47,2***	***9,3***	***19,7***	***29,0***	***0,7***	***1,7***	***4,8***	***1,3***	***0,60***	***0,37***	***0,26***
Shales of Mastranderbreen														
123,65	7,5	10,3	3,0	38,9	6,5	19,5	26,0	3,3	3,1	7,9	0,0	0,60	0,29	0,23
125,45	4,0	5,3	1,2	36,7	13,9	33,8	47,7	1,1	0,0	3,4	0,7	0,44	0,23	0,19
126,50	5,5	6,5	3,1	41,7	0,0	21,2	21,2	0,0	0,8	14,4	6,7	0,66	0,36	0,32
Average	***5,7***	***7,4***	***2,4***	***39,1***	***6,8***	***24,8***	***31,6***	***1,4***	***1,3***	***8,6***	***2,5***	***0,60***	***0,29***	***0,25***
Siltstone of Mastranderbreen														
128,50	1,2	2,3	0,5	26,6	21,0	44,0	64,9	1,2	1,8	1,0	0,5	0,29	0,31	0,19
Sandstones of Grumantbyen														
129,10	0,6	1,2	0,2	48,9	18,0	26,4	44,4	1,5	2,5	0,8	0,0	0,52	0,21	0,12
130,70	1,1	2,0	0,4	34,2	17,7	37,9	55,6	2,5	2,4	1,2	0,5	0,38	0,26	0,16
131,60	0,9	2,4	0,3	38,4	23,3	30,7	54,0	1,7	2,4	0,0	0,0	0,42	0,24	0,10
135,00	0,5	1,4	0,4	38,9	22,4	31,6	54,0	1,3	2,4	0,8	0,4	0,42	0,42	0,21
Average	***0,8***	***1,7***	***0,3***	***40,1***	***20,3***	***31,7***	***52,0***	***1,8***	***2,4***	***0,7***	***0,2***	***0,41***	***0,28***	***0,15***
Conglomerate														
132,50	0,4	0,8	0,2	44,2	19,4	23,1	42,5	7,9	2,8	0,9	0,4	1,04	0,31	0,21

Appendix 6: Mineral estimation from bulk XRD in BH 10/06

BH 10/06														
Depth	Illite %	Chlorite %	Kaolinite %	Quartz %	K-feldspar %	Plagioclase %	Feldspar %	Calcite %	Dolomite %	Siderite %	Pyrite %	Quartz/ Feldspar	Kaolinite /Illite	Kaolinite /Chlorite
Shales of lower Gilsonryggen														
475,55	3,7	2,4	3,0	43,4	9,3	18,9	28,2	1,7	0,0	10,8	6,8	0,61	0,45	0,55
479,50	3,4	2,5	1,9	40,2	8,3	17,2	25,5	0,8	1,3	1,8	22,6	0,61	0,35	0,42
482,35	0,0	0,1	0,4	1,0	27,7	25,4	53,1	0,8	2,1	29,0	13,4	0,02	1,00	0,84
485,45	6,1	4,3	2,8	37,2	6,8	12,9	19,7	1,1	2,5	2,1	24,4	0,65	0,31	0,39
488,50	3,4	2,6	2,4	32,7	9,4	14,5	23,9	2,0	2,9	1,5	28,5	0,58	0,41	0,47
492,90	2,2	1,9	1,9	32,2	6,3	13,7	19,9	0,0	0,0	2,8	39,2	0,62	0,47	0,50
496,85	3,7	1,5	2,6	27,6	3,8	6,8	10,6	1,3	4,6	46,8	1,2	0,72	0,41	0,63
501,80	0,7	1,6	0,2	4,1	0,6	2,3	2,9	0,0	0,9	89,1	0,2	0,58	0,20	0,10
505,15	2,6	4,2	2,0	44,5	12,6	18,9	31,5	2,7	3,8	8,6	0,0	0,59	0,44	0,33
508,95	3,0	3,8	2,1	56,8	8,5	14,4	22,8	1,1	1,1	8,2	1,3	0,71	0,41	0,36
511,20	4,0	3,9	1,9	53,1	11,3	19,5	30,8	1,6	2,4	1,7	0,5	0,63	0,32	0,33
511,90	0,7	3,7	0,8	37,3	16,9	36,3	53,2	0,9	1,9	0,7	0,6	0,41	0,55	0,18
512,90	1,3	2,9	1,1	44,0	19,3	27,3	46,5	0,8	2,1	0,5	0,7	0,49	0,46	0,27
Average	***2,8***	***2,8***	***1,9***	***37,5***	***11,7***	***18,8***	***30,5***	***1,2***	***2,0***	***9,5***	***11,6***	***0,6***	***0,5***	***0,4***
Sandstones of upper Grumantbyen														
514,90	0,3	2,0	0,5	56,0	16,6	19,7	36,3	0,9	2,5	0,9	0,5	0,6	0,61	0,20
516,25	0,3	3,0	0,3	65,9	16,2	8,4	24,5	2,6	1,9	0,6	1,0	0,7	0,55	0,10
518,05	0,0	1,4	0,3	59,3	15,7	18,0	33,7	1,3	2,8	0,8	0,4	0,6	1,00	0,16
Average	***0,2***	***2,1***	***0,4***	***60,4***	***16,2***	***15,4***	***31,5***	***1,6***	***2,4***	***0,8***	***0,6***	***0,7***	***0,7***	***0,2***

Appendix7 : TOC, TC and Rock-Eval analyses

Depth	TOC	TC	S1	S2	S3	S2/S3	Tmax	HI	OI	PP	PI
BH 7/08											
58,80	1,46	1,63	0,24	1,45	0,42	3,45	441	99,31	29,00	1,70	0,14
62,25	1,32	1,51	0,29	1,13	0,74	1,53	438	85,60	56,00	1,40	0,20
70,40	1,31	1,35	0,53	1,86	0,20	9,30	435	141,98	15,00	2,40	0,22
74,80	1,87	1,86	0,81	3,64	0,18	20,22	432	194,65	10,00	4,50	0,18
80,45	1,30	2,03	0,32	1,40	0,81	1,73	437	107,69	62,00	1,70	0,19
86,90	1,84	1,90	0,35	2,28	0,23	9,91	439	123,91	13,00	2,60	0,13
91,55	1,58	1,38	0,31	1,41	0,24	5,88	439	89,24	15,00	1,70	0,18
BH 9/06											
104,05	1,82	1,86	0,74	2,74	0,28	9,79	436	150,55	15,00	3,50	0,21
109,35	1,42	1,66	0,32	1,58	0,27	5,85	436	111,27	19,00	1,90	0,17
115,05	3,03	3,60	0,52	3,32	0,71	4,68	437	109,57	23,00	3,80	0,14
118,90	1,12	1,41	0,22	1,04	0,72	1,44	438	92,85	64,00	1,30	0,17
123,65	1,50	1,77	0,32	1,53	0,52	2,94	441	102,00	35,00	1,90	0,17
126,50	1,29	1,82	0,32	1,13	0,58	1,95	435	87,59	45,00	1,50	0,22
BH 10/06											
475,55	1,27	1,63	0,45	1,30	0,56	2,32	440	102,36	44,00	1,70	0,26
485,45	1,13	1,15	0,63	1,36	0,18	7,56	436	120,35	16,00	2,00	0,32
492,50	1,58	1,64	0,92	2,16	0,23	9,39	432	136,71	15,00	3,10	0,30
501,80	3,28	8,29	0,29	0,81	4,51	0,18	443	24,69	138,00	1,10	0,26
508,95	1,30	1,62	0,30	0,94	0,59	1,59	442	72,31	45,00	1,20	0,24
518,05	0,11	0,11	0,10	0,07	0,32	0,22	452	63,64	291,00	0,20	0,59

Acknlowdgments

I feel instigated from within to extend my thanks to Allmighty Allah whos magnanimous and chivalrous enabled me to percieve and pursue my abmitions and objectives. Special praises to Prophet Mohammad (PBUH) how is well wether for humanity as a whole.

I feel great honour in expressing my avid gratifications to Professor Henning Dypvikand Jeno Nagy at the Department of Geosciences. Special thanks to Henning Dypvik for always being available for discussions of my problems. Thanks to Jeno Nagy for his friendly and supportive way of discussing new ideas.

Thanks to Dwarika Maharjan for the support and teamwork during the field work at Svalbard and the entire length of this thesis. We will always be great friends.

The finalcial support of World Wide Universities Network during the field trip to Svalbard associated with this thesis is highly appretiated. Thanks SNSK for providing us their core storage unit in Svalbard.

Mofak Nauroz has been very helpful in determining the geochemical analysis of my samples. Thanks to Berit Løken Berg for her guidance in XRD analysis.

I would also like to thank all my classmates and juniors for their support and confidence in me and for the help during the course of this thesis.

At last but definitely not the least, I would like to thank my Family for their unendind love and affection, I owe a lot to them. Especially my dear sister for always believing in me.

P.S. “Kaddi sochaya vi nai si k Norway aa k Thesis vi pura keraa ga :….(”